Characterization of dielectric barrier discharges for analytical applications

Dissertation

zur Erlangung
des akademischen Grades
„Dr. rer. nat“
der Fakultät Physik
der Technischen Universität Dortmund

von

Felix David Klute
aus
Recklinghausen

Dortmund 2019

1. Gutachter: PD. Dr. Joachim Franzke
2. Gutachter: Prof. Dr. Manfred Bayer
Vorsitzender der Prüfungskommission: Prof. Dr. Matthias F. Schneider
Vertreter der wissenschaftlichen Mitarbeiter: Dr. Davide Bossini

Datum der Einreichung: 26.11.2018
Datum der mündlichen Prüfung: 28.01.2020
Eingereicht bei der Fakultät für Physik der Technischen Universität Dortmund.

ABSTRACT

This work will focus on the characterization of different dielectric barrier discharges (DBD) that are used in analytical applications. These discharges are primarily used as ion sources that provide charged species for the subsequent detection with atmospheric mass spectrometers (MS) or ion mobility spectrometers (IMS). The main method of investigation for the DBDs will be based on optical methods such as temporally-, spatially-, and spectrally-resolved optical emission spectroscopy (TSSR-OES). The small size of the DBDs investigated in this work complicates physical probing with e.g. Langmuir-probe, which means that optical measurements such as the TSSR-OES is the only feasible approach to characterize the mechanisms of said DBDs.

The findings of the these characterizations will be correlated with mass spectrometric measurements to evaluate the analytical performance of each discharge at different parameters. Combination of fundamental discharge characteristics respectively parameters to a meaningful ionization efficiency of a given plasma source will eventually improve the understanding of soft-ionization mechanisms that are a key part of current analytical applications and greatly help optimizing them.

Diese Arbeit konzentriert sich auf die Charakterisierung verschiedener dielektrisch behinderter Entladungen (DBD), die in analytischen Anwendungen verwendet werden. Diese Entladungen werden in erster Linie als Ionenquellen verwendet, die geladene Spezies für den späteren Nachweis mit atmosphärischen Massenspektrometern (MS) oder Ionenmobilitätsspektrometern (IMS) bereitstellen. Die Hauptmethode der Untersuchung für die DBDs wird auf optischen Methoden wie der zeitlich, räumlich und spektral aufgelösten optischen Emissionsspektroskopie (TSSR-OES) basieren. Die geringe Größe der in dieser Arbeit untersuchten DBDs erschwert die physikalische Untersuchung mit z.B. Langmuir-Sonden, was bedeutet, dass optische Methoden wie die TSSR-OES der einzig mögliche Ansatz zur Charakterisierung der Mechanismen der DBDs sind.

Die Ergebnisse dieser Charakterisierungen werden mit massenspektrometrischen Messungen korreliert, um die analytische Leistung jeder Entladung bei verschiedenen Parametern zu bewerten. Die Kombination von grundlegenden Entladungseigenschaften bzw. Parametern zu einer aussagekräftigen Ionisationseffizienz für eine bestimmte Plasmaquelle wird letztendlich das Verständnis von weichen Ionisationsmechanismen, die ein wichtiger Bestandteil aktueller analytischer Anwendungen sind, verbessern und wesentlich dazu beitragen diese Anwendungen zu optimieren.

CONTENTS

1 INTRODUCTION

Ionization sources are integral parts of analytical applications such as mass spectrometers (MS) or ion mobility spectrometers (IMS). These two methods can be used to identify and quantify analytes by either sorting them by their molecular masses in the case of MS or using the substance specific mobility in a gaseous phase for IMS [1–5].

Both methods require that the analytes are ionized prior to the measurement, due to the use of electric fields to either identify their masses or their mobility. Some of the ion sources usually used for these analytical detectors are e.g. electrospray ionization (ESI) [6, 7], UV photoionization lamps, β-radiation electron emitters or atmospheric pressure chemical ionization (APCI) [8–10]. An important aspect of these sources is that they are capable of the so called "soft ionization" which means that they can ionize whole molecules without breaking them up by dissociation or other destructive processes. One of the main processes of soft ionization is the addition of a positively charged hydrogen atom $[H]^+$ to a molecule [M] to form a protonated molecule $[M+H]^+$.

All these sources are commonly used, their applicability however often depends on several factors and they all are subject to several restrictions. This creates a constant demand for alternative ionization sources and subsequently lead to a steady increase of research in the field of plasma based ionization sources. Plasmas genereted by dielectric barrier discharges especially are of high interest due to the their properties thy offer to analytical applications [11–17].

Plasma discharges in general are extensively studied since the early 1920's [18] and play important roles in several industrial branches such as semiconductor fabrication [19, 20], material processing [21–23], lighting media [24, 25], energy production, waste treatment [26, 27], sterilization [28, 29] and many more. Dielectric barrier discharges (DBD) are a special form of plasma discharges and are the base of the recent interest in plasma based ionization sources that arose with the introduction of the dielectric barrier discharge for soft ionization (DBDI) [30–32].

The DBDI and similar designs use dielectric capillary tubes which allow for a compact, robust and also cheap construction of discharge systems which can be easily implemented into existing analytical applications. These discharges demonstrate promising attributes as ionization sources and could either complement or completely replace established sources such as APCI or ESI.

A DBDI can be operated in atmospheric pressure at ambient conditions without the need to isolate it from the outer atmosphere. This greatly simplifies its operation and reduces the requirements to an analytical application. Furthermore, a DBDI can be used with a variety of gases and gas mixtures, as long as the geometry and

power supply allow for the ignition and operation of a plasma. The choice of gas is not completely irrelevant as it greatly influences the properties of the plasma and its ionization efficiency due to the potential reactive species a plasma can generate.

A very common gas used for DBDs is helium as it greatly simplifies the ignite and subsequent operation of plasma due to its properties. As a noble gas it is chemical inert and therefore safe to use under almost all circumstances. A closer look at the physical properties of helium also reveals that helium atoms in a plasma reach relatively high energetic states which can easily break chemical bonds in collisions with molecules and thus create high energetic reactive fragments.

Recent studies show that these reactive species might play a major role in the atmospheric ionization capabilities exhibited by the DBDI and similar DBD based discharges [33, 34]. This means that the matter of the correct gas choice might not only be related to the simple question of cost optimization and ease of operation but might be more fundamentally rooted to the overall potential ionization efficiency of a discharge.

The aim of this work is the characterization of capillary DBDs like the DBDI to identify fundamental mechanisms in the formation and development of the plasma. Understanding these mechanisms should lead to a clearer insight to the interaction between high energetic plasma species with atmospheric molecular components and the formation of highly reactive species that might be an essential catalyst for chemical reactions under atmospheric conditions.

The main means for the investigation of these interactions is temporally-, spatially- and spectrally-resolved optical emission spectroscopy (TSSR-OES) which allows for a detailed observation of selected emission lines of the discharges on plasma relevant time and position scales. With the help of this optical method it is possible to observe the influence of global parameter changes to the plasma, such as e.g. a change to the applied voltage, electrode gap, gas flow or gas mixture, and correlate these changes to the observed development of the plasma. At the same time these observations can be correlated to the changes of the ionization efficiency of a DBD that is used with the same global parameters. A suited method to determine the ionization efficiency of DBD is to use it with a mass spectrometer and determine the influence of the global plasma parameters in the detected mass spectra.

Combination of these two different approaches might subsequently lead to a more complete picture on how an atmospheric plasma generate soft ionized molecules and potentially lead to new methods to directly influence and optimize this generation process. This would greatly help out the development of ionization sources for analytical applications and open up new paths for more sensitive and efficient devices.

2 THEORY

The exact description of a plasma is often difficult due to the fact that the choice of the correct model requires detailed knowledge of the given discharge to ensure that the assumptions used in the model are valid. This work primarily deals with atmospheric dielectric barrier discharges driven with high frequency voltages in the 10 kHz range. These discharges are mainly used for the ionization or excitation of analytes. The theoretical discussion of this work will only deal with this very special kind of plasma discharges and important mechanisms that are necessary to understand the formation and development of the plasma.

2.1 Plasmas and dielectric barrier discharges

A common glow or direct discharge is usually operated with a DC voltage ranging from some 100 V to several 1 kV depending on parameters such as electrode gap, gas pressure and the composition of the gas. Application of a constant electric field between two electrodes leads to acceleration of electrons and ions that are in the gas volume between these electrodes. The accelerated charged particles can collide with neutral atoms and molecules and ionize them if the energy gained by the acceleration is high enough. If the applied voltage surpasses a certain break-down value, which can be described by the Paschen's-law [35], the degree of ionization is high enough for a self-sustained plasma discharge to form. This kind of plasma is also referred to as a Townsend discharge named after John Sealy Townsend who first described this kind of plasma mechanism.

By putting one or more dielectric layers on the electrodes such a direct discharge can be transformed into a so called dielectric barrier discharge or short DBD. Application of a voltage will lead to an initial polarization of the dielectric layers which is further illustrated in figure 2.1. This polarization is caused by sorting the charged species inside of the dielectric layers along the axis of the applied electric field and can be expressed by the polarization density P which is, in the case of a homogeneous and linear electric field E, given by,

$$P = \epsilon_0 \chi_e E \tag{2.1}$$

where ϵ_0 is the electric permittivity of vacuum and χ_e is the electric susceptibility of the material. χ_e in principle indicates a materials ability to be polarized and is related to the electric permittivity in the following way:

$$\chi_e = \epsilon_r - 1. \tag{2.2}$$

This means the higher the relative permittivity or dielectric constant ϵ_r of a material, the better said material can be polarized by an applied electric field. A common

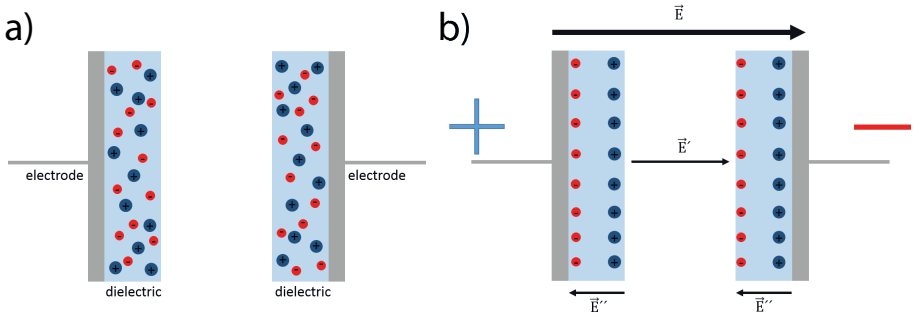

Figure 2.1: a) Parallel electrode configuration with dielectric layers covering the surface. The blue + and red - represent the unsorted charged species in the absence of an externel electric field $\vec{E}$. b) Application of an external voltage creates the electric field $\vec{E}$ between the electrodes which sorts the charged species inside the dielectric leading to the formation of $\vec{E}'$ and $\vec{E}''$.

material that is considered to be suited dielectric for dielectric barrier discharges is glass with a dielectric constant in the range of 3.5 to 10 depending on the exact composition of the glass[1].

The composition of the dielectric and the applied voltage play a major role in the polarization process, however another important factor is the geometry of the system which will be discussed in more detail in the following.

2.1.1 Capillary dielectric barrier discharges

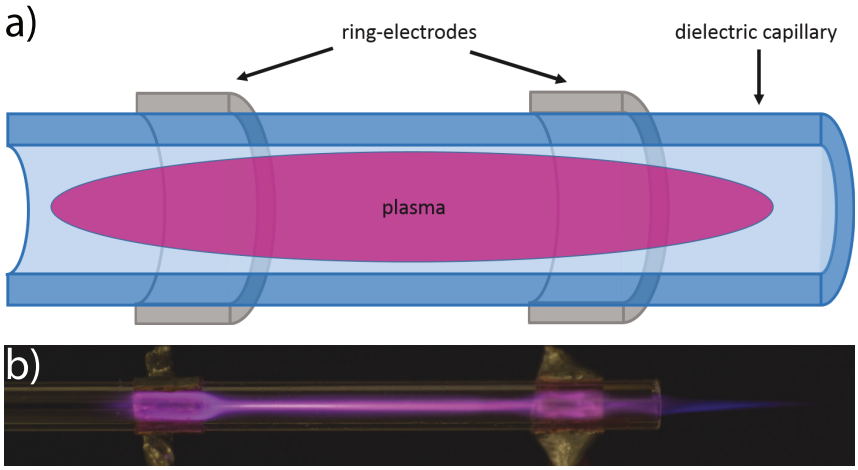

Figure 2.2: a) Schematic of a capillary dielectric barrier discharge. The dielectric tube (blue) is the basis of the discharge. The voltage is applied at the ring electrodes (grey) which are wrapped around the dielectric tube. b) Image of a capillary DBD in operation with partially opened electrodes.

Capillary dielectric barrier discharges use hollow glass, quartz or ceramic tubes as a dielectric material and are often found in analytical applications. The diameters

[1]The dielectric constant of fused silica or quartz glass which is used in the majority of this work is $\epsilon_r(\text{quartz}) = 3.75$

and lengths of these capillaries can vary depending on the application but they are in general cheap and robust and can be exchanged with low effort in the case of contamination or damage.

Constructing a dielectric barrier discharge out of such a dielectric tube is comparatively easy as the separation of the generated plasma from the electrodes can be achieved without much effort as one can see from figure 2.2. The capillary is filled with a gas mixture that is suited for the operation of plasma, in the most cases helium or other noble gases, while the ring-electrodes are affixed to the outside of the capillary and cannot come into contact with the the inner volume of the capillary. The plasma is able to ignite inside of the capillary due to the polarization of the dielectric material.

Using the cylindrical symmetry of the capillary it is possible to illustrate the polarization of the capillary in only two dimensions in figure 2.3. The application of an external voltage to the ring electrodes will lead to the polarization of the dielectric material in the direct vicinity of the electrodes. This realignment of the charged species inside of the capillary will lead to shift of the surface charge inside of the capillary and subsequently to an inner electric field $\vec{E}'$ which in turn can accelerate charged species along the axis of the capillary and ignite a plasma if the right conditions are met.

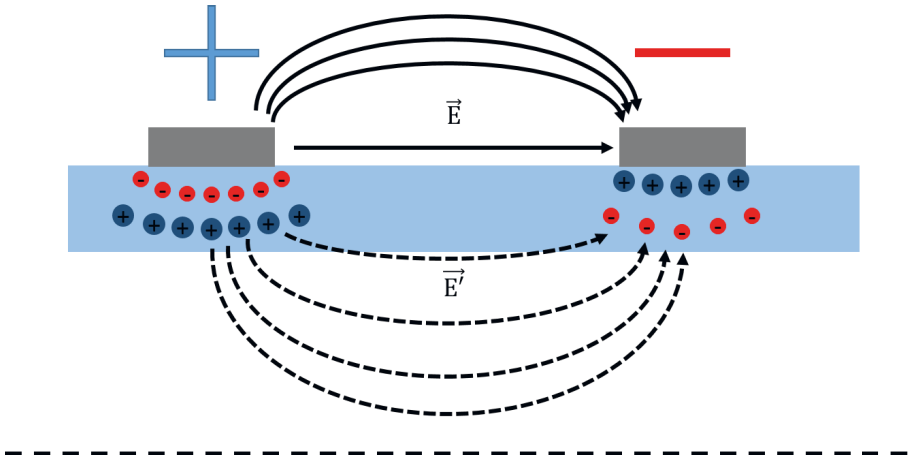

Figure 2.3: Illustration of the polarization inside of a dielectric capillary tube. Application of a voltage leads to the creation of an electric field $\vec{E}$ between the ring electrodes outside of the capillary. The voltage furthermore leads to the polarization of charged species inside of the dielectric and the creation of an inner field $\vec{E}'$. The dotted line at the bottom implies the cylindrical symmetry axis of the capillary.

Contrary to a direct discharge, a DBD cannot rely on a steady flow of electric current or secondary electrons from the surface of the electrodes as they are covered by the dielectric material. The initial ignition process, which will be discussed later on in more detail, has to be repeated perpetually to sustain a quasi continuous plasma discharge under these conditions. This is the reason why capillary DBDs and DBDs in general are operated by suited AC voltage supplies. These power supplies periodically switch the direction of the applied voltage and the discharge process can be restarted over and over again. The operation of a dielectric barrier discharge only seems to be continuous to the human eye because it is to slow to follow the quick

ignition processes on a microsecond scale, similar to the normal everyday lighting which is modulated by the electric grid frequency of 50 Hz.

With the help of suited optical detectors it is possible to resolve the ignition processes of dielectric barrier discharges and observe the highly dynamic processes in the plasma. Studies by Horvatic et al. in 2015 [36] measured the temporally- and spatially-resolved emission of several significant emission lines of a capillary dielectric barrier discharge operated in helium. These kind of discharges are often referred to as "plasma jets" due to their characteristic plasma plume that forms outside of the capillary orifice in open atmosphere.

These plumes have been claimed to be afterglows of the plasma that forms inside of the capillary and then carried out by the gas flow. However Horvatic et al. showed that the plasma instead starts in the vicinity of the powered front ring electrode and develops from there in two directions at the same time, downstream out of the capillary orifice to form the plasma jet and upstream of the capillary towards the grounded ring electrode.

The authors of the study refer to the inner plasmas as early plasma and coincident plasma due to the time frame given by the accompanying current measurements of the discharge. This work will carry on these studies and try to develop a comprehensive approach for a better understanding of the discharge dynamics. The most plausible model that explains the observed discharge behavior so far is based on streamer propagation in plasma discharges which will be further discussed in the following.

2.2 Streamer propagation in capillary DBDs

The development of a plasma in atmospheric DBDs has already been the focus of several studies. The formation of discrete "plasma packages" on a nanosecond scale that can be observed in capillary DBDs in particular, has lead to the coinage of the term "plasma bullets" for these phenomenons [37, 38]. The authors of Horvatic et al. 2015 [36] decided to refer to the observed phenomenon as "plasma jet" and while it is an open question to debate which term more fittingly describes the observed phenomenon, it is more important to clearly describe the underlying mechanism that leads to the observed formation of distinct plasma packages and their propagation.

The mechanism that best describes the measurements conducted throughout this work is that of an atmospheric streamer driven plasma discharge. The description for these kinds of discharges by Fridman [39] is fairly detailed and can be easily followed however it does not describe the formation of streamer like discharges in a DBD. However the described streamer mechanism can easily be adapted to the DBD case and will therefore be the basis for the following explanations.

A streamer discharge can occur when the product between discharge gas pressure and electrode gap referred to as $p \cdot d$ is too large for the formation of a normal Townsend avalanche discharge. A streamer discharge starts with an initial avalanche where electrons are rapidly accelerated towards a positively charged HV electrode or anode. Such an anode can form on the inside of a dielectric capillary by polarization

due to an external electric field as shown in figure 2.3. The formation of this kind of anode will accelerate free electrons on the inside of the capillary towards the dielectric surface and leave behind positive charged species inside the capillary volume as depicted in figure 2.4 (a). At the same time the acceleration of the electrons will lead to collisions with the neutral background gas atoms and excite them, which will lead to the emission of photons and potentially photoionization (see 2.2.1).

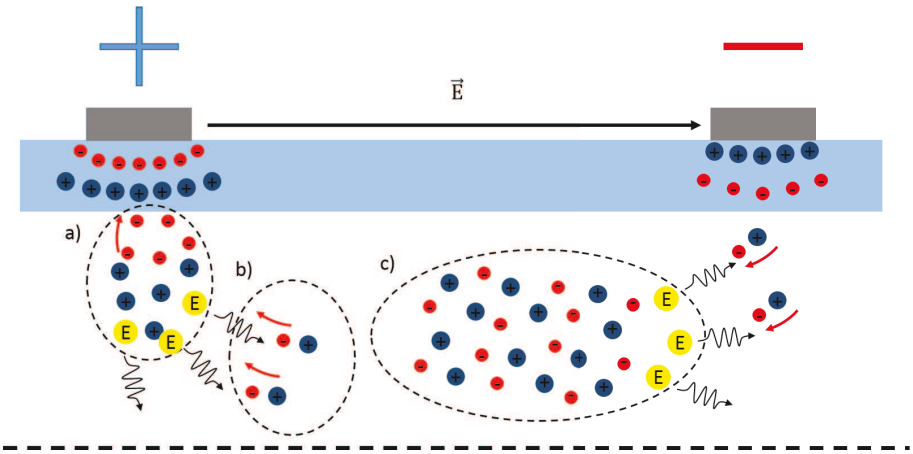

Figure 2.4: Schematic of streamer development and propagation in a capillary DBD. a) Initial acceleration of electrons (-) towards the capillary surface. The positive ions (+) are left behind in the capillary volume. Colission with the electrons create exited atoms (E) that emit photons. b) Creation of new electron-ion-pairs by photo-ionization. The new secondary electrons are accelerated towards the left behind ions and create a quasi neutral plasma channel. c) Propagation of the plasma channel along the capillary axis due to continuous photo-ionization.

Newly created secondary electrons will be accelerated towards the positive species that were left behind of the initial avalanche and create a quasi neutral plasma channel shown in figure 2.4 (b) and (c). This creation of new electron-ion-pairs and acceleration of the electrons propagates through the capillary like a wave until the formed quasi neutral plasma channel reaches the other electrode respectively the cathode. The velocity of this excitation wave is highly dependent on parameters such as the applied field or the gas pressure but in general it can be assumed to be in the range of $10 \cdot 10^4$ m/s up to $10 \cdot 10^5$ m/s and is therefore much faster than any movement that can be conducted by any heavy particles such as ions or neutral atoms and molecules.

Considering that the secondary electrons compensate the charge of the ions in the quasi neutral plasma channel, the movement of the gas background is only caused by the initial gas flow with which the capillary is flushed. The linear gas velocity of DBDs used throughout this work is in the order of only some 10 m/s even assuming best case scenario and therefore several orders of magnitudes slower than the propagation velocity of the excitation waves.

The quasi neutral plasma channel forms a conductive connection between anode and cathode as soon as the streamer reaches the vicinity of the opposite electrode. This leads to the ignition of a so called spark discharge which can lead to the formation of very high peak currents. However, in the case of a DBD the maximum

amount of current that can flow is restricted due to the dielectric layers that shield the electrodes. The amount of charge that can flow during the spark discharge, previously referred to as coincident plasma, is directly proportional to the capacitance of the discharge and therefore the amount of charges it can hold. This limitation of potential current that can flow through a DBD also means that a spark discharge in this kind of arrangement cannot be sustained indefinitely.

Optical measurements in fact reveal that no significant amount of emission can be measured from the discharge capillary after only some microseconds have passed. This means the plasma extinguishes long before the polarity of the AC voltage is switched to start a new discharge cycle and once more stresses the need for a repeated re-ignition to sustain a quasi continuous operation of plasma.

2.2.1 Photoionization in gas mixtures and its effect on plasma development

An important part of the streamer mechanism is the photoionization as was mentioned before, which creates secondary electrons and improves the overall degree of ionization to sustain a plasma [40, 41]. Photoionization itself is highly dependent on the gas with which the plasma is operated as it determines the photons and their energies available for said ionization. The most important gas to consider for this work is helium as it is used in the majority of the discharges throughout this work and also one of the most common gases used for DBDs.

Helium as the second element in the periodic tables has the first complete electron shell and is therefore considered a chemical inert noble-gas. He has two electrons which occupy the $1s^2\ {}^1S_0$ state when the atom is in its unexcited ground state. The first excited state of He is the $1s2s\ {}^3S_1$ state which has an energy of 19.81 eV which means that an He atom has to gain at least this amount of energy for one of its electrons to reach this higher energy state.

An atmospheric He DBD is normally operated in the range of 1 kV to 3 kV, which means it should be easy for an electron to gain the needed amount of energy. However the high amount of particles at atmospheric pressure drastically reduce the free mean path of the electrons to around 10 nm to 100 nm meaning that an electron can only travel a few nanometer before it will hit a particle in its way. The energy an electron can gain per collision is thus drastically reduced and only in the order of some 0.01 eV to 0.1 eV per collision, assuming an electric field in the order of 1 kV is applied over a 1 cm gap.

The reason electrons can gain any meaningful amount of energy is that they are colliding mainly with He atoms which will only take energy from a collision with an electron when the energy is high enough to excite an electron state in the He atom. All collisions with electrons which have a lower energy will be inelastic and mostly conserve the energy of the electrons. This means that an electron can slowly build up energy over several collisions until it has enough to excite the first state of He atom which is $1s2s\ {}^3S_1$.

The $1s2s\ {}^3S_1$ state is a so called triplet state due to its spin multiplicity which results from the parallel spin orientation of its two electrons. The $1s^2\ {}^1S_0$ ground state

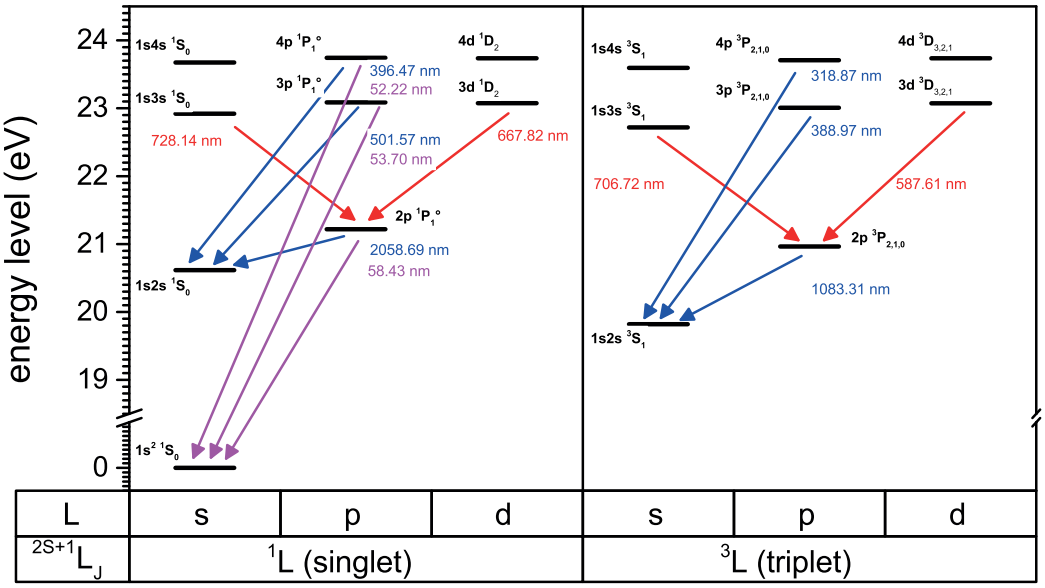

Figure 2.5: Energy states of the helium atom. The states are sorted in singlet and triplet states according to their 2S+1 spin multiplicity. The downward pointing colored arrows represent possible optical transitions from the indicated upper level to the associated lower level with respected color coded wavelengths.

of He has spin multiplicity of 1 due to the anti-parallel orientation of the electrons which otherwise could not occupy the same electronic state. An optical transition cannot change the orientation of an electron spin due to the conservation of the spin momentum. For this reason, the 1s2s $^3S_1$ cannot relax back to the ground state via emission of a photon.

The only way for a He atom in the 1s2s $^3S_1$ state to lose energy is via collisions which take much longer than optical transitions and increases the lifetime of the excited state. For this reason this state is referred to as He metastable state. The metastable states play an important role in the further excitation of He as they function as energy reservoirs from which higher energetic states can be further excited by relatively low energetic electrons and particles.

Two other important energy states are the 1s2s $^1S_0$ and 1s2p $^1P_1^\circ$ states which are the first two singlet energy states of helium. In particular the 1s2p $^1P_1^\circ$ state is of interest as this state can directly de-excite to the ground state via resonant optical transition as it also has an anit-parallel spin orientation. The energy of the emitted photons is 21.21 eV which corresponds to a wavelength of only 58.43 nm and belongs to the vacuum ultra-violet (VUV) spectrum of light.

Optical transitions generally have a shorter lifetime than atomic collisions which means that the singlet energy states 1s2p $^1P_1^\circ$ and the associated 1s2s $^1S_0$ should also have a much shorter lifetime than the metastable 1s2s $^3S_1$ triplet state. The lifetime of the emitted photons is reduced due to the high particle density at atmospheric pressure leading to an almost instantaneous re-absorption of the emitted photon. The most likely candidate to absorb the VUV photons is a helium atom in its

ground state, as it is the most abundant constituent of helium atmosphere, leading to a re-excitation of the 1s2p $^1P_1^\circ$ energy state. This process can be repeated several times, which overall extends the lifetime of the energetic 1s2p $^1P_1^\circ$ state making it "quasi-metastable".

As shown helium possesses metastable and quasi-metastable states in both spin multiplicity branches that have significant lifetimes even at high particle density at atmospheric pressure, which usually leads to a high probability of collision and depopulation of energetic states. As mentioned before, these states can be considered as energy reservoirs which simplify the further excitation of higher energetic states, as their high lifetimes increase the chance of them to interact with another energetic particle that further increases their energy. These energy reservoir states are important for the ionization processes in a helium plasma, not only as a stepping stone for the direct ionization of helium but also considering that a helium atmosphere under more realistic conditions does not exclusively consist of only helium atoms.

The helium used throughout this work has a purity of 99.999 % and is referred to as Helium 5.0. A purity of 99.999 % at the same time means that 0.001 % or in other word 10 out every one million volume particles ($10\,\mathrm{ppm_V}$) of the gas mixture is an unknown particle that is not helium. This means that $2.5 \cdot 10^{14}$ of the overall $2.5 \cdot 10^{19}$ particles a cubic-centimeter of volume filled with atmospheric pressure helium can be seen as an additional trace impurity. This number of particles is quite interesting as it is in the same order of magnitude as the number of helium metastables per volume element in a capillary DBD as determined by previous studies [42].

As the amount of trace additions is on a scale that seems to be relevant for a plasma, it is not unreasonable to assume that they can impact the formation and development of said plasma to a certain degree. Preliminary measurements have revealed that an increase of the trace amount of the nitrogen concentration in a helium discharge can influence the behavior of the plasma drastically. First explanations of the observed effects imply that nitrogen enhances the ionization processes in the plasma due to the much lower ionization energy.

The energies of the molecular bands of nitrogen are much lower than the atomic levels of helium as shown in figure 2.6. Furthermore the ionization energy of molecular nitrogen is only 15.6 eV which means that helium metastables, helium quasi-metastables as well as the resonant photons emitted by this state carry enough energy to ionize molecular nitrogen. The energy of the helium is even high enough to excite the upper state of the first negative emission system of the N_2^+-ion which could explain the high amount of emission from the 391.56 nm line that can be usually measured in helium discharges.

Further indication of the importance of nitrogen for the ionization of a atmospheric capillary DBD helium plasma can be found when the same discharge is operated with argon instead of helium. The energetic states of argon have less energy than helium and it also requires less energy to be ionized, therefore it could be assumed that the operation of argon is easier than the operation helium. Actual measurements however show that argon needs higher voltages to be operated than helium and can be considered to be the harder to ignite gas. This contradiction can

be explained by the fact that the argon metastable states have a lower energy than helium metastable and cannot ionize nitrogen in the same way as helium most likely can.

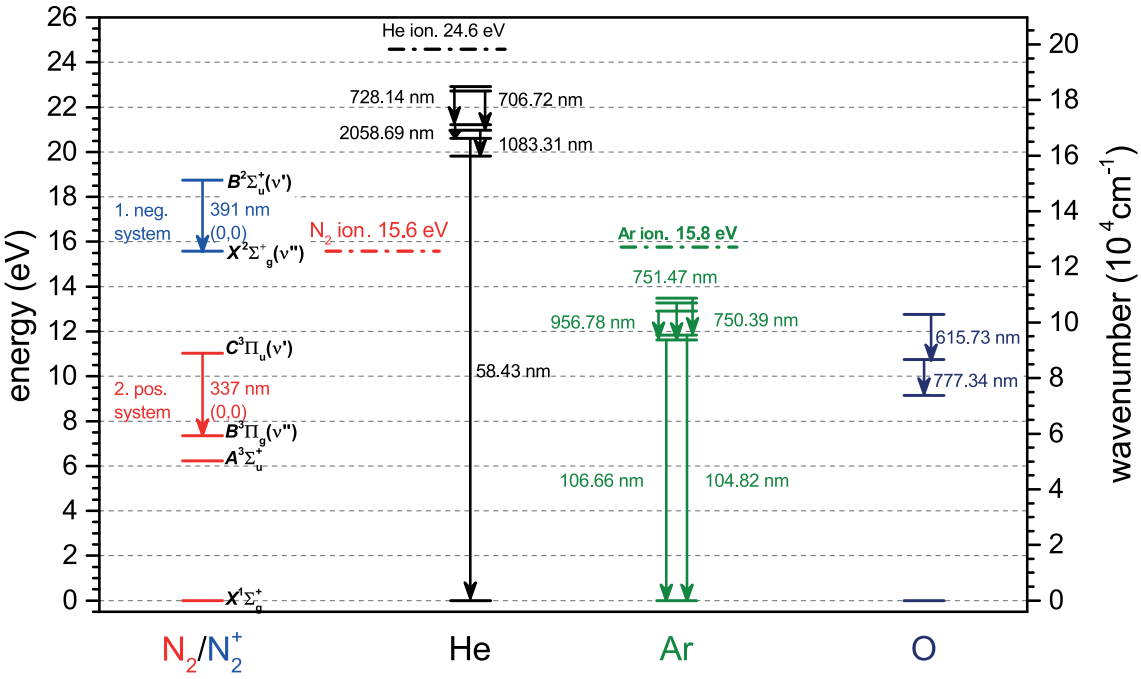

Figure 2.6: Energetic states of N_2 (red),N_2^+ (blue), He (black), Ar (green) and O (dark blue). The schematic shows some selected energy levels and associated optical transitions with their respective wavelengths.

It is possible to find and add a substitute to argon with a lower ionization energy than the argon metastables which have an energy of 11.55 eV, which in turn would verify the supposed importance of nitrogen for the ionization of helium in an indirect way. A potential substitute for nitrogen in argon could be e.g. propane (C_3H_8) with an ionization energy of 10.95 eV and will be extensively tested in this work to demonstrate the importance of additional trace gas components in a noble-gas mixture for the ionization efficiency of the plasma.

3 THE DBDI: A MODEL CASE FOR DIELECTRIC BARRIER DISCHARGES IN ANALYTICAL CHEMISTRY

This part will focus on the characterization of a specific dielectric barrier discharge (DBD) which is used in several analytical application, the dielectric barrier discharge for soft ionization (DBDI) [17].

As the name implies it can be used as a soft ionization source for the detection of molecules, but at the same time it is also a suitable source for the detection of atomized species. To use the DBDI efficiently for these contradicting tasks, it is crucial to understand the ionization and excitation mechanisms of the discharge in great detail. Nevertheless, the DBDI has already established itself as an excellent ionization source for mass spectrometer applications without a direct correlation of such knowledge and therefore is an ideal starting point for systematic studies.

Measurement of the plasma emission offers an efficient way to gather information about the DBDI and will therefore be the key part of the characterization efforts. After a brief introduction of the standard DBDI used primarily as ionization source for mass spectrometer applications, a detailed discussion of the experimental arrangements and the experimental results will follow.

3.1 The dielectric barrier discharge for soft-ionization

Most notable feature of the DBDI might be its characteristic design, which helps to create cheap and reproducible discharges and at the same time simplifies coupling of ionization source and instrument. Core part of the DBDI design is a disposable capillary pipette (5 µl minicaps by Hirschmann Laborgeräte) which has an inner and outer diameter of 440 µm and 900 µm, respectively. The electrodes which supply the HV to sustain the discharge are wrapped tightly around the glass capillary and soldered to fix them to the glass surface. The discharge gas, usually helium, can be directly fed through the capillary.

The plasma that is ignited in the discharge gas does not come into direct contact with either one of the electrodes (see figure 3.1). This configuration has several advantages purely for the plasma discharge itself as well as for analytical applications: The dielectric barrier limits the total amount of charges, in other words the total electrical current that can flow through the discharge. This ultimately limits the total power that can be coupled into the plasma, therefore reducing heating effects that otherwise could damage the discharge or measuring instruments. Another advantage that the strict separation of plasma and electrode surface offers is very

unique requirement needed for the detection of analytes.

An analytical procedure in general has to be very sensitive and be able to detect minuscule trace amounts of chemicals. To achieve this high degree of sensitivity, it is necessary to create very clean and stable measurement environments. The influence of electrode surfaces on the plasma itself will be discussed in more detail in the following chapter 4, however it can be assumed that a direct contact between plasma and electrode surface will undoubtedly lead to interactions that might disturb a stable plasma operation.

Some of these electrode plasma interaction such as, secondary electron emission, sputtering and ion emission only to name some of the most prominent ones, are vital processes for several industrial techniques such as plasma enhanced chemical vapor deposition (PECVD) [43]. For analytical applications these effects can be assumed to be in general undesired and only add to the uncertainty of a measurement.

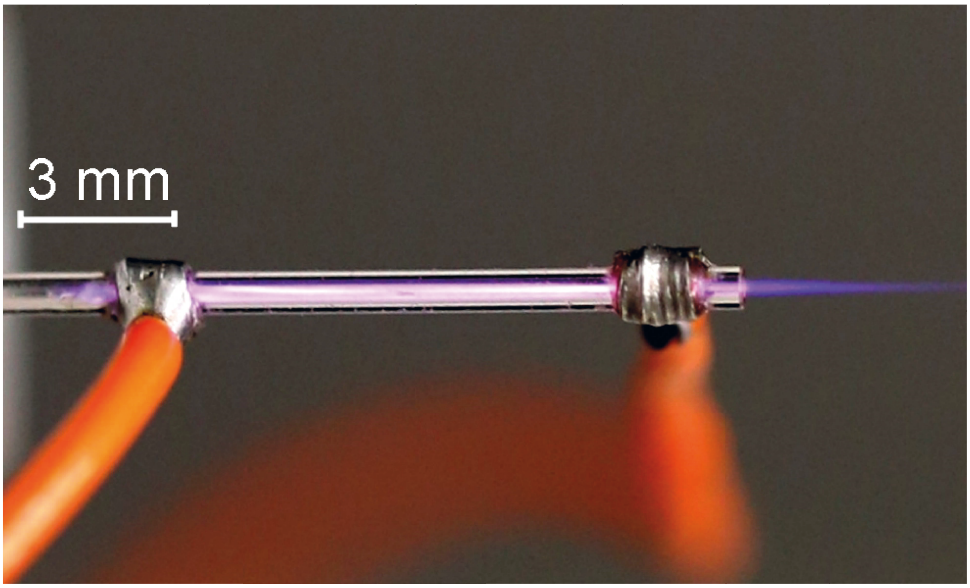

Figure 3.1: Photograph of a DBDI that will be discussed in the following parts of this work.

Despite the advantages a DBD offers to analytical applications, the operation of a DBD is at the same time quite demanding. Compared to a direct plasma discharge, which can be operated with either a DC or an AC voltage supply, a DBD has to be operated with an AC supply exclusively. The reason for this is, that the free flow of charges is hindered in the DBD case due to the dielectric barrier. Therefore, charges that are created during the first change of the electric potential would lead to a short period of excitation and ionization until these initial charges are neutralized and the discharge is extinguished.

To uphold a quasi continuous DBD plasma it is necessary to repeat the initial ignition process, which is realized by using AC voltage supplies that use a fixed frequency. The DBDI is usually operated with a square-wave HV generator operated at 20 kHz with a maximum voltage amplitude of 3.5 kV_{pp}. These square-wave generators are in-house built specifically for the operation of the DBDI and are replacements for previously used HV generators that utilized a quasi-sinusoidal waveform [36, 44, 45]. Implementation of the square-wave voltages instead of the quasi-sinusoidal volt-

ages creates a more stable and reproducible plasma and also inhibits the discharge to switch into a "filamentary" regime that is unfavorable for the soft ionization of analytes [46].

This filamentary regime occurs when the previously used quasi-sinusoidal voltage applied to the DBDI exceeds a critical point after which additional current spikes arise in the discharge. While the homogeneous regime at low voltages can be characterized by the occurrence of a single discharge ignition peak per discharge half-cycle the existence of additional discharge peaks indicate that the filamentary mode is caused by multiple plasma ignitions per voltage half cycle. These multiple ignitions can only occur with the quasi-sinusoidal voltage applied, due to the fact that it has higher frequency parts that superimpose the main frequency that is used to operate the plasma.

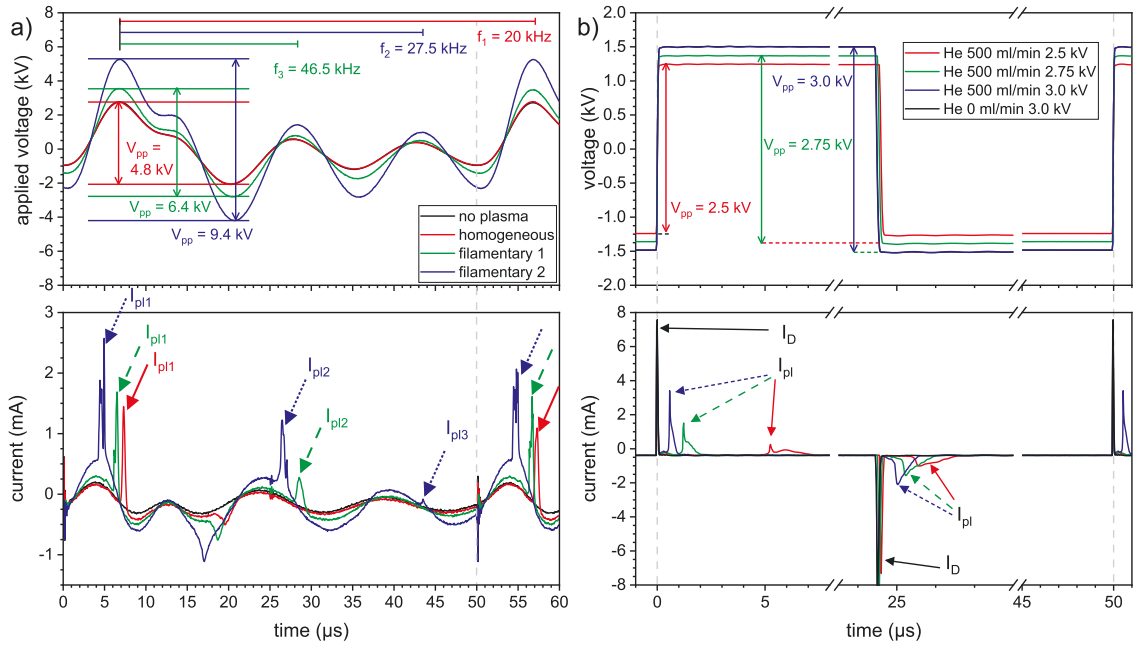

Figure 3.2: a) Voltage (upper part) and current (lower part) of the previously used quasi-sinusoidal HV generator that was used to operate the DBDI. The sinusoidal fundamental frequency $f_1 = 20\,\mathrm{kHz}$ is superimposed by additional frequencies that would equal frequencies of $f_2 = 27.5\,\mathrm{kHz}$ and $f_3 = 46.5\,\mathrm{kHz}$. Increase of the applied voltage leads to the ignition of additional discharge phenomena at these higher frequencies (colored arrows). b) Voltage (upper part) and current (lower part) of the currently used square-wave HV generator. The time axis is interrupted between $8 - 23\,\mu\mathrm{s}$ and $28 - 45\,\mu\mathrm{s}$ to better resolve the relevant features of the plasma discharge. The plasma currents (I_{pl}) and displacement currents (I_{D}) are marked with respective arrows.

This will lead to steady and modulated polarization of the DBDI as shown in 3.2 (a), and effectively a higher frequencies with which the plasma is operated. This very well could lead to the increase of the rotational temperatures of the N_2^+ molecular emission bands observed by Müller et al. indicating that the overall discharge temperature is rising in the filamentary regime due to an increase of the overall plasma power. In turn, the plasma might switch from a "soft" to "hard" regime which is detrimental for the soft ionization of analytes.

Problems caused by the plasma uncontrolled switching to a filamentary regime can be easily circumvented by usage of the square-wave HV generator, which only operates with a single "clean" frequency as can be seen in 3.2 (b). While this generator was primarily intended for the time and space resolved optical characterization of the DBDI, it also leads to a complete suppression of the filamentary regime and its most characteristic feature, namely the multiple plasma ignitions during a voltage half cycle. An appearance of multiple discharge ignitions is physically impossible using the square-wave HV generator, due to the fact that only a single temporally well defined polarization will occur, yielding a sharp displacement current I_D marked in figure 3.2 (b) by respective arrows.

The displacement current I_D will always occur when the generator switches its polarization either from negative HV to positive HV or vice versa independent of an actual ignition of a plasma. The plasma currents (I_{pl}) on the other hand can only be measured in the presence of an ignited plasma and are therefore characteristic to the operation of these plasmas. As presented in figure 3.2 (b), only a single plasma current will develop per voltage half-cycle after the initial fast polarization indicated by the displacement current independent of the amplitude of the applied voltage. This means no filamentary regime occurs during the operation with a square-wave generator.

The absence of a filamentary regime however, does not mean that the plasmas generated by the square-wave generator will be exclusively "soft". Instead, mass spectrometer measurements using the DBDI with the square-wave generator have shown that increasing the voltage beyond a certain ideal operation voltage will also deteriorate the ionization efficiency. In contrast to the the sudden switch to a filamentary regime, this slow deterioration of the ionization efficiency can not be linked to a critical voltage anymore, making the definition of suited operation parameters for the DBDI in a way more complicated. A detailed understanding of the DBDI and its mechanisms is necessary to efficiently use it in analytical applications.

One approach presented in the following is the use of temporally-, spatially- and spectrally-resolved optical emission spectroscopy (TSSR-OES) as a non invasive plasma diagnostic. It will be shown that these measurements give reproducible and predictable results, that help understand excitation and ionization mechanisms in the DBDI and can also be linked to time resolved plasma current measurements that can be done in parallel. These current measurements require virtually no additional experimental effort and can be executed during mass spectrometric measurements without disturbing them. This creates an ideal monitor for the mass spectrometer applications and helps optimizing them in a more controlled way.

3.2 Temporally-, spatially-, and spectrally-resolved optical emission spectroscopy

The temporal, spatial- and spectral-resolved optical emission spectroscopy (TSSR-OES) is the key diagnostic for this work. It allows for detailed investigation of discharge mechanisms with nanosecond and micrometer resolution, without disturbing the plasma itself. While the instruments used for the detection of the discharge light underwent some drastic changes, the core part of the experimental arrangement, a 1 m Czerny-Turner grating spectrometer from McPhearson instruments, remained the same throughout most parts of this work.

Usually, photo-multiplier tubes (PMT) are used with theses kinds of spectrometer arrangements, due to the fact that they can sufficiently amplify the weak emission that is still able to pass the long optical paths of the spectrometer, while still retaining a high temporal resolution. A satisfactory spectral and spatial resolution can additionally be achieved with the help of the spectrometer entrance slits.

To create a resolved map of the emission, the discharge has to be moved perpendicular in front of the entrance slit to create data points for each point of the discharge [47]. This restricts the spatial resolution as well as it reduces reproducibility. For these reasons the PMTs were eventually replaced by an ICCD camera from Andor instruments. This special kind of CCD camera has an integrated light intensifier with additional gating options, giving it better low light capabilities and time resolution than the available PMTs.

For simplicity and clarity, the following description of the experimental arrangements of the TSSR-OES will assume that only the ICCD was used as a detector and all presented emission data were taken by this upgraded arrangement.

Experimental arrangement

Core part of the TSSR-OES is the Czerny-Turner grating spectrometer from McPhearson instruments. A Czerny-Turner grating spectrometer usually consists of two mirrors M1 and M2 that are used to image the light that enters through the entrance slit S1 onto a rotatable grating G through the outlet slit S2 onto a detector as shown in figure 3.3.

The concave mirrors and the grating are positioned in a way that they form an optical plane at the position of S1 and S2, meaning that an object positioned at S1 will be imaged with a ratio of 1:1 at S2. Using a detector like the Andor iStar DH720-18F-03 ICCD camera essentially makes the use of slits redundant, due to the fact that the camera produces 2D resolved pictures as presented in figure 3.4. Therefore, the slits of the spectrometer are only necessary when a PMT is used and are otherwise usually removed when the ICCD camera is installed.

Without slits, the plasma can be positioned directly in front of the spectrometer. This reduces the loses that would be caused by the additional lens L that would be otherwise necessary to accurately image the discharge. The rotational axis of the discharge capillary has to be oriented parallel to the ridges of the transmission grating to achieve spectral and quasi spatial resolution at the same time. As one can see in

figure 3.4 (a) it is possible to produce complete spatially resolved 2D images, if the angle of the grating is set to 0^{th} order. The spatial resolution is effectively reduced to 1D if the dispersion angle of the grating changes and a specific wavelength is selected, due to the minimal dispersion that is given by the instrumental profile.

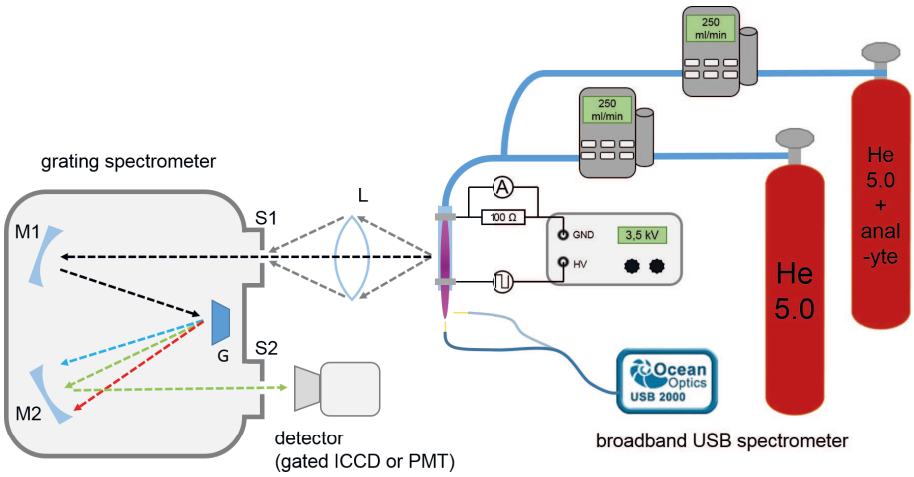

Figure 3.3: Schematic of the experimental arrangement used to characterize the DBDI. The arrangement can be divided in an optical part, shown mainly in the left, that is used to investigate the emission of the plasma discharge and a generator part that supplies the discharge with the necessary voltage and gas. The commercial Ocean Optics USB broadband spectrometer only requires an optical fiber aligned to the discharge to obtain time integrated optical spectra. It can be used as an additional monitor when the DBDI is operated in combination with an analytical detector, e.g. a MS or gaschromatograph (GC).

Assuming a perfect monochromatic, point-shaped light source, the instrumental profile would still cause the dispersed light to be spatially distributed across the detector surface. For the case of a spatially resolved imaged discharge, as described above, this would mean that the spatial information of the imaged discharge will be overlapped with additional emission contributions and will give a slightly blurred image that might be hard to interpret.

For this reason, and also to reduce data size and measurement time, the ICCD camera was usually operated in single track binning mode. This mode enables the camera to reduce and bin the vertical data rows of the CCD chip to a single data row which only contains the rotational axis and intensity information of the discharge. These 1D binned data rows can be easily displayed as simple line plots as shown in figure 3.4 (c) or can be used to produce 2D heatmaps as is done from figure 3.6 on page 36 onward.

Time resolution is achieved by the triggered short gate times of the ICCD, with 5 ns being the shortest gate times available for the iStar DH720. The gate time is the time interval in which light is effectively intensified by the cameras image intensifier tube. Even if the camera chip is illuminated respectively read out for longer time intervals, the camera is only effectively collecting light during the gate on time. It is possible to take several individual images with short gate times in succession and advance the trigger point of each measurement, to image a time series that shows the time dependent development of a plasma discharge with high time resolution.

The time resolution is therefore given by the shortest gate time possible as well as the step width by which the gate can be shifted time wise. The smallest step size given by the software of the camera is 25 ps meaning that several images with 5 ns gates can be superimposed to generate super sampled data points with 25 ps time resolution. This option was never enabled during this work and it can be assumed that the highest time resolution achieved for all presented measurements is 5 ns, or higher if longer time periods were investigated.

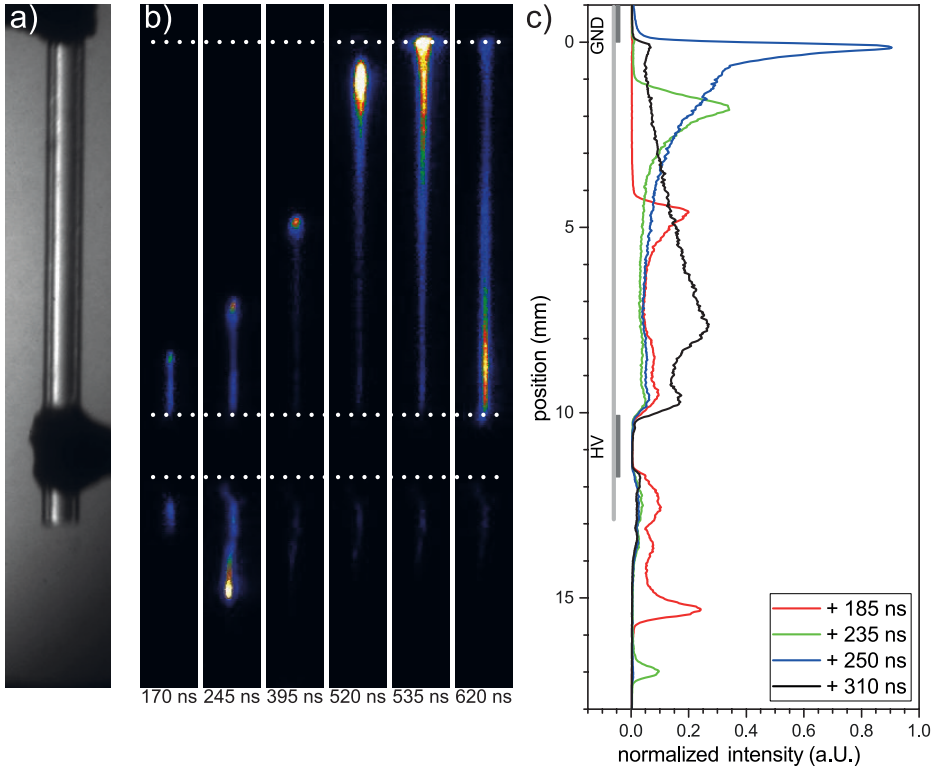

Figure 3.4: Different imaging modes of the ICCD camera. a) Monochromatic full 2D image of a DBDI used for alignment purposes. b) Cropped monochromatic 2D image series of the emission development of a DBDI. Each shown frame has a time resolution of 5 ns. Only some representative frames of the series are shown. c) Single track binned 1D data of a comparable series as shown in b).

A maximum time resolution of 10 ns was deemed to be more than sufficient for depicting the development of a typical discharge half cycle which in general takes $2 - 3\,\mu s$. A full screening of this time frame with 10 ns resolution already means that 200 to 300 individual images have to be taken. Using the highest theoretical resolution of 25 ps would increase this number to 80 000 to 120 000, which cannot be handled by the camera software anymore. Depending on the intensity of the observed emission line and therefore possible long integration times, a full time series with only 200 to 300 individual images can take up to several minutes, requiring a very stable measurement environment and plasma in particular.

For easier handling, the capillary of the DBDI is embedded in a 3D printed structure, which is shown in figure 3.5 and is used as a support structure for the in general delicate glass or quartz capillaries used for the DBDI. The capillaries are glued into the 3D structure with a two component adhesive two prevent any air leakage to the gas feed. The 3D structure itself is printed with a threading that fits to commercial swaglock connectors that are used on the tubing of the gas supply, enabling an easy connection of the DBDI.

The HV generator, that supplies the necessary voltage to ignite a plasma, is connected to the electrodes that are usually directly "soldered" to the glass surface of the capillary (see figure 3.1 and 3.5 (b)). The soldering is primarily used to enhance the mechanical bonding of the cables that are wrapped around the capillary and to ensure a good contact between metal and glass surface. First attempts to sputter electrodes directly unto the capillary surface showed promising results, indicating that the electrical contact is increasing, however it was not possible yet to produce and connect the sputtered electrodes reliably enough to justify the additional effort compared to the relatively easy soldering process.

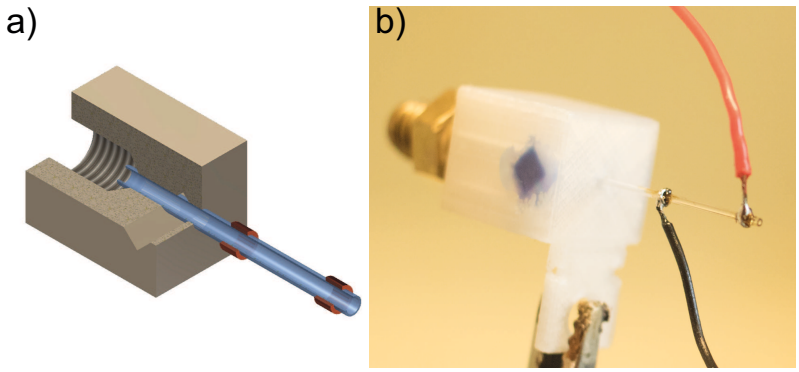

Figure 3.5: CAD model a) and photograph b) of a DBDI embedded in a 3D printed support structure. The sectional view in the CAD model shows how the DBDI capillary is inserted in the 3D structure. In addition one can identify the square holes for the two component adhesive and the threading used for the commercial Swagelok connectors.

The cables connecting capillary and generator have to be kept as short as possible, to minimize disturbances to the plasma. As mentioned in chapter 2.1 a dielectric barrier discharge can be simply seen as a capacitor. The capacitance of this capacitor can be easily disturbed by external influences, due to the fact that it is very small and can be noticeably changed by just touching the capillary. While these changes of the capacitance can be easily detected by e.g. changes in the time resolved plasma current, they should be avoided at all cost when long term measurements with the TSSR-OES are implemented.

The HV generator has two connections, one HV output which alternates with a given frequency between a positive and negative voltage and a fixed ground connection. When the generator is set to output 3.0 kV, the HV output alternates between +1.5 kV and −1.5 kV while the ground remains fixed at 0 kV. This creates a potential difference between both outputs that is passed on to the electrodes when they are connected.

A 100 Ω resistor can be put between the grounded electrode and the ground connector of the generator. An oscilloscope can be used to measure the time resolved voltage drop over the resistor which subsequently gives an estimate for the amount of current/charge that flows through the discharge. It has to be kept in mind that this is purely an estimate for the total amount of charges, due to the fact that no distinction between ion and electron current can be made and also leak currents cannot be excluded and are highly probable in this arrangement. However, due to its simplicity and non invasive nature the current measurement is an ideal tool to compare different discharge parameters and will give valuable information, as will be shown later on.

The gas to the DBDI is supplied by at least one mass-flow controller (MFC) from Analyt-MTC, to ensure a stable and controlled supply of the operating gas. A stable gas supply is exceptionally important for the DBDI, considering that it is operated under ambient conditions which makes it susceptible to pressure variations. Using the MFC also simplifies the use of different gases, due to the fact that a MFC can always supply the same volume of gas independent of its atomic weight.

While the DBDI is in general operated with helium 5.0 which has a purity of 99.999 %, the use of different gases and mixtures, such as argon, argon mixed with propane, nitrogen and air is of particular interest for this work. For this reason, the output of several MFCs can be combined to create a constant mixed gas flow [47]. This allows for very accurate and minor supply of certain gas additives to the gas flow in the range of only some ppm_V or even ppb_V if necessary. It will be shown that even minuscule changes of the gas composition in this range can have a noticeable influence on the discharge ion formation and ignition behavior, which will be discussed in detail in the following chapter of this work.

3.3 Investigation of the discharge development

This chapter of the work will give a detailed, general description of the discharge development to retrace some of the notations that developed throughout the different scientific studies dedicated to the characterization of the DBDI prior to this work. Figure 3.6 shows the plasma development of a representative DBDI that was operated with what could be referred to as standard conditions. The gas flow was set to 500 ml/min He 5.0 and the applied voltage was set to 3.0 kV at a frequency of 20 kHz.

The discharge development can be broken down into three stages as shown in the graph, the 1^{st} stage or “early stage”, the 2^{nd} stage or “coincident stage” and the 3^{rd} stage or “afterglow stage”. The 2^{nd} and 3^{rd} stages were treated as one in previous works that still used PMTs instead of the ICCD camera, due to the lack of temporal resolution and the weak nature of the afterglow stage that made a clear separation impossible.

The distinction of the early and coincident plasma stage already took place during the first temporally, spatially- and spectrally-resolved optical studies on the DBDI [36, 44]. The 1^{st} stage addresses the development of the first emission phenomena directly after the positive HV polarization ignites the plasma. The initial positive

polarization can be clearly identified by the positive displacement current I_D[1] in the upper part of figure 3.6 that is depicting the time resolved discharge current. For this reason, I_D is usually used as the origin of the temporal coordinate and also as a trigger signal.

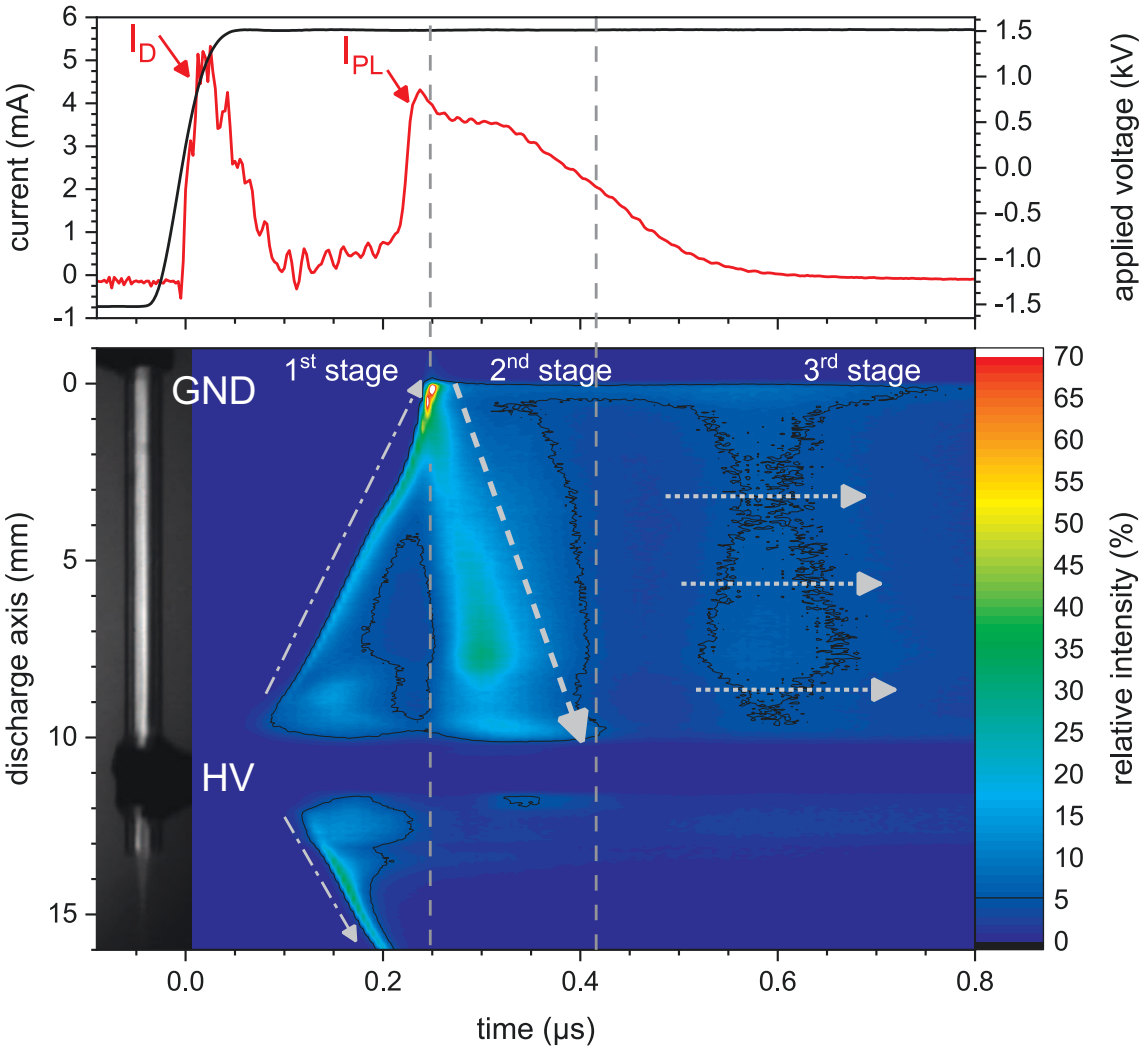

Figure 3.6: Development of the temporally, spatially- and spectrally-resolved optical emission of the DBDI. The upper part shows the applied voltage (black) and the measured discharge current (red). The arrows highlight the displacement current I_D and the plasma current I_{pl}. The lower part shows the spectrally integrated emission. The image of the DBDI serves as a guide to comprehend the position scales, similarly the arrows help to follow the propagation of the emission in the individual stages. The color scale of the graph is normalized to the maximum intensity but was capped at 70 % to help visualize the weak emission in the 3rd stage. The plasma was operated with an applied voltage of 3.0 kV and a He 5.0 flow of 500 ml/min.

The lower part of figure 3.6 shows the time and space resolved emission and reveals that emission emerges simultaneously to the appearance of I_D. The emission is starting at both edges of the positively powered HV electrode and spreads in both directions, upstream of the gas flow towards the grounded electrode and downstream

[1]The negative polarization can be identified by a negative amplitude I_D respectively

into the ambient atmosphere. In previous works these phenomena were referred to as "early plasma" for the upstream and "jet" or "plasma jet" for the downstream directed emission. From now on they will be referred to as "streamer" or "streamer like discharge" in an attempt to create a more coherent description as was already attempted in chapter 2.2.

As discussed streamers are photoionization driven excitation waves, that travel at fairly high speeds up to 100 km/s. The initial, preferably fast and sudden, polarization rapidly accelerates first seed electrons that in turn excite He atoms by collisions. The excited He atoms themselves give of emission to relax to lower energy levels, which creates the first strong emission signals that can be observed during the ignition process of the DBDI.

A very interesting transition for the development of the streamer is the He $2p\,^1P_1^\circ \longrightarrow 1s^2\,^1S_0$ at 58.4 nm which has an energy equivalent of 21.2 eV and is shown in figure 2.6 on page 11. This very high energetic and deep UV light is able to ionize every atom or molecule apart from neon and helium itself, which makes it a very potent ion producer. At the same time the lifetime of the upper $2p\,^1P_1^\circ$ is prolonged by a trapping effect that is caused by constant re-absorption of emitted photons by ground state He atoms.

This prolonged lifetime increases the chance for an emitted UV photon to be absorbed by an atom or a molecule that is subsequently ionized in the process. While many studies dealing with streamers already differentiate gases in classes that are suited for photoionization (e.g. He) and classes that are not (e.g. O_2), these studies still suspect that the photoionization happens in the main component of the operation gas. Assuming He is used as discharge gas, this would mean that by for example two photon processes the UV emission at 58.4 nm would keep the upper $2p\,^1P_1^\circ$ state populated until a second suited photon with an energy equivalent of at least 3.4 eV would be absorbed by an excited He atom in this state to subsequently form a He^+ ion which has an ionization energy of 24.8 eV.

While this process is by no way impossible and the trapping of the $2p\,^1P_1^\circ$ does also increase the chance for it to happen, it's still more probable for an emitted UV photon to directly ionize a gas component with a lower ionization energy than He. The influence of existing or purposefully added gas additions, on the ignition behavior of a streamer like discharge will be discussed for different operation gases later on in chapter 3.4.2. For now it is enough to identify photoionization as the driving ionization mechanism in a streamer like discharge.

The newly generated ions are forming a positive streamer head that is attracting and accelerating additional electrons towards its center, which leads to further excitation. This self-intensifying process leads to a wave like accelerated propagation away from the location of the initial polarization, that can be interpreted as the movement of a "plasma bullet" as described in chapter 2.2. This propagation takes place until the initial excitation is simply used up and the streamer extinguishes, which is the case for the outside jet, or until the streamer reaches the grounded electrode and starts the 2^{nd} stage of the discharge.

The streamer head leaves behind a quasi neutral tunnel filled with positive and negative particles while it propagates through the capillary. This tunnel can be interpreted as a volume that contains free charge carriers, which means it can be seen as a conductor. The conductor starts at the HV electrode and is short-circuited as soon as the streamer head connects to the grounded electrode, which leads to a sudden re-acceleration of charged species.

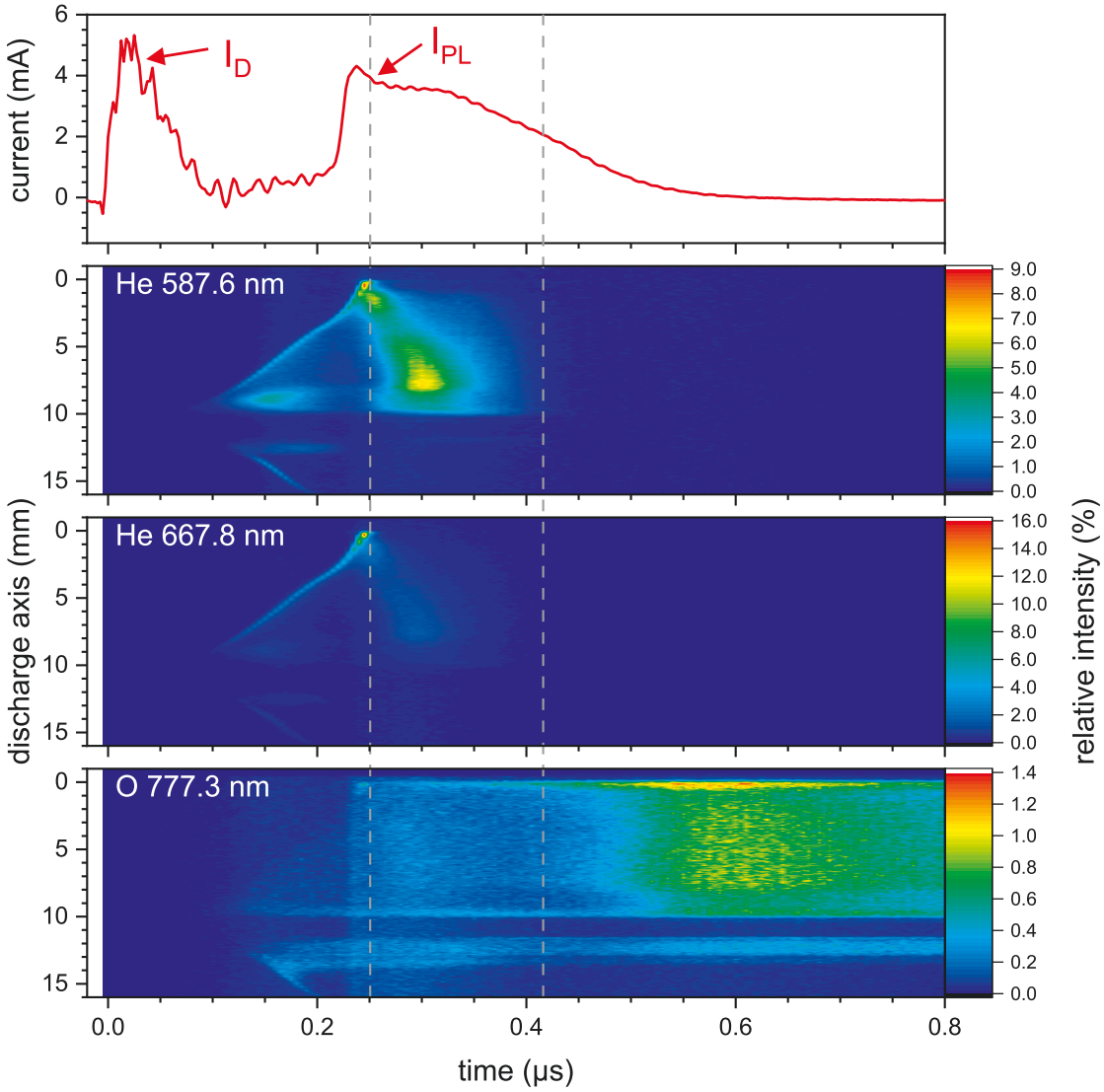

Figure 3.7: Development of the He 587.6 nm (top), He 667.8 nm (middle) and O 777.3 nm (bottom) line. The presentation of the data is the same as in figure 3.6. The intensity scale of each spectrally resolved graph was normalized to the maximum number of counts given by the spectrally integrated graph in figure 4.5 to determine the relative contribution of each line. The current signal and the dotted lines help to recognize the individual plasma stages. The plasma was operated with an applied voltage of 3.0 kV and a He 5.0 flow of 500 ml/min.

The re-acceleration can be identified in two ways: One indication is the sudden rise in the time resolved current which is referred to the plasma current I_{pl} and indicated by an arrow in the upper part of figure 3.6 and 3.7. The other indicator is

the occurrence of new emission that is seemingly spreading the opposite way of the original streamer direction. This new emission can be very bright and appears to be less sharp and focused than the bullet like appearance of the initial streamer.

The re-ignition like process was previously described as coincident plasma, due to the fact that the emission occurred at the same time as the plasma current. It was interpreted to be the "harder" part of the plasma that causes dissociation of molecules and also produces atomic emission of dissociated fragments such as the prominent oxygen radical emission at 777.3 nm. These findings were already published in the context of this work [47], but the mechanism responsible for the dissociation of molecules and the subsequent excitation of the fragments could not exactly be identified.

While the findings of the previous study are in general right and the dissociation of molecules and excitation of atomic fragments indeed happens after the discharge proceeds to its 2nd stage, the higher time resolution of the ICCD camera reveals that further differentiation of the coincident stage is advisable. As one can see from figure 3.7, the emission of the oxygen 777.3 nm line that originates from the $3p\,^5P_{3,2,1} \longrightarrow 3s\,^3S^\circ_2$ transition does noticeable increase after the ignition of the 2nd plasma stage, but at the same time one can also see, that the maximum of this emission arises at a considerably later point in time. In addition, it is clearly visible, that the emission of the 777.3 nm line first increases and then slightly decreases in the 2nd plasma stage before it rises again in the 3rd stage and reaches it maximum and decays very slowly with a half-life period of 700 ns.

This afterglow like behavior, that is described in different studies in one way or another [48, 49], strongly hints to a mechanism primarily involving the He metastable states such as $2s\,^1S_0$ or $2s\,^3S_1$. The energetic He metastables deexcite via collisions and create secondary excited species which can subsequently give of their energy via emission after the initial plasma is already extinguished.

Figure 3.7 also shows the TSSR-OES results for the He $3d\,^1D_2 \longrightarrow 2p\,^1P^\circ_1$ transition at 667.8 nm, He $3d\,^3D_{3,2,1} \longrightarrow 2p\,^3P_{2,1,0}$ transition at 587.6 nm. The reason for considering two He lines at the same time is, that the 667.8 nm line belongs to the so called singlet states of the helium atom and the 587.6 nm line to the so called triplet states. The naming of these states can be traced back to the introduction of the the term symbol notation $^{2S+1}L_J$ that used in quantum-mechanics to identify atomic energy levels. Here, the term $2S+1$ refers to the orientation of initial spin of the two electrons in the He atom, with parallel spin orientation giving $S = 1 \Rightarrow 2S + 1 = 3$ and anti-parallel orientation giving $S = 0 \Rightarrow 2S + 1 = 1$.

Therefore, singlet refers to He atoms with electrons that have an anti-parallel spin orientation while triplet refers to the He atoms with parallel oriented electrons. The difference between singlet and triplet states in the He atom is of particular interest as soon as excitation and relaxations processes from or to the $1s^2\,^1S_0$ ground state of the He atom are considered. This ground state has to be a singlet state, otherwise the electrons have the same spin orientation and would occupy the same quantum-mechanical state which is not allowed.

At the same time this also means that optical transitions to the ground state can only occur from another singlet state of the He e.g. the $2p\,^1P^\circ_1$ state with $J = 1$.

The transition from the equivalent triplet state $2p\,^3P_{2,1,0}$ on the other hand would be forbidden, due to the fact that the photon having an integer spin could not switch the electron spin during the optical transition.

Excitation of He from the ground state into the triplet state and the vice versa deexcition have to take place by other processes than optical transactions. These processes are primarily collisions of He with accelerated electrons or other suited particles. This however means, that the excitation and subsequently the emission of triplet states is enhanced in the presence of a high number of excited He in particular He^m states such as $2s\,^3S_1$ which have long lifetime and can efficiently transfer their energy in atomic collisions without "losing" it in optical transitions.

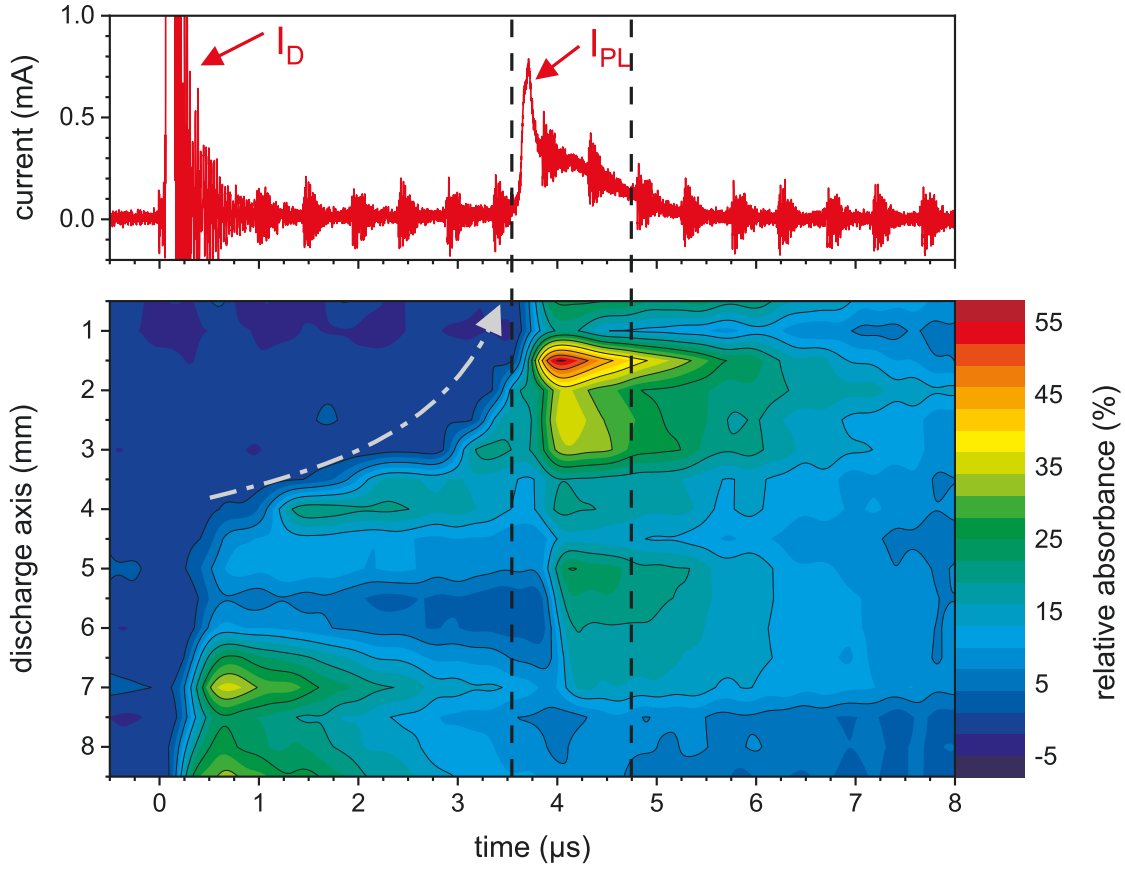

Figure 3.8: Time and space resolved absorption measurement of the He 1083.3 nm line. The discharge had to be operated at a very low voltage to delay the ignition of the 2nd plasma stage and still resolve the development of the discharge. The absorption was only measured in between the electrodes due to the fact that no significant He^m absorption could be measured beyond the electrodes anymore.

Directly comparing the emission of the He 667.8 nm and 587.6 nm in figure 3.7 one can directly see that the 587.6 nm triplet line has a far stronger emission in the region which can be associated with the re-ignition during the 2nd plasma stage than the 667.8 nm singlet line. This implies that the spark like re-ignition during the 2nd stage leads to an increased production of He^m.

This assumption can be further asserted by absorption measurements of the He 1083.3 nm line that transitions from the $2p\,^3P_{2,1,0}$ down to the metastable $2s\,^3S_1$

state. These measurements were done at the laboratories of P. B. Farnsworth of the Department of Chemistry and Biochemistry at the Brigham Young University in Provo USA. The time and space resolved absorption measurement works similar to the first TSSR-OES arrangements presented in chapter 3.2. The DBDI is positioned in the optical path of a continuous wave diode laser that is tuned to the resonance wavelength of the 1083.3 nm transition and can be moved in such a way that the discharge axis is scanned by the laser beam. The emission of the laser is measured with a suited PMT and oscilloscope to obtain time resolution.

The absorption measurements cannot be compared directly to the emission measurements that are presented in figure 3.6 and 3.7, due to the fact that they were not taken with the same plasma discharge respectively the same laboratories and the discharge parameters for the absorption measurements were chosen in such a way, that the comparatively long lifetimes of the He^m are pronounced throughout the discharge development. Nevertheless, a clear maximum of the He^m absorption can be seen after the plasma current arises after around 4 µs which indicates the transition to the 2^{nd} plasma stage. Therefore it can be assumed that an increased He^m production indeed takes place after the discharge transitioned to the 2^{nd} stage.

Another strong argument for the involvement of noble gas metastables in the dissociation and excitation of molecules can be found if other gases besides He are considered. For this reason, the DBDI was operated in He and Ar and the emission of the discharge was measured with an optical fiber that is connected to a commercial compact USB 2000 spectrometer from Ocean Optics.

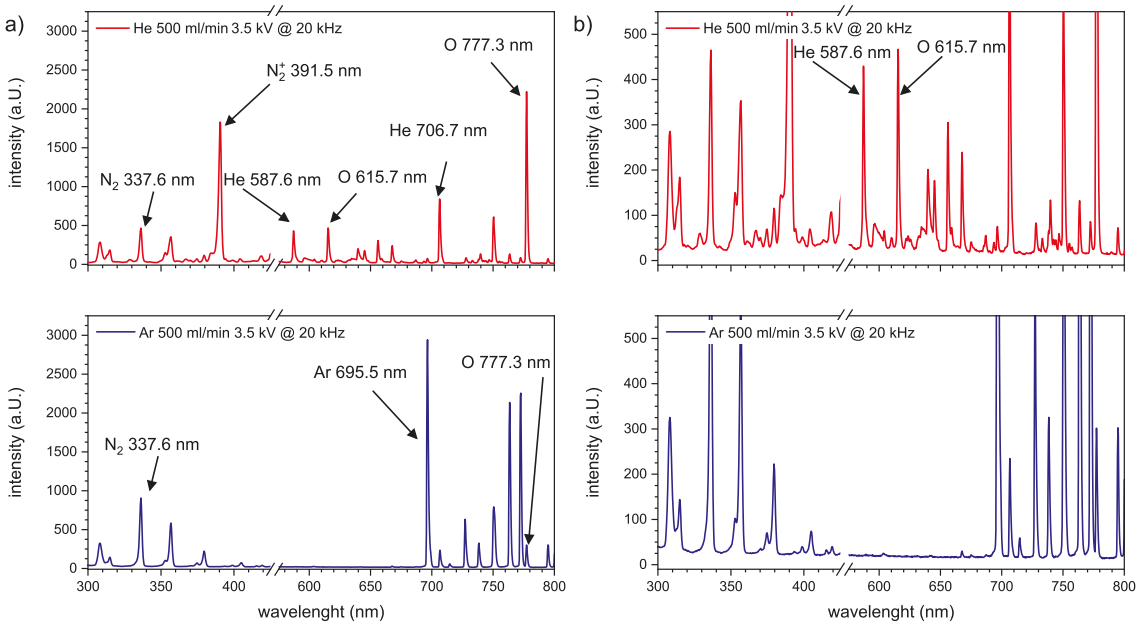

Figure 3.9: a) Time integrated emission spectra of a DBDI operated with 3.5 kV at 20 kHz in 500 ml/min He (red, top) and 500 ml/min Ar (blue, bottom). The spectral range from around 400 to 600 nm was cut out to concentrate on the relevant ranges. b) Spectra taken with a higher integration time to enhance the darker lines. The intensity scaling was normalized to the one used in a) to obtain comparable values again [50].

As presented in figure 3.3, this optical fiber can be either aligned parallel to the discharge axis to gather all the emission of the plasma from the front, or perpendicular if only the emission of one point in the discharge is of particular interest. Compared to the TSSR-OES system, the advantage of the commercial USB spectrometer is the possibility to observe several emission lines at the same time over a wide spectral range of several hundreds of nanometer.

The comparison of such broadband spectra is shown in figure 3.9. As mentioned before, the discharge was operated in He and Ar. The other discharge parameters, e.g. the applied voltage or the gas flow, were kept the same for both plasmas, to make sure that the observed differences are caused by the choice of the plasma gas. However, the electrode distance of the DBDI had to be slightly reduced for a plasma to be able to ignite in pure Ar, even with the maximum generator output of 3.5 kV.

The alternative way of operating the discharge in He and Ar at the same conditions would be to use a suited additive for the Ar discharge that would help in the ionization process during the streamer development. One of such additives can be propane (C_3H_8) which leads to lower operation voltages for a DBDI operated in Ar, as will be shown in later chapters of this work (see chapter 3.4.2).

Addition of propane was not a valid option of reducing the operation of the Ar discharge at this point in time, due to the fact that the addition of propane could very well change the collision energetics in the discharge, which are important for the following considerations. Examples for relevant collision processes that could lead to the dissociation of molecular oxygen and subsequently to the emission of atomic oxygen are given in equation 3.1 and 3.2:

$$\underbrace{He^m\left(2s^3S_1\right)}_{19.8\,eV} + \underbrace{O_2\left(X^3\Sigma_g^-\right)}_{0\,eV} \rightarrow \underbrace{He\left(1s^2\,^1S_0\right)}_{0\,eV} + \underbrace{O\left(3p\,^5P_{[3-1]}\right)}_{10.7\,eV} + \underbrace{O\left(3s\,^5S_2^\circ\right)}_{9.1\,eV} \quad (3.1)$$

$$\underbrace{Ar^m\left(4s^2\,[3/2]_2^\circ\right)}_{11.5\,eV} + \underbrace{O_2\left(X^3\Sigma_g^-\right)}_{0\,eV} \rightarrow \underbrace{Ar\left(3s^2 3p^6\,^1S_0\right)}_{0\,eV} + \underbrace{O\left(3p\,^5P_{[3-1]}\right)}_{10.7\,eV} + \underbrace{O\left(\ldots\right)}_{0.8\,eV} \quad (3.2)$$

Both metastable atoms He^m and Ar^m could collide with an oxygen molecule in the $X\,^3\Sigma_g^-$ ground state, dissociate it and produce oxygen fragments that still have considerable amount of energy. However only He^m carries enough energy to produce two energetically nearly equivalent oxygen radicals, while the energy of the Ar^m is used up nearly completely to produce a single oxygen radical in the $3p\,^5P_{3,2,1}$ state, which is the upper level of the 777.3 nm transition shown in figure 2.6.

The consequence of this energy difference of both metastable species is a reduced emission of the 777.3 nm line in the case of Ar which is around ten times less compared to He in the presented case in figure 3.9. Even more striking however is the fact that other emission lines of the oxygen radical are not excited at all in the Ar plasma. One of these lines is at 615.7 nm and can only be observed in He. The reason for this is, that the upper level $4d\,^5D^\circ$ of this transition has an energy of 12.8 eV depicted in figure 2.6 on page 11, which is more than 1 eV higher than the Ar^m could potentially carry into the collision. This means that only emission lines below the energy threshold given by the involved noble gas metastable will be excited efficiently in a plasma that is operated in a comparable regime to the DBDI.

The completion of the afterglow stage, which is dominated by collisions driven by excited metastables, concludes the discharge development during the positive half-period of the applied voltage. However, the complete discharge development also encompasses an ignition process during the negative half-period of the applied voltage which is shown in figure 3.10.

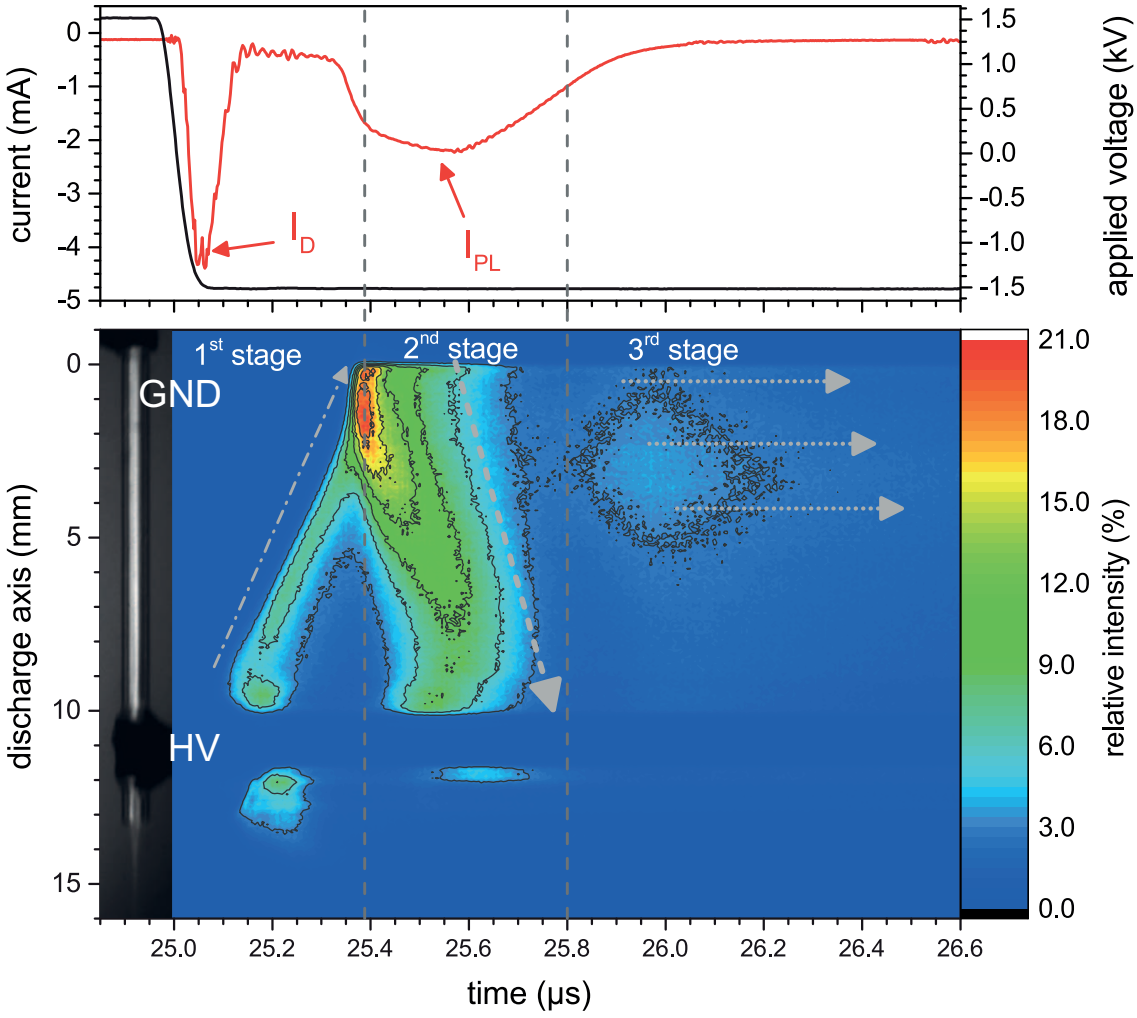

Figure 3.10: Development of the temporally, spatially- and spectrally-resolved optical emission of the DBDI during the negative voltage half-cycle starting at 25 us. The presentation is the same as in figure 3.6, the only difference is that the intensity scaling that was normalized to the maximum number of counts obtained during the positive voltage half-cycle. The plasma was operated with an applied voltage of 3.0 kV and a He 5.0 flow of 500 ml/min.

The ignition during the negative half-cycle strongly resembles the positive version on first glance, with the emission propagating essentially in the same direction as indicated by the grey arrows. The development of the discharge can again be divided into three stages that can be characterized by the same features as in the positive half-cycle, however the negative half-cycle can still be clearly differentiated from the positive half-cycle. The most obvious difference is the time resolved currents and the relative intensities that are shown in figure 3.6 and 3.10. Displacement current I_D and plasma current I_{pl} have a positive amplitude during the positive half-cycle of

the discharge, which change to a negative amplitude when the discharge switches to the negative half-cycle after 25 µs.

While the amplitudes of the negative currents are to some extent smaller than the positive ones the overall charge, given by the current during a specific time interval and obtained by integration of the time resolved currents, is the same for each half-cycle. The reason for this is that the charge generated during the positive half-cycle has to be compensated during the negative half-cycle, otherwise the quasi-neutrality of the plasma would be violated. This neutralization is caused by a negative electron wave, which is fundamentally different from the positive streamer propagation that was described before.

In contrast to the positive polarization where electrons are attracted to the HV electrode, they are suddenly repulsed from the HV electrode during the negative polarization. This leads to a collision dominated wave like phenomenon traveling to the GND electrode which in the end ignites a spark like second discharge with a reversed current flow compared to the positive half-cycle.

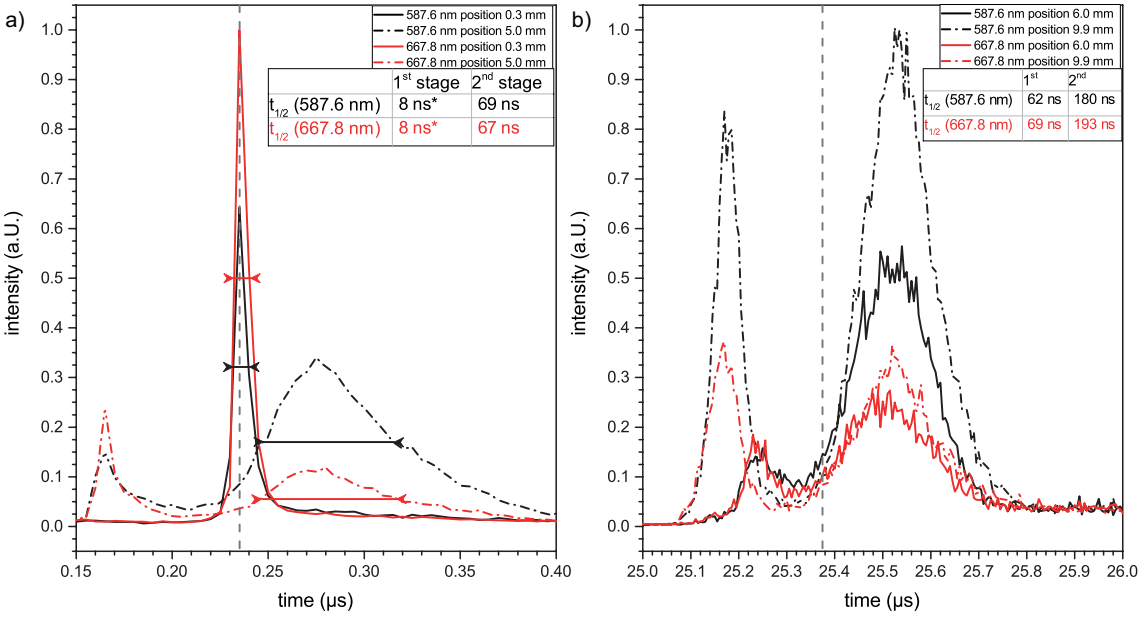

Figure 3.11: Temporal distribution of the He 587.6 nm (black) and 667.8 nm (red) emission lines during the positive a) and negative b) voltage half-cycles. The temporal profiles where taken from different points of the TSSR-OES spectra.

Comparing the relative intensities of figure 3.6 and 3.10, on first glance it seems that the negative half-cycle is much darker than the positive because it only peaks at 21 % of the positive half-cycle. This false conclusion is caused by the different overall timescales of the positive and negative half-cycles. While the positive half-cycle is essentially finished after 800 ns, the negative half-cycle takes roughly double as long meaning that it is significantly slower.

Similar to the total amount of charges, the total amount of light emitted during both discharge half-cycles is again the same. While the same amount of electrical charges can be expected due to the quasi-neutrality of the plasma, it is surprising to find the exact same amount of light emission during both discharge half-cycles

too, considering that the excitation mechanisms are clearly different. This difference becomes apparent when the half-life times $t_{1/2}$ of the He 587.6 nm emission lines presented in figure 3.11 are compared for the positive and negative voltage half-cycles.

The temporal profiles show the time dependent development of the emission at certain fixed points, which were chosen in a way that it is possible to clearly assign the emission to either the 1st or the 2nd plasma stage. The lifetimes of the He states is clearly shorter in the 1st stage of the plasma for both voltage half-cycles and does increase considerably after the ignition of the 2nd stage. At the same time, it is obvious that the lifetimes of the negative half-cycle are much longer than the lifetimes of the positive half-cycle, in particular if one considers that the lifetime obtained for the 1st of the positive half-cycle is effectively limited by the maximum time resolution of the TSSR-OES and could very well be even shorter than the 8 ns given in figure 3.11.

The results presented in figure 3.11 (a) vividly illustrates the transition of the temporal well defined and sharp streamer like discharge of the 1st to the collision dominated spark like discharge of the 2nd stage. The emission events of this spark like regime have a broader temporal distribution, due to the fact that the collisions are orders of magnitudes slower than the photoionization that drives the positive streamer. Another difference between the two regimes is the intensity of the reduced electric field which can be estimated by the ratio of the 587.6 nm and 667.8 nm line.

As mentioned before, these lines belong to the singlet and triplet states of the He and the ratio of these lines can directly be used to measure electric fields under certain discharge conditions [51]. The model described by Ivković et al. is only applicable in a plasma regime with a relatively low He metastable density, due to the fact that the emission triplet lines is over pronounced and therefore would yield a false line ratio. Therefore, it is only applicable in the positive streamer regime of the 1st positive plasma stage. All other stages are dominated by He metastables as was discussed before and also show a higher He 587.6 nm line compared to the 667.8 nm line as expected by the model for this case.

This concludes the description of a complete discharge cycle of a DBDI that is operated with a square-wave HV generator with 3.0 kV applied at 20 kHz using helium as discharge gas. To summarize: The plasma starts after the first initial positive polarization that occurs after the HV generator switches from the low (−1.5 kV) to the high (+1.5 kV) amplitude. This polarization rapidly attracts electrons towards the HV electrode, which in turn excite He atoms and leave behind a positive cloud of ions.

While the excited He atoms create new ions via photoionization, the ions create a high electric field which attracts new electrons and starts a wave like propagation that leads away from the HV electrode. This positive streamer propagates either until the initial polarization is depleted or it reaches the GND electrode. As soon as the streamer reaches the GND electrode it closes the external electric circuit, which leads to a short circuit and a spark like re-ignition of the discharge.

The spark like re-ignition can be characterized by a rapid acceleration of charged particles through the ion channel that was formed by the streamer. The high amount

of electron collisions throughout this stage lead to a strong occupation of He^m states that are primarily responsible for the dissociation and excitation of molecules and molecular fragments in the third and last afterglow stage of the DBDI.

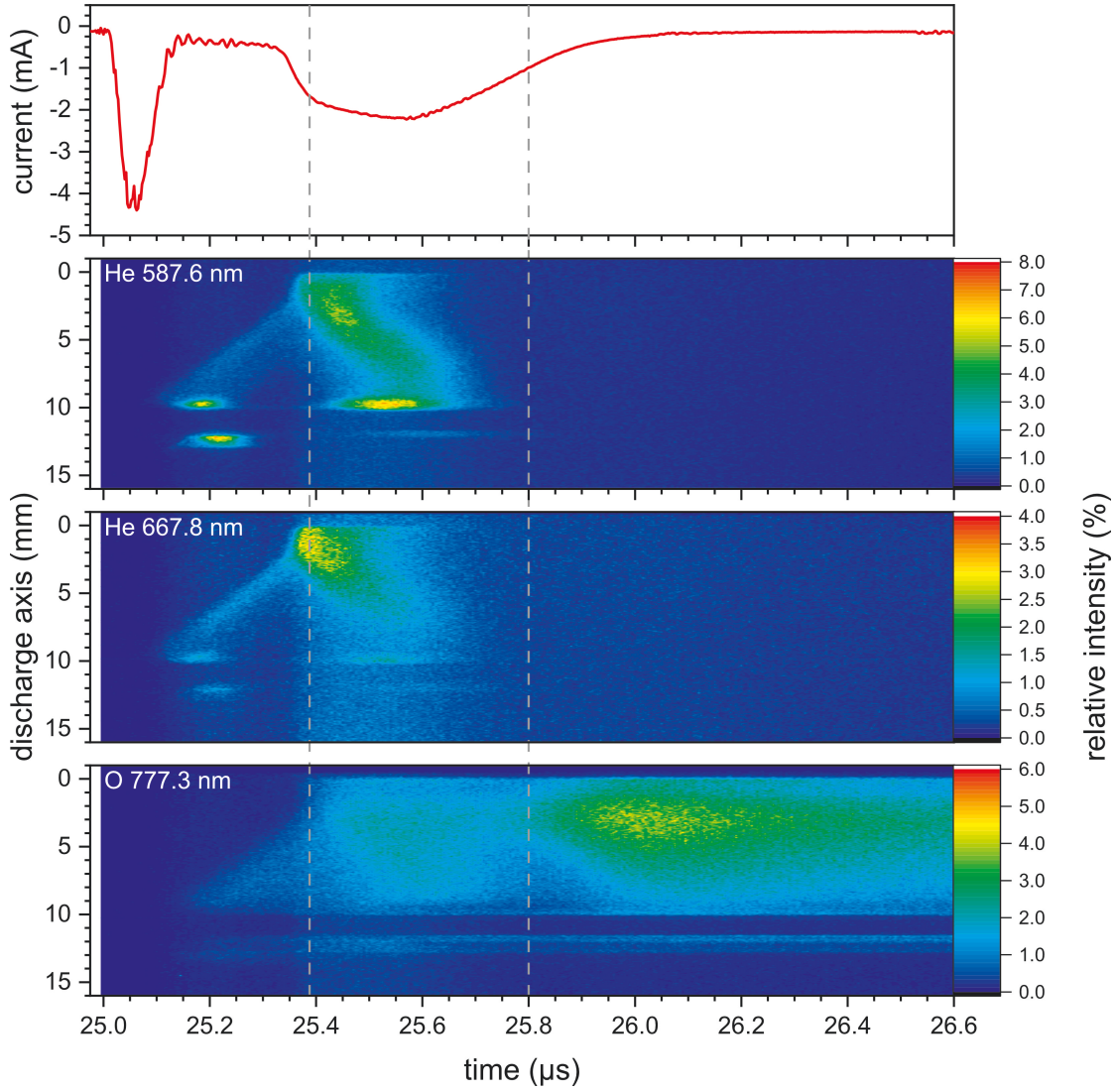

Figure 3.12: Development of the temporally, spatially- and spectrally-resolved optical emission of the DBDI during the negative voltage half-cycle starting at 25 µs. The presentation is the same as in figure 3.6, the only difference is that the intensity scaling that was normalized to the maximum number of counts obtained during the positive voltage half-cycle.

The positive half-cycle is essentially finished after this point in time and the discharge remains in a passive state until it is re-ignited after the negative polarization occurs 25 µs later. Contrary to the positive streamer, electrons are repulsed from the HV electrode by the negative electric field, creating a collision dominated electron wave that travels towards the GND electrode. This electron wave does not produce an as strong electric field as the positive streamer and therefore the photoionization is less efficient and focused. Similar to the positive streamer however, the arrival of the electron waves ignites a spark like discharge which transitions and finishes in a metastable collision dominated afterglow phase.

The complete discharge development should not be seen as a singular event, but instead as a series of accumulated reproducible events that create a stable equilibrium with a noticeable memory effect. This memory effect is primarily caused by charged species and reaction products that survive longer than a half-period and therefore until a new discharge ignition takes place. This means that charges created in the positive half-cycle of the discharge influence charges in the negative half-cycle and vice versa. Therefore, it takes some time until a discharge "warms up" and also for changes to a once found equilibrium to take effect.

The next part of this work will discuss the systematic influence of different parameters on the discharge development and also highlight how some of the observed effects can only be explained by a memory effect and stable equilibrium conditions created by the discharge itself.

3.4 Influence of external parameters on the discharge development

The previous part of the work dealt with the general description of the discharge development with a focus on the fundamental ionization and excitation mechanism. For this reason, the discharge was operated at quasi standard settings that were arbitrarily chosen as suited parameters. The voltage was set to 3.0 kV, the gas flow was set to 500 ml/min and the same DBDI capillary was used for all measurements.

The last point in particular is important for reproducible measurements, due to the fact that all DBDI capillaries are handmade with slight differences that can have drastic influences on the discharge development, as will be shown later on. This part of the work will therefore begin with the easier to control parameters which are the applied voltage and gas-flow and then move on to the more complex geometry of the DBDI itself.

3.4.1 Applied voltage: Influence of amplitude, duty-cycle and frequency on the discharge development

The first approach that is considered is to either reduce or increase the voltage applied to the DBDI. Figure 3.13 summarizes the results of the voltage variation in a range of 1.9 kV to 3.5 kV with 100 V voltage increments. Reducing the voltage from 3.0 kV to 2.5 kV shown in figure 3.13 (a) has two effects on the plasma discharge. The first, and most obvious is an increase of time until the discharge transitions from the 1^{st} to the 2^{nd} plasma stage. This time, given by Δt clearly increases from 0.263 µs to 0.875 µs after a voltage decrease of 500 V. The second effect is a decrease of the total amount of charge that is coupled into the discharge.

The charge Q is given by the electrical current that flows in a certain time interval and can therefore be obtained by integration of the time resolved plasma currents. However, a direct comparison of the hatched areas in figure 3.13 (a) is quite difficult, due to the fact that the amplitude and width of the current peak changes quite drastically. Therefore, figure 3.13 (b) directly shows the integrated charge Q in

dependence of the applied voltage for the plasma current peaks occurring in the positive and negative half-cycles.

Considering that the current during the negative half-cycle also has a negative sign it is more convenient to depict the absolute value $|Q|$ instead of the normal charge Q which is of course also negative during the negative half-cycle. The charge that is obtained in that way shows essentially the same absolute charge during the positive and negative half-cycles and a linear dependence on the applied voltage in a range of 3.5 kV down to 2.6 kV.

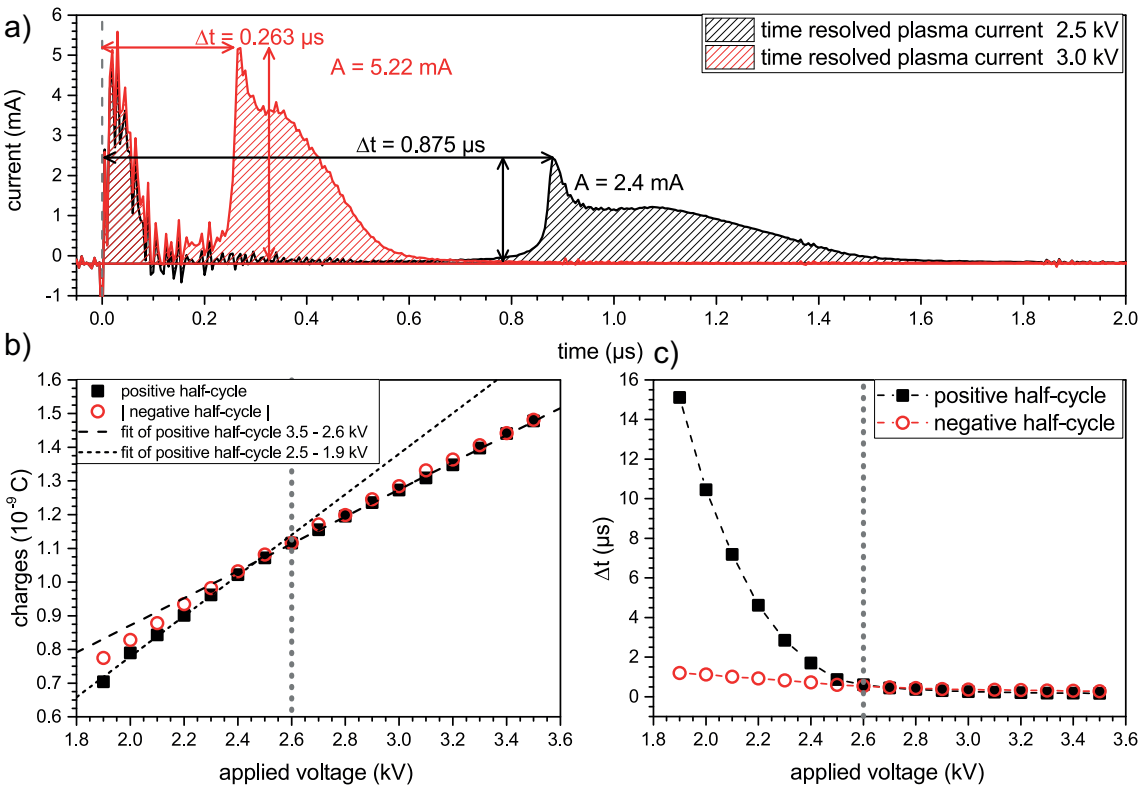

Figure 3.13: Influence of the applied voltage on the ignition behavior and total amount of charges in the DBDI. The upper part a) shows two time resolved current signals at representative voltages (3.0 kV (red) and 2.5 kV (black)) and shows the changes in ignition time delay (Δt) and charge (hatched areas). The lower part shows the dependence of the total amount of charges Q b) and Δt c) on the applied voltage.

This is in good agreement with the assumption that the DBDI can in principle be seen as a capacitor and the quasi neutrality requirement of a plasma. The charge Q a capacitor can hold is given by $Q = C \cdot U$ with U being the applied voltage and C the capacitance of the system. Assuming that the presence of a plasma does not drastically change the capacitance of the system, an increase of the voltage leads to a linear increase of the charge. However, this linear dependency only seems to be valid until a minimal voltage of at least 2.6 kV.

Below this voltage a clear bend in the linear dependency of the charges in the positive half cycle occurs and linear fits of the respective ranges also show clearly different slopes as one can see in figure 3.13 (b). This effect is more pronounced in the positive half-cycle indicating that something drastically changes in the discharge

in the voltage range below 2.6 kV that mostly effects the development of the positive half-cycle. Taking a closer look on the behavior of Δt for different voltages further strengthens this assumption.

Similar to the charges before, the development of Δt can be differentiated in a seemingly linear range from 3.5 kV down to 2.6 kV and a non-linear range from 2.5 kV down to 1.9 kV that primarily affects the positive half-cycle. While the slight kink in the presented charge can be easily overlooked or attributed to measurement uncertainties, the deviation of Δt in the low voltage regime is far too extreme to be explained in that way.

The shift of Δt spans over two orders of magnitude considering that the shortest time for the second plasma stage to develop at the maximum voltage was $\Delta t_{min}(3.5\,\mathrm{kV}) = 0.17\,\mu\mathrm{s}$ and the longest time measured was $\Delta t_{max}(1.9\,\mathrm{kV}) = 15.11\,\mu\mathrm{s}$ and therefore increases by a total of 14.94 µs. The total increase of Δt during the negative half-cycle is only 0.92 µs with $\Delta t_{min}(3.5\,\mathrm{kV}) = 0.272\,\mu\mathrm{s}$ and $\Delta t_{max}(1.9\,\mathrm{kV}) = 1.19\,\mu\mathrm{s}$, which means that Δt is only increased by roughly a factor of five or in other words half an order of magnitude. The reason for these clearly different Δt shifts can be identified in the contrasting excitation mechanisms during the positive and negative half-cycle and become apparent if the time and space resolved emission of the DBDI for different representative voltages is compared as is done in figure 3.14.

The description used to characterize the development of the 1st plasma stage was until now purposefully simplified to focus on the important principle mechanisms. While the statement that the 1st plasma stage is dominated by a positive streamer that propagates from the HV to the GND electrode is still true, it has to be specified now that it does not do so in a smooth and constant way as implied by the straight arrow in figure 3.6. The middle part of figure 3.14 instead shows that the positive streamer in the 1st plasma stage could itself be divided into two stages that starts off with a linear regime where two comparable fast traveling excitation fronts expand down- and upstream from the HV electrode.

In previous descriptions it was assumed that the upstream excitation front propagates until it reaches the GND electrode and triggers the second stage of the plasma, whereas the downstream front slowly uses up the initial excitation in the ambient atmosphere and in the absence of a guiding dielectric or grounded surface cannot trigger a re-ignition of a new plasma stage and subsequently extinguishes. For the case of low voltages it also seems as if the upstream excitation only travels until it reaches a certain point at which it halts its initial constant propagation and switches to an accelerated propagation regime.

While the medium velocity of this regime $\bar{v}_{d2} = 7.9\,\mathrm{km/s}$ is only slightly slower than the velocity of the first linear regime $v_{d1} = 8.7\,\mathrm{km/s}$ it is still obvious from the curvature of the arrow that a strong acceleration of the propagation takes place in this second regime. For higher voltages the difference of v_{d1} and $\bar{v}_{d2}$ is negligible and it can very well be assumed that the upstream excitation front develops and propagates in one smooth process.

Due to this dependence on the voltage it is likely to assume that the occurrence of a second propagation regime is closely connected to the absolute amount of charges in the discharge and the electrical fields produced between the dielectrics in the DBDI that subsequently determine the transport of these charged species. The measurement of the field between the dielectrics in the DBDI is a very complicated task and was not yet realized due to technical limitations and an overall complicated measurement parameter regime. Still it can be assumed that the field between the dielectrics inside the DBDI is more or less directly proportional to the applied voltage and therefore should change in a comparable way as the applied voltage.

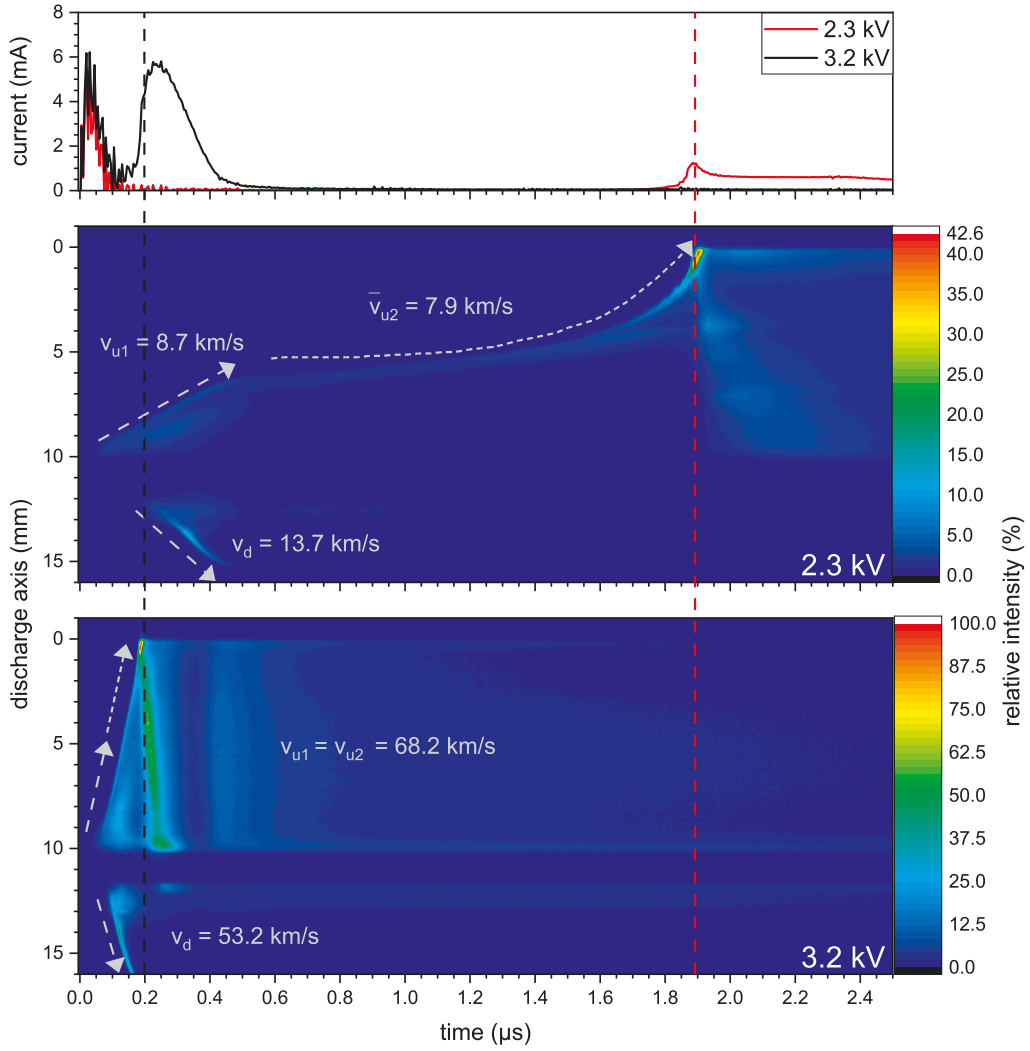

Figure 3.14: Development of the temporally, spatially- and spectrally-resolved optical emission of the DBDI for 2.3 kV (black) and 3.2 kV (red). The colored dotted vertical lines indicate the transition form the 1st to the 2nd plasma stage and the grey arrows help identifying the down-and upstream excitation fronts of the streamer development. The color scale was normalized to the maximum intensity of the measurement series that was reached at an applied voltage of 3.5 kV.

The reduced velocity of the excitation fronts for the lower voltages could very well be explained by a weaker electrical field and therefore slower acceleration of the initial electrons that start the streamer propagation. A smaller electric field also leads to a lower number of electrons that is involved in the initial formation of the streamer, due to a reduced polarization of the dielectric. This subsequently produces excitation fronts that seemingly stops midway in the capillary. This weaker form of a streamer needs an extended accumulation phase in which it gathers new electrons in the vicinity of the positive streamer head to upkeep the excitation, ionization and propagation.

As this accumulation phase continues the streamer gets stronger, which leads to the noticeable acceleration until it reaches the grounded electrode and triggers the 2nd plasma stage. The difference between the initial and the accumulation stages of the streamer can be even more drastic than presented in figure 3.14 as one has to consider that the time until the streamer finally reaches the grounded electrode can easily be prolonged to several microseconds as shown in figure 3.13 (c).

A decrease of the voltage beyond a critical value however, will lead to ignition times which are too long for the plasma to fully develop during a single positive half-cycle. An incomplete discharge cycle usually means that no stable plasma can form and a further operation is not possible. Nevertheless it is still possible to change the applied voltage in way that the full development of the plasma is interrupted before the 2nd stage ignites.

The method in question is called “plasma tuning” and was first presented by Schütz et al. in 2016 in the context of this work and is used to improve the analytical performance of the DBDI as an ambient ionization source [52]. The “plasma tuning” method was first developed after the initial characterization measurements of the DBDI which revealed that the plasma discharge ignites in several stages, as was published [47] and also described in the previous part of this work (see chapter 3.3).

The conclusion of the initial characterization of the DBDI was that the outer “jet plasma” is the part plasma that is primarily responsible for the soft ionization of molecules while the inner “coincident plasma” is responsible for dissociation and excitation. Therefore, to enhance the soft ionization capabilities of the DBDI, it was assumed that the operation of a “jet only” discharge without the inner coincident plasma contribution is beneficial or at least easier. This kind of “jet only” DBDI can be realized without too much effort if the duty cycle of the applied voltage is changed.

The duty cycle gives the time ratio of the positive and negative half-cycles and is usually set to a ratio of 50/50 or 50 % for the standard DBDI. However, by changing this ratio and shortening the positive half-cycle it is possible to switch the polarity before the full discharge development is completed and the transition to the 2nd discharge stage is suppressed, as shown in figure 3.15.

Another thing that should be taken into consideration is the fact that changing the duty cycle already influences the discharge development before the 2nd stage is fully suppressed. Decreasing the duty cycle from 50/50 to 17.5/82.5 respectively

17.5 % at the same time drastically increases Δt from 0.73 µs to 5.96 µs. The reason for this increase of Δt is similar to the increase that occurs when the applied voltage is reduced, however a reduction of the duty cycle does not effectively decrease the total number of charges in the discharge, it only influences the amount of time these charges decay before a new discharge ignition occurs.

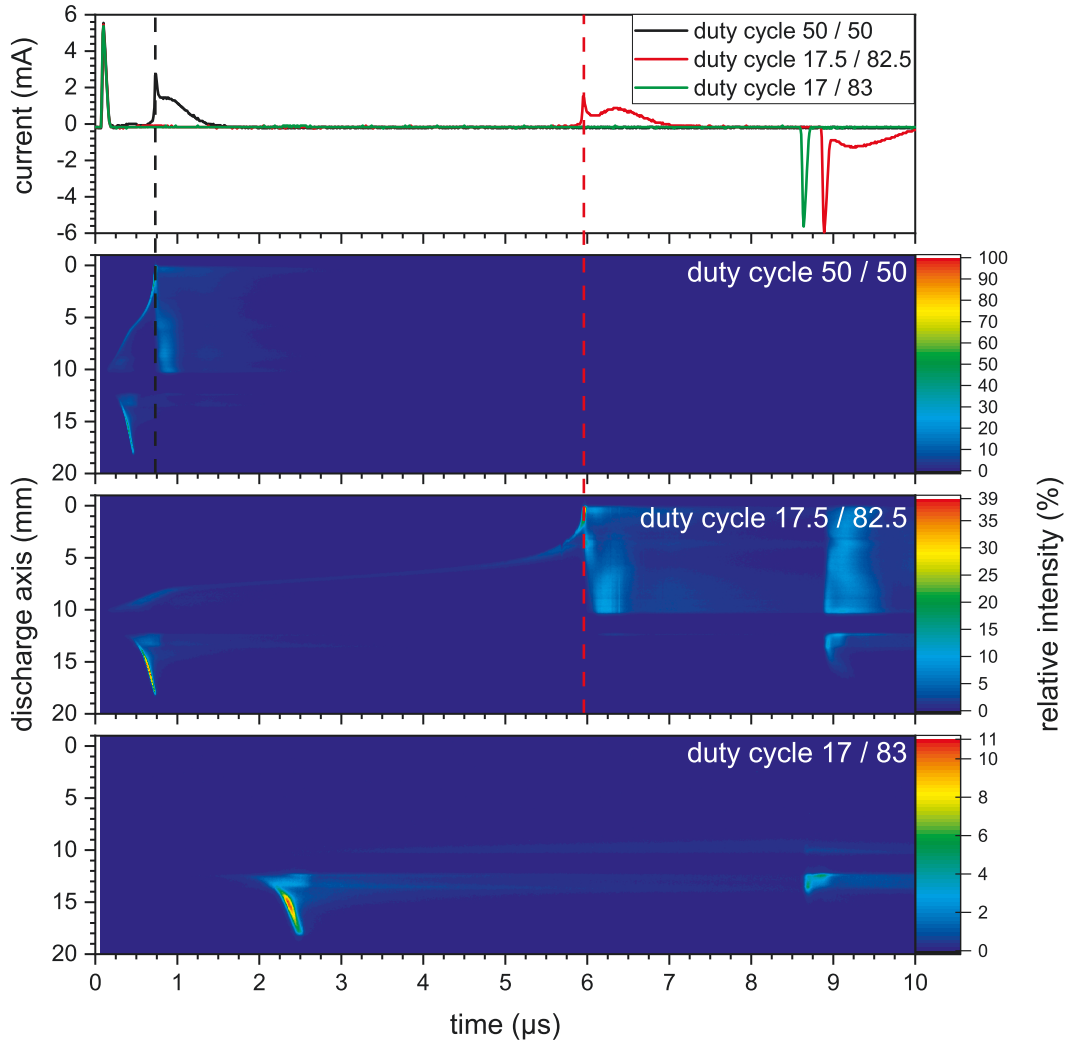

Figure 3.15: TSSR-OES measurement of a DBDI operated with 500 ml/min He and a voltage of 2.7 kV. The duty cycle was set to 50/50, 17.5/82.5 and 17/83, whereas the latter two can be identified by the earlier occurrence of the negative displacement currents at 8.9 µs and 8.65 µs respectively.

The time between the positive HV polarization that starts the positive discharge half-cycle and the negative HV polarization that starts the negative half-cycle amounts to 25 µs at an applied frequency of 20 kHz. Changing the duty cycle to 17.5/82.5 shortens the time between positive and negative half-cycle to 8.75 µs and prolongs the time between negative half-cycle and the next positive half-cycle to 41.25 µs. It has to be stressed again that the whole discharge development described in the previous parts is not a singular event but a repetition of periodic, similar events that form a relative stable equilibrium.

A relevant factor for this equilibrium is the amount of charged and excited species, which are produced in one discharge half-cycle and survive until the next half-cycle starts. This amount of charged and excited species is directly influenced by the duty cycle in such a way that more species, which are produced during the positive half-cycle, survive until the negative half-cycle ignites, due to the fact that it starts sooner. The amount of species supplied to the next positive half-cycle on the other hand is reduced due to the increased decay time, resulting in a more pronounced accumulation phase during the 1st plasma streamer stage and an increase of Δt.

The shift of charged and excited species caused by the change of the duty cycle can also be identified by its influence on the current peak shapes and the linked excitation mechanisms in the discharge, which is not as obvious as the already discussed change of Δt and requires a more detailed examination of the measurements. The plasma current peaks, both during the positive as well as in the negative half-cycle, have a very particular shape that was not discussed in great detail yet. The plasma current peaks seem to consist of at least two current contributions that can be clearly differentiated into a 1st and a 2nd peak, whereas one can directly take from figure 3.16 (a) and (b) that the expression and discernability of these peaks strongly depend on the duty cycle.

The peaks during the positive positive half-cycles can be best distinguished for low duty cycle values and begin to merge when the the duty cycle is increased until they seem to be a singular current peak. The same behavior occurs for the negative half-cycle except that the best separation of the peaks occurs at high duty cycle values and the merging occurs when the duty cycle is reduced.

While the impact of the duty cycle on the current shape and time delay Δt is very notable, at the same time it does not influence the total amount of charges that are produced in the discharge as one can see in figure 3.16 (e). Considering that the duty cycle clearly influences the excitation mechanisms and development of the plasma, it is interesting that it obviously is not changing the total amount of charges that are present in the discharge. This further implies that the charged and excited species are only shifted from one half-cycle to the other, due to a change to the established equilibrium.

Another indicator that documents the strong impact of this changed equilibrium, can be observed in the emission of the plasma presented in figure 3.16 (f). The normalized intensities of some chosen emission lines that are representative for excited species in the discharge such as He, N_2 and O, show similar non-monotonous fluctuations as the positive peak height, which means that the duty cycle impacts the emission in a similar way.

Figure 3.16 (f) also shows that some emission lines are impacted more by the duty cycle than others, which changes the overall ratios of the emission lines. This strongly hints at changes in the excitation mechanism and the most noteworthy emission lines in this case are the He lines which are He 667.8 nm, 706.7 nm and in particular 587.6 nm. The intensity of these lines heavily depends on the occupation of the helium metastable states, as was discussed before and a strong decrease as can be observed in figure 3.16 (f) subsequently indicates a decrease of the He metastables.

This observation fits very well with the previous conclusions that a change of the duty cycle shifts the established equilibrium and favors one voltage half-cycle on the expanse of the other. This effect can best be observed in the duty cycle range below 50 % which represents the case of a weakened positive voltage half-cycle in favor of the negative one. The positive streamer discharge has to develop in an environment that suffers from an increased loss of charged and excited species due to increased decay times.

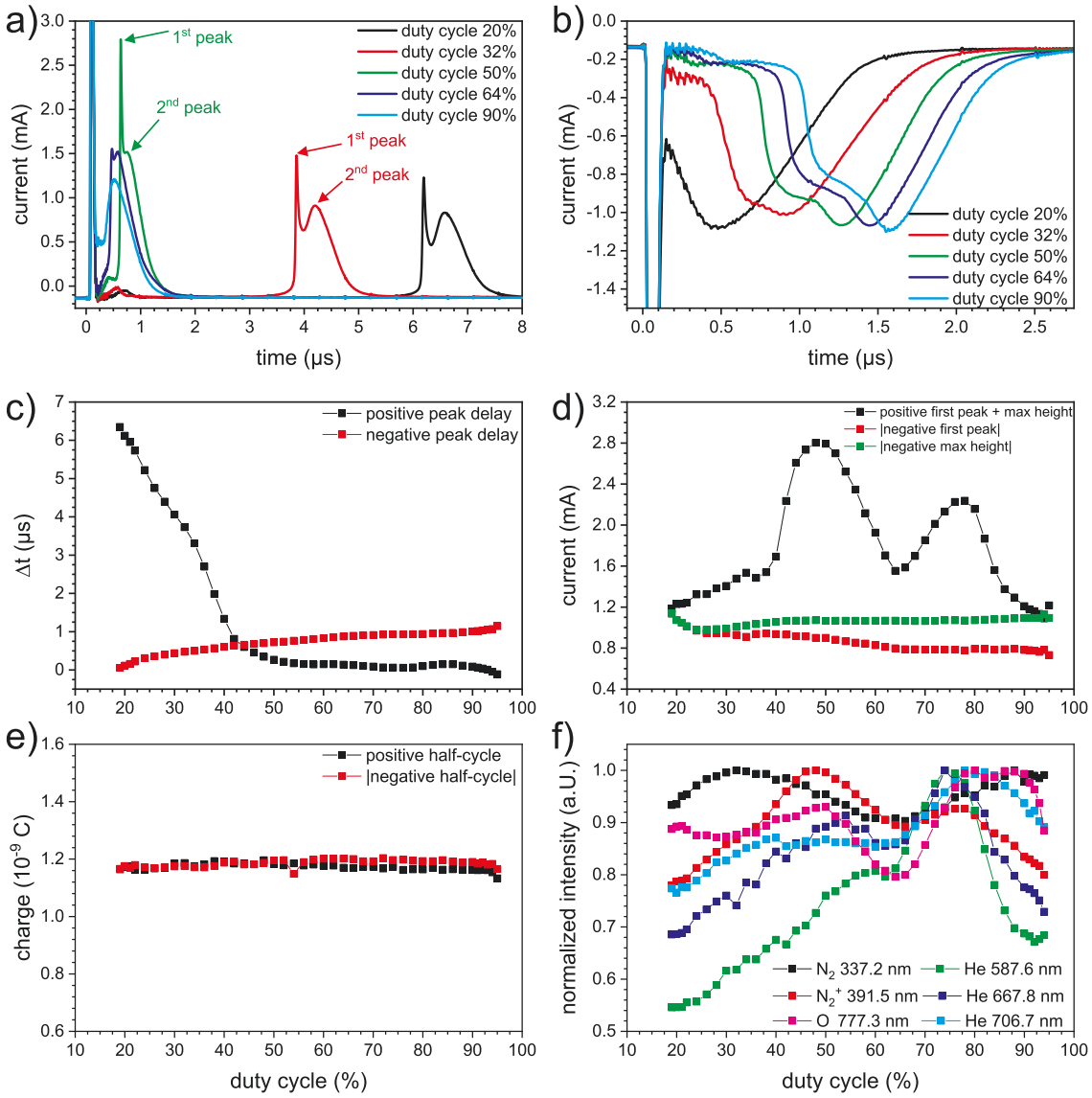

Figure 3.16: Time resolved current measurements a) positive, b) negative, current peak delay c), current peak heights and current maximum d), integrated charges e) and normalized intensity f) in dependence of the applied duty cycle for a DBDI operated with 2.7 kV at 20 kHz and 500 ml/min He. The results from c) - f) all show discharges without a suppressed 2nd plasma stage (duty cycle $\geq$ 20 %) to either avoid missing points due to non existing data c) and e) or jumps in the presented curves d) and f).

This leads to stronger expressed accumulation phases of the streamer that could already be identified to be less pronounced in the case of a reduced applied voltage.

This increased accumulation phase will subsequently create a less dense interaction regime during this discharge half-cycle, where excitation processes involving He metastables statistically decrease. At the same time the negative discharge half-cycle starts in an environment where it is proving generally more species from the previous positive half-cycle than it normally would receive from the standard 50 % case.

This concludes the examination of the two important plasma parameters that are related to the applied voltage, namely the amplitude of the applied voltage and the duty cycle which determines the ratio between positive and negative voltage half-cycle. The amplitude of the applied voltage is a rather straightforward parameter that directly controls the total amount of charges coupled into the discharge and influences the discharge development in a quite predictable way. The behavior due to changes of the duty cycle is partly surprising and requires interpretations that involve the shift of established equilibrium of charged and excited species in the discharge, which is hard to predict without suited observables or models.

Nevertheless, the duty cycle is a particularly powerful parameter that enables additional control over the discharge and its excitation mechanisms as was already presented by Schütz et al. [52]. However, further work on the duty cycle in particular is necessary since some of the mechanism in the plasma tuning that lead to an actual improvement of the analytical performance are still not fully understood at this moment.

While the investigations presented in this part of the work document most of the changes the applied voltage and duty cycle have on the plasma discharge and its development itself, a distinct connection to the analytical performance of the DBDI is not possible at this moment in time. One reason for this is that the mechanism of soft ionization occurring in the DBDI itself is still a topic for investigations. The mass spectra used to evaluate the impact of the duty cycle, and the overall analytical performance of the DBDI only show the finished soft ionized molecule without giving much information on the reaction chain that leads from the DBDI to the signal of this soft ionized molecule measured by the mass spectrometer. It can only be concluded that changes to the duty cycle can have various benefits on the analytical performance of the DBDI, but it cannot be said what the exact mechanism behind the improvement is.

One approach to explain this improvement is that the overall chemical reactivity of the atmosphere in and around the DBDI is changed due to the shift of charged and excited species during the variation of the duty cycle, as was discussed before and can be partly observed in the fluctuating plasma emission. The gas composition plays an important role in the operation of the DBDI, in particular due to the fact that the DBDI is normally operated under ambient conditions. The following part of this work will highlight the influence that gas flow and gas composition can have on the behavior of the discharge and will try to elaborate in how far these two parameters cannot be as easily separated as other discharge parameters can be.

3.4.2 Gas-flow and -composition

Gas-flow, -pressure and -composition, including the choice of the main gas component, are crucial factors for a plasma discharges. The DBDI is usually operated in ambient atmospheric conditions and uses helium as the main gas component, due to previous studies which evaluated the anayltical performance of the DBDI or DBDI like discharges [53].

The gas choice for the operation of dielectric barrier discharges is not restricted to He and in principle any gas can be used provided the requirements for the plasma to ignite are still fulfilled. The choice of other gases such as e.g. argon, nitrogen or even synthetic air for a DBD based ion source would provide several advantages to potential ambient MS applications, such as e.g. a higher cost efficiency due to lower gas prices or a better compatibility to ambient measurement conditions. However, the aforementioned studies by Meyer et al. determined that DBDIs operated in He outperform DBDIs operated in pure Ar.

One of the main reasons for this, claimed by these studies, was that DBDIs operated in He produce a homogeneous and "soft" plasma while the other gases produce a filamentary and "hard" plasma. This reasoning was already discussed during the introduction of chapter 3.1, where the problematic behavior of the previously used quasi-sinusoidal HV generator also implied a sudden mode change of the He DBDI from a "soft homogeneous" to a "hard filamentary" mode.

Careful evaluation of the ignition behavior displayed by the DBDI revealed that an increase of the quasi sinusoidal voltage simply leads to multiple discharge ignitions during a fixed plasma voltage-cycle, which in turn leads to a sudden rise of power that is converted in the discharge due to a quasi higher effective applied frequency. Use of the newer square-wave HV generators solved this problem by inhibiting multiple ignitions during a single voltage half-cycle, subsequently making the behavior of the DBDI more predictable and demonstrating that no sudden change to a so-called filamentary mode occurs in DBDIs that are operated in He. The better analytical performance of He can be explained by the fact that He can be operated with lower applied voltages than Ar, presumed all other experimental conditions are the same.

The DBDI can be operated with voltages in the range of 2.0 kV using He as discharge gas and still produce a stable plasma discharge. This leaves over 1.5 kV of the generator output to tune the discharge to a given analytical application and optimize the signal yield of the mass spectrometer. The same DBDI operated in Ar does not produce a stable plasma in a voltage range below $4.0 - 5.0$ kV and therefore far exceeds the maximum output of the standard square-wave generator. Simple solutions to still use Ar as discharge gas is to either use generators with a higher maximum voltage amplitudes such as the older quasi-sinusoidal HV generators, or to change the geometry of the DBDI enabling an Ar plasma to be operated at lower voltages. The latter solution will be discussed in following parts of this work in chapter 4 onward which deals with the influence of the discharge geometry on the development of the plasma.

The former solution, which is an increase of the discharge voltage, turned out to be unsuitable for analytical applications as reported on by Meyer et al. due to the fact that a DBDI operated at high voltages will dissociate analytes instead of soft ionizing them. The question that needs to be solved before Ar can be used as discharge gas for the DBDI, therefore is why the DBDI can be operated at lower voltages when it is operated in He.

The following part of this work will focus on this question, using the characterization of the DBDI up to this point and focus on the role of gas impurities for the formation of ions and on the overall ionization mechanism of the plasma discharge.

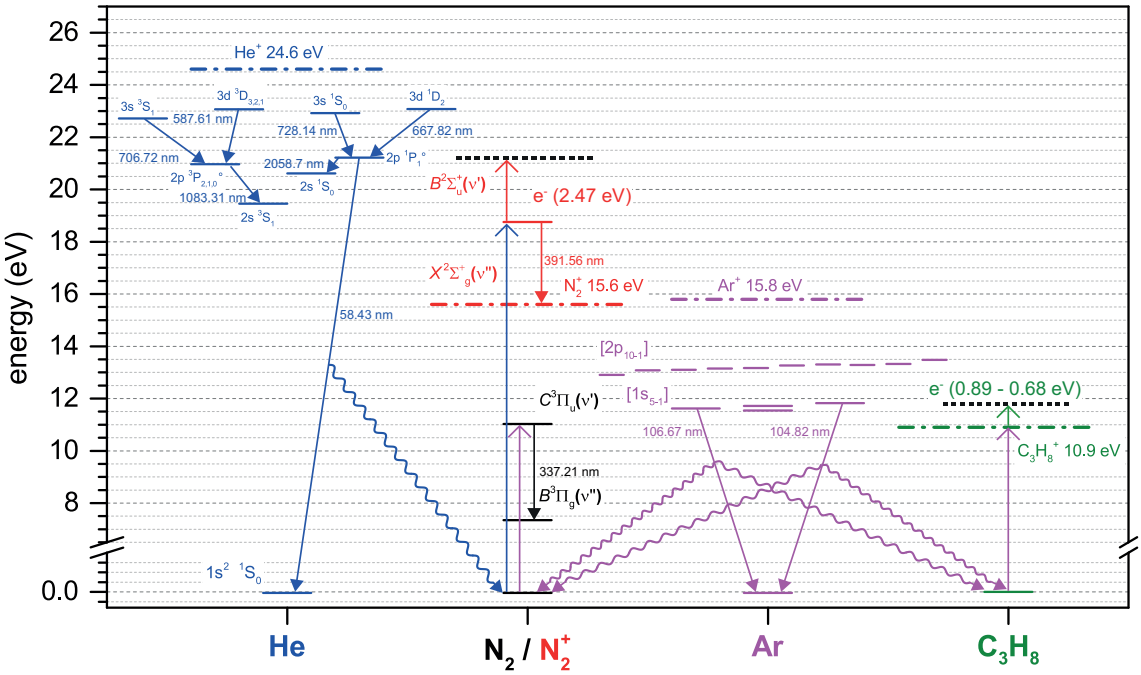

Figure 3.17: Selected energy states (horizontal lines) and optical transitions (downward arrows) of He (blue), Ar (pink), N_2/N_2^+ (black/red) and C_3H_8 (green). The waved-arrows and following upward arrows show possible photon-absorption paths that visualize how energy can be transferred from one atom/molecule to another. The upward arrows represent the energy gain of the excited electrons. Upward arrows passing a ionization threshold (dash-dotted lines) mean that the energy gain of an electron is sufficient for the formation an ion and an additional free electron.

Thus far the development of the plasma in the dielectric barrier discharge was described as multi-stage development with an initial streamer dominated early plasma phase that transitions to a spark like discharge as soon as the streamer fully develops and reaches the grounded electrode. It was mentioned in chapter 2.2.1 and 3.3 that ions are formed primarily by photoionization and not by direct electron collision or atom collisions with heavy metastables [40, 41]. It could also be shown in chapter 3.3 that metastable collisions are much more likely responsible for the dissociation of molecules and subsequent excitation of the fragmented atoms (see figure 3.9 and equations 3.1 and 3.2).

The most likely source of photoionization in a He discharge is the resonant transition $1s2p\ ^1P_1^\circ \longrightarrow 1s^2\ ^1S_0$, which is called resonant due to the fact that the excited

He returns to the ground state and emits the complete energy it had before in the form of a photon with a very small wavelength of only 58.43 nm, as illustrated in figure 3.17. These vacuum ultra violet (VUV) photons have an energy equivalent of 21.22 eV, which means that they can directly ionize every atom except neon ($E_i(\mathrm{Ne}) = 21.56\,\mathrm{eV}$) and helium ($E_i(\mathrm{He}) = 24.59\,\mathrm{eV}$).

It can be assumed that the standard DBDI studied so far is contaminated with a considerable amount of additional gas impurities although it was operated with He 5.0 exclusively, which means the He has a purity of 99.999 %. At the same time this means that at least 0.001 % of the gas is not He, which are 10 particles out of 1 000 000 He particles.

Nitrogen has an ionization energy of $E_i(\mathrm{N_2}) = 15.6\,\mathrm{eV}$ and represents the most abundant part among these residual impurities found in He, and it can be assumed that the percentage of N_2 in the gas mixture of the usual DBDI is even higher, due to the fact that it is operated in an open environment at ambient atmosphere.

N_2 is an ideal gas component in regards of the photo-ionization, due the fact that the VUV photons created by the 1s2p $^1P_1^\circ \longrightarrow$ 1s^2 $^1S_0$ transition can be absorbed by N_2. In turn, an electron is excited in the N_2 over the ionization threshold forming a free electron and N_2^+ ion, as indicated in figure 3.17.

The energy transferred to the N_2 is sufficient to create electrons with considerable energies of over 2 eV and at the same time can produce N_2^+ ions in the excited $B^2\Sigma_u^+(\nu')$ state which forms the upper state of second negative emission system of the N_2^+ ion with 391.56 nm being the most prominent emission band. This photo ionization is very efficient in the He DBDI, due to the fact that the concentration of the N_2 is in a range of only some 10 $\mathrm{ppm_V}$ to 100 $\mathrm{ppm_V}$ and also due to the atmospheric pressure that leads to a radiative trapping of the 1s2p $^1P_1^\circ$ state of the He.

The resonant nature of the 58.43 nm transition leads to a direct reabsorption of the emitted photon by a ground state He atom, restoring and therefore trapping the 1s2p $^1P_1^\circ$ state that emitted the photon initially. This emission and re-absorption of these VUV photons is repeated continuously and artificially prolongs the lifetime of the upper state, especially under atmospheric conditions where the free mean path of the photons is reduced due to the high density of particles.

The trapping of this state is only released, when the VUV photon is absorbed by an atom or molecule other than a He in the ground state, e.g. either a He in an excited state or a N_2 molecule in ground state and therefore lost from the constant, spiral-like emission and re-absorption process. The loss of the VUV photon will lead to the formation of an ion and free electron, which means that the energy deposited in the excited He states is efficiently transferred towards the formation of charged species in the plasma discharge that are essential for its development.

One sign for this energy transfer can be seen in figure 3.18 which shows the distribution of He 667.8 nm and N_2^+ 391.6 nm emission lines inside the discharge capillary at different points of time. The emission of the N_2^+ ion (blue) clearly trails behind the emission of the He 667.8 nm (red), which is an evidence for the initial excitation of high energetic He states and subsequent transfer of energy to N_2.

A systematic study was conducted in the context of this work, to find further evidence of the overall importance of N_2 for the ionization mechanism of the DBDI

[54]. One of the biggest challenges of this systematic study was the fact that it nearly impossible to conduct a control measurement between pure and polluted He gas mixtures to indisputably show the effect of N_2 on the ion formation of the DBDI.

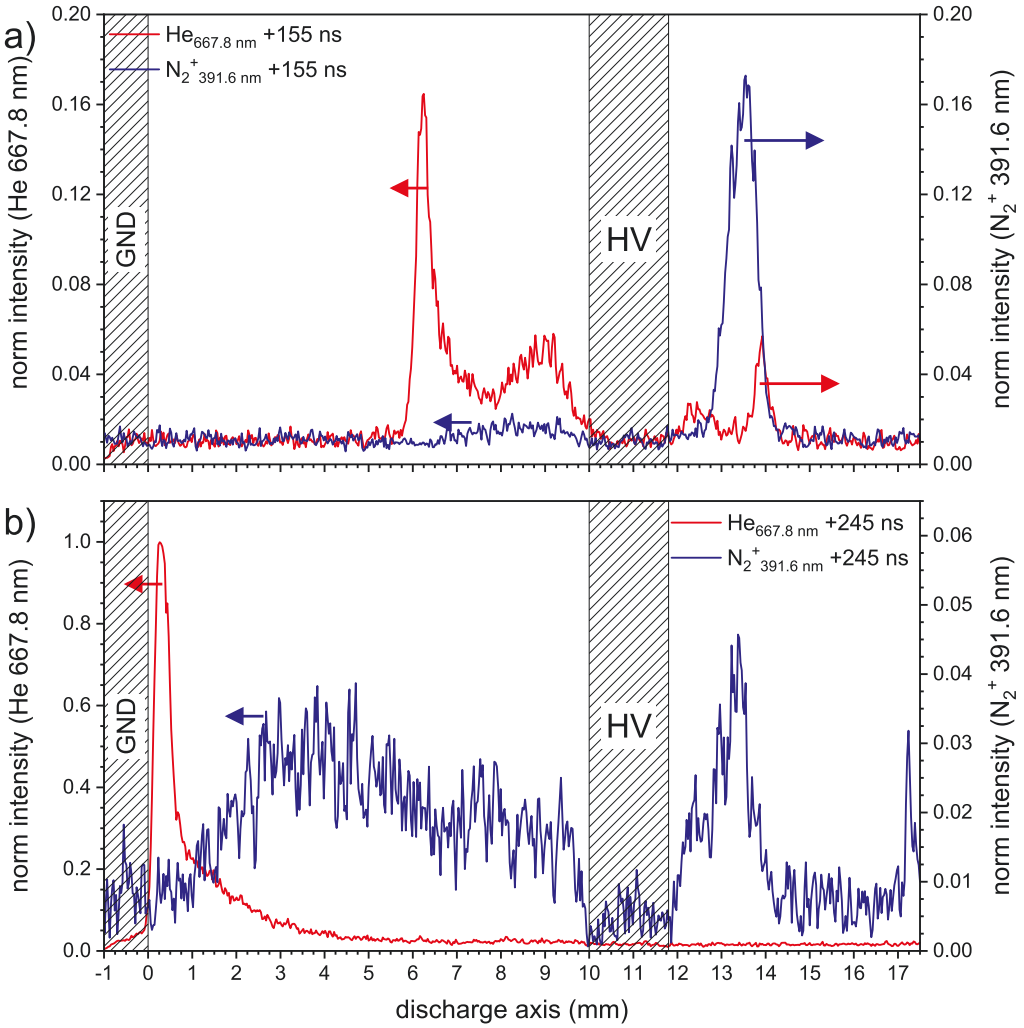

Figure 3.18: Distribution of the emission produced by the He 667.8 nm (red) and N_2^+ 391.6 nm (blue) line. a) Shows the plasma at an earlier stage of the plasma development (+0.155 ns after Trigger). b) Shows the plasma directly before the transition to the 2nd plasma stage at +0.245 ns after the trigger.

As already mentioned, the used He 5.0 still has a considerable amount of N_2 and although several methods exist to further purify the gas, such as e.g. cleaning the gas by appropriate filters, none of these methods were feasible for this study. The ambient operation of the DBDI gives access to a sufficient supply of N_2 from the atmosphere. In addition, preliminary tests showed that it is simply not possible to operate the DBDI in a reasonable voltage, respectively, power range without a minimum amount of N_2 still left inside, which means that even if it would be possible to create a completely pure He gas mixture it would not be possible to operate the DBDI in it.

For this reason a comparison with a model-system using argon as discharge gas was introduced. The energetic states of Ar are significantly lower than the states of

He, as presented in figure 3.17. The paschen notated $2p_{10-1}$ and $1s_{5-2}$ states create the well known emission system of the Ar discharge that creates the characteristic emission consisting of multiple strong lines in the near-IR range, partly shown in figure 3.9 (b).

In addition to this excited emission system, Ar also has resonant transition lines to the ground state, the 104.82 nm line originating from the $1s_4$ state and the 106.67 nm line originating from the $1s_2$ state. The energy of these photons is slightly below 12 eV and therefore significantly smaller than the energy that the photons created by the resonant He transitions carry. This makes the Ar resonant transitions a much less potent source of photoionization.

Absorption of these photons by N_2 could lead to the excitation of the $C^3\Pi_u(\nu')$ energy band, which is the upper state of the second positive emission system of the neutral N_2 molecule, but the energy is not sufficient to form an ion and free electron. Subsequently this means that N_2 is not a "suited" addition to Ar, as it does not help the formation of ions in the plasma discharge, due to the high ionization threshold energy of N_2 which is in the range of the Ar ionization energy itself. A suited gas addition to Ar can be found in C_3H_8 (propane), which has an ionization energy of $E_i(C_3H_8) = 10.9\,\text{eV}$ which is therefore clearly lower than the resonant transitions of Ar.

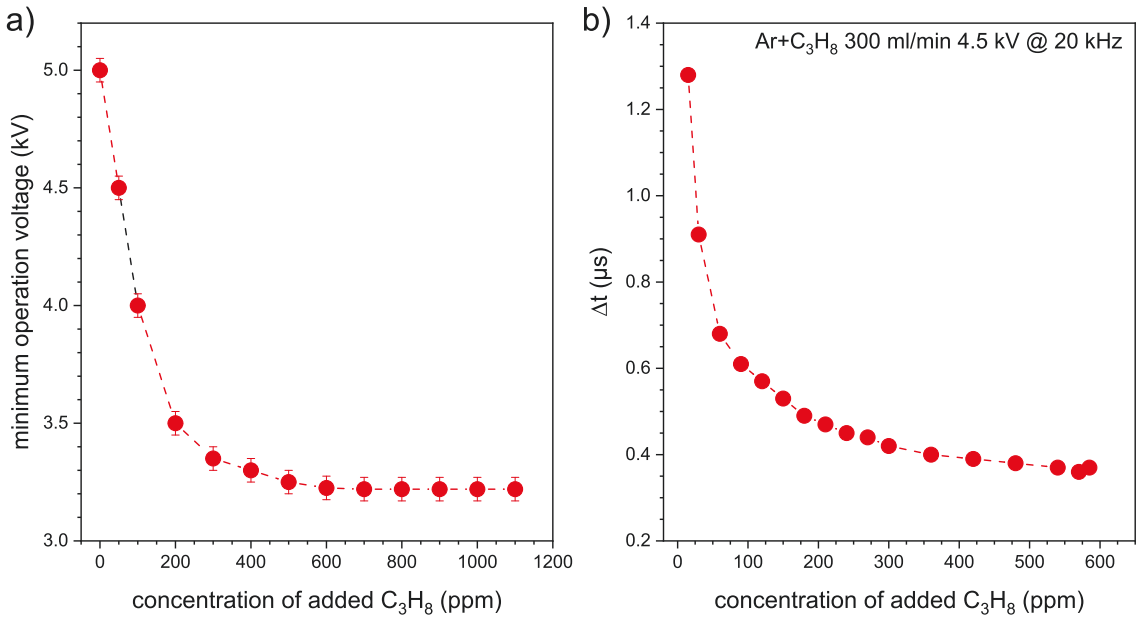

Figure 3.19: Influence of the C_3H_8 concentration on a Ar discharge. a) An increase of C_3H_8 percentage decrease the minimum operation voltage, which is required to still maintain a stable plasma ignition. b) Increase of C_3H_8 concentration at a constant applied voltage of 4.5 kV decreases Δt revealing an acceleration of the transition from 1st to 2nd plasma stage [54].

Adding C_3H_8 to Ar clearly affects a plasma discharge that is operated with this gas mixture, as the minimum operation voltage significantly decreases, with an increase of the C_3H_8 in the gas mixture, as shown in figure 3.19. The minimum operation voltage is, as the name implies, the minimum voltage required to operate a stable

discharge or prevent the discharge formation from breaking down. While the definition of a stable discharge is highly subjective and the exact voltage at which the discharge formation breaks down can be hard to determine, the minimum operation voltage proofed to be the best experimental value to describe the impact that the added C_3H_8 has on Ar as the main gas component of the DBDI.

The investigated DBDI operated in pure Ar without additional C_3H_8 requires at least 5.0 kV to be operated in seemingly stable way over the period of at least a couple of minutes. It has to be noted however that, the discharge was ignited respectively started at a higher voltage of 6.0 kV until it stabilized and warmed up. A customized HV square-wave generator was used for these measurements that used two power supplies and can provide roughly twice the HV amplitude output of the standard square-wave generators used so far.

An addition of 50 ppm_V C_3H_8 to the Ar leads to a significant decrease of the minimum operation voltage of 500 V from 5.0 kV down to 4.5 kV as shown in figure 3.19. However, before the applied voltage is reduced and a new minimum operation voltage is determined, the discharge needs a couple of minutes before a new equilibrium state sets in and the gas mixture with the new concentration of C_3H_8 is sufficiently flushed and stable.

The reason for the decrease of the operational voltage can be found when the development of the plasma discharge is taken into consideration, in particular Δt as it represents the transition form the 1st to 2nd plasma stage and therefore marks the full ignition of the plasma. Figure 3.19 (b) illustrates the reduction of Δt with rising C_3H_8 concentration for a fixed applied voltage of 4.5 kV.

The reduction of Δt and quickened transition of the plasma stages is caused by a more efficient ionization during the 1st stage of the plasma. C_3H_8 can absorb the VUV photons of the resonant Ar transitions and form $C_3H_8^+$ ions. This means that C_3H_8 is a suited acceptor of this radiation and will make the photoionization process in the discharge more efficient in contrast to N_2 which would only absorb the photons without providing ions and subsequently only disturb the discharge.

The enhanced ionization efficiency and reduced time of the plasma stage transition caused by a higher percentage of C_3H_8 mean that the discharge can be sustained at gradually lower voltages respectively minimal operation voltage, as shown in figure 3.19 (a). The influence of the C_3H_8 concentration on the discharge development is strongly non linear and the strongest reduction of the minimal operation voltage can be observed in the range between 0 ppm_V to 200 ppm_V added C_3H_8.

A further increase of C_3H_8 concentration leads only to moderate decrease of the operation voltage and Δt, subsequently leading to saturation for concentrations above 1000 ppm_V. The Ar-C_3H_8 model demonstrates that deliberate addition of a suited gas in a low concentration range can clearly influence the discharge development by increasing the efficiency of the photoionization that occurs during the 1st plasma streamer stage.

It has to be mentioned at this point that adding suited gases to increase the ionization efficiency, does not increase the total amount of charges that are formed in the DBD, as presented in figure 3.20 (a). The relative strong deviation of the

individual measurement values from the obtained mean values for Q, indicated by the large error bars, are primarily caused by the rather unstable output of the customized HV square-wave generator that has to be used for voltages above 3.5 kV.

It can be assumed that the charge Q is independent from the C_3H_8 concentration provided all other parameters, in particular the applied voltage, can be kept constant. This means that increasing the ionization efficiency only accelerates the formation of ions but the overall amount or yield of ions remains a constant value predetermined by the applied voltage and capacitance of the discharge.

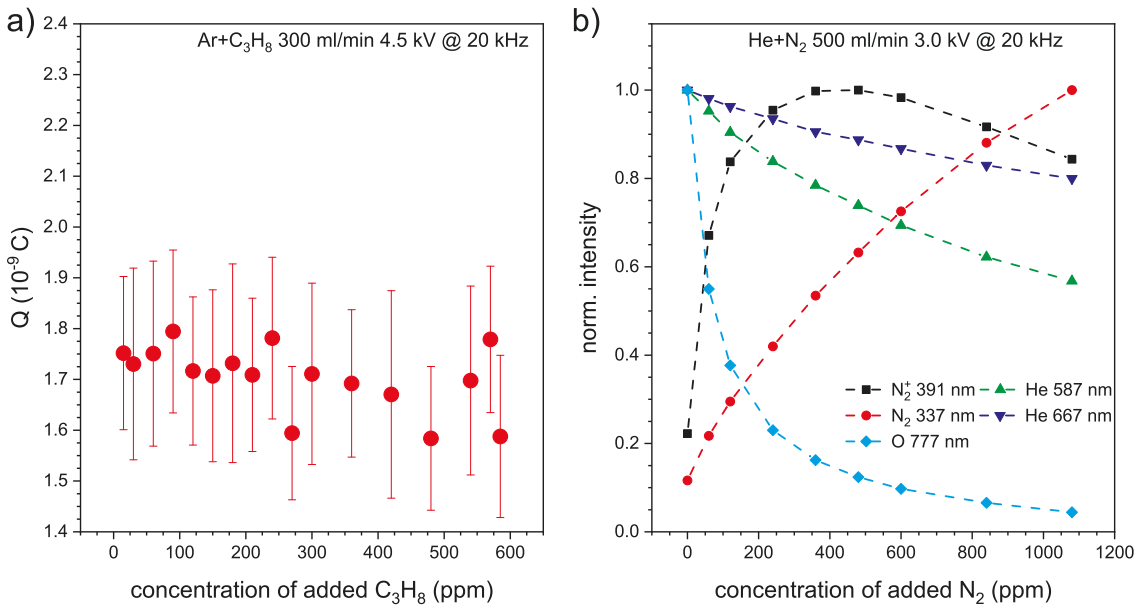

Figure 3.20: a) Total amount of charges Q depending on the concentration of C_3H_8 admixed to discharge operated with 300 ml/min of Ar at 4.5 kV and 20 kHz. Q was obtained by taking nine time resolved measurements of the discharge current without averaging, integration of the signals and assessing a mean value. The strong deviation of the individual values form the obtained mean values, indicated by error bars, is caused by the custom HV square-wave generator that uses to power supplies and runs not as smooth as the normal HV square-wave generators. b) Normalized intensity of selected emission lines in dependence of the N_2 concentration in a discharge operated with 500 ml/min of He at 3.0 kV and 20 kHz [54].

The acceleration of the photoionization as presented in figure 3.19, shows a strongly non-linear dependence subsequently leading to saturation at higher concentrations of C_3H_8. Further increase of the additional gas component beyond this saturation is actually disadvantageous for the discharge development, as can be seen in figure 3.20 (b).

The presented measurement, using He as discharge gas again, illustrates the effect of increasing the N_2 concentration on the intensity of several normalized emission lines that represent species in the discharge that are most likely affected by the addition of N_2. Initial increase of the N_2 concentration leads to an enhancement of the N_2^+ 391.56 nm and N_2 337 nm emission, indicating that production of excited N_2 neutrals and more importantly N_2^+ ions is improved, as was expected and also intended. Increase of the concentration of N_2 beyond 400 ppm_V however, only increases the

neutral N_2 337 nm emission while a slow decrease of the 391.56 nm sets in. This behavior implies that a further increase of the N_2 concentration does not improve the ionization efficiency of the discharge anymore, on the contrary an increase beyond a certain concentration level seems to be detrimental for the discharge development.

Several emission lines decrease with the addition of N_2 to the discharge which can be expected due to the fact that an enhanced excitation of N_2 naturally means that the excitation of other species becomes less favored. However, the exceptionally strong decrease of the He 587.6 nm and O 777.6 nm line suggest that a high level of N_2 primarily disturbs mechanisms in the discharge that are related to He metastable states, by either disturbing the formation or the collision reactions of the metastables.

The most likely explanation for the observed strong decrease of He metastable reactions is a decline in the formation of He metastables, caused by a lack of electrons that are quenched by N_2 before they can reach the necessary energies to excite He. The energy an electron can gain in an electric field is given by the strength of the field respectively the acceleration the particle gains and the length of the path that the electron can travel before it collides with an atom or another suited acceptor of the energy it gained thus far.

It can be assumed that most of the energy an electron has gained is preserved throughout a collision, due to the fact that a collision between a low energetic electron and a atom can be regarded as highly inelastic, caused by the high mass difference of the two particles. An electron can only lose its energy when it has gained enough energy through successive collision, to excite an electron in the He atom to a higher energy state.

Introduction of N_2 in the gas mixture means that electrons have new collision partners with lower energy states available, which means that an increase of N_2 will naturally decrease the amount of high energetic electrons and therefore also reduce the amount of excited He species.

In conclusion it can be said, that suited additions to the main gas component of a discharge such as N_2 or C_3H_8 play an important role in the ionization mechanisms of the DBDI. Addition of said gases in the range of some 100-1000 ppm_V lead to an increase of the photoionization efficiency during the 1^{st} plasma stage, which in turn means that the discharge can be operated and sustained at significantly lower voltages.

In particular for the case of Ar, which does not a have natural gas addition such as N_2 in He, addition of C_3H_8 helps to operate the discharge in voltage regime that is suited for analytical applications. DBDIs using pure Ar previously had to be operated in a higher voltage regime, resulting in strongly fragmented mass spectra that could not compete with mass spectra obtained by DBDIs operated in He at much lower voltages. However Schütz et al. [55] demonstrated that using Ar in combination with C_3H_8 and an appropriate duty cycle tuning can have several advantages for mass spectrometric measurements.

4 GEOMETRY OF DBDS: COMPARISON OF FULL- AND HALF-DIELECTRIC BARRIER DISCHARGES

So far all investigations on the DBDI were carried out with a standard version of this particular type of plasma discharge, which primarily consists of a glass capillary with an inner diameter of $d_i = 466\,\mu m$, outer diameter of $d_o = 900\,\mu m$ and two approximately 1 mm wide electrodes that are fixed directly on the glass capillary. The distance of the front electrode to the capillary orifice is usually 1 mm and the distance between the electrodes, also called electrode gap, is generally 10 mm.

The electrodes are made out of copper cables that are wrapped around the capillary and then fixed by soldering. While this method produces a very sturdy bond between copper cable and glass surface, it is very difficult to produce two DBDs with exactly the same electrode configuration. This reproducibility problem was avoided in the previous chapter by only using a single DBDI in all of the measurements but is not a practical solution for the actual problem.

This chapter deals with the geometry of the DBDI and the influence that the electrode width, electrode gap and capillary dimensions have on the development of the plasma. Another important part of this chapter will be the discussion and comparison of different discharge types. These different types of discharges are so called full- and half-dielectric barrier discharges and a systematic comparison of these types of discharges was published in 2017 in the context of this work [56].

The motivation for this kind of comparison originates from the many different kind of DBD based plasmas that are used in the field of analytical chemistry as ionization sources for ambient mass spectrometers. These discharges are often simply defined as dielectric barrier discharges without further regard to operational parameters or geometry, which leads to a wide variety of different discharges that are used for analytical applications that can drastically differ from each other.

Two very prominent examples of DBDs used in analytical applications are the dielectric barrier discharge for soft ionization (DBDI) and the low temperature plasma probe (LTP) [12]. The DBDI is primarily used for the soft ionization of analytes for the subsequent measurement with a mass spectrometer and usually needs a supply that provides the analytes in a gaseous form. The LTP can be used as a desorption ionization source, which means that it can desorp analytes from a carrier surface and ionize the analyte after or while lifting it from the surface. Attempting to use a LTP in the same way as a DBDI usually leads to strongly fragmented mass spectra indicating that the direct ionization mechanism of the LTP is harder than the DBDI for potential analytes.

Both discharges, DBDI and LTP, are quite different regarding their capillary diameters, applied voltages, power consumption and gas flows, but the most striking difference is the electrode configuration. The DBDI belongs to the aforementioned full-dielectric barrier discharges, with two ring electrodes on the outside of the capillary, which means that the electrodes cannot come into direct contact with the plasma itself. The LTP has only a single ring electrode outside of the capillary and a pin electrode inside of the capillary that comes into direct contact of the plasma, making the LTP only a half-dielectric discharge.

The aim of the systematic comparison of these two discharges was to find out if the difference in the analytical performance of both discharges is only based on the difference in operational parameters such as the applied voltage or the gas flow, or if it is a more fundamental reason due to the full- and half-dielectric barrier discharge configurations.

This chapter will first illustrate the influence of general geometric factors on the discharge behavior, which include the electrode width, electrode gap and capillary diameter and will afterwards present the results of the systematic comparison of the two discharge types.

4.1 Influence of electrode- and capillary-properties on the discharge development

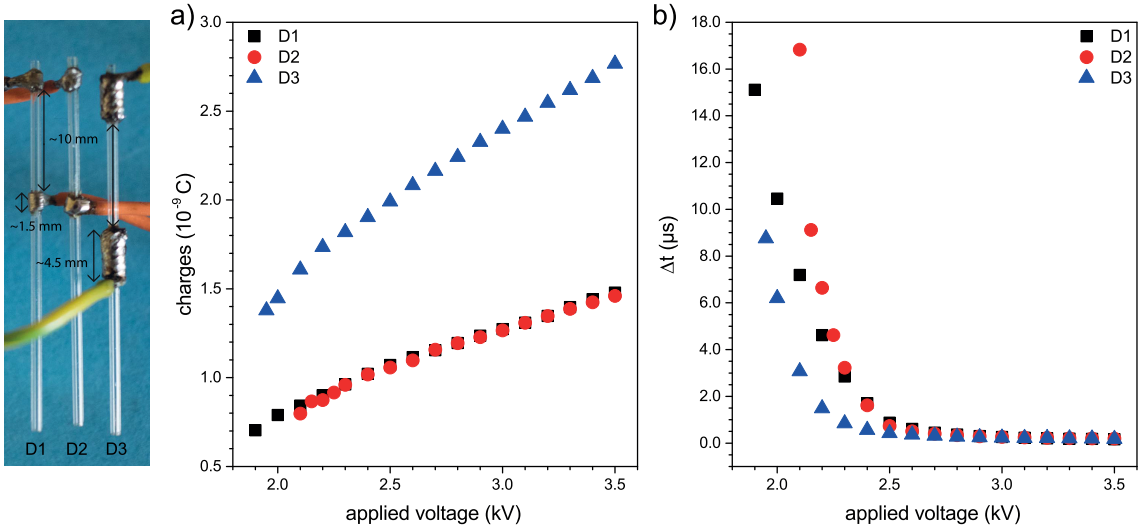

Figure 4.1: Assessment of the total charge Q, shown in a) and Δt in b), of three different DBDIs D1, D2 and D3. D1 is the capillary used throughout the previous measurments and D2 a copy of D1. D3 is a DBDI version with much wider electrodes compared to the other two discharges. It was attempted to keep the electrode gap at 10 mm and the distance of the front electrode to the capillary orifice roughly the same for all three DBDIs.

The geometric proportion of a dielectric barrier discharge is a crucial factor predetermining the overall charge that can be handled by the discharge at a given constant applied voltage. A DBD is in principle a capacitor and the charge coupled into such

a capacitance is give by $Q = U \cdot C$ where U is the applied voltage and C the capacitance. The geometry of a DBDI is mostly cylindrical and the capacitance of a cylindrical system is given by:

$$C = \frac{2\pi\epsilon_0\epsilon_r L}{ln\,(r_2/r_1)} \tag{4.1}$$

The permittivity of the vacuum ϵ_0 and the dielectric material ϵ_r are constant values of the material, r_1 is the inner and r_2 the outer radius of the capillary and L the length of the electrodes covering the cylindrical surface. The DBDI is not a cylindrical capacitor, therefore equation 4.1 can only be seen as a very rough estimation for the capacitance of the the DBDI. However, it can be assumed that to change the amount of charge Q that is coupled into the discharge either a change of the voltage U as was demonstrated in figure 3.13, or a change of the capacitance C via geometric variation of r_1, r_2 or L, is required.

The easiest geometric change to the capacitance of the DBDI is a variation of the electrode surface that is in contact with the dielectric, which can be achieved by either an increase or decrease of the electrode width, as is presented in figure 4.1. This measurement includes the acquired total charge Q and Δt values for three individual DBDIs.

D1 is the discharge that was used in all previous measurements so far and D2 is a copy of D1 with special attention to try and keep the electrode size and distances as close to D1 as possible. On this note, it is not surprising that the dependence of the charge Q to the applied voltage is nearly identical for D1 and D2 in the higher voltage regime above 2.5 kV and only slight variations are occurring in the more unstable low voltage regime. However, it has to be mentioned that D2 cannot be operated at voltages below 2.1 kV and attempting to do so will lead to the extinguishing of the discharge.

The reason for this can be seen in figure 4.1 (b), which reveals that the Δt belonging to discharge D2 shows a much stronger response to the applied voltage than Δt of D1. This means that although the two discharges D1 and D2 are very similar and show a very similar charge dependence, they still demonstrate a considerable difference in the much more sensitive dependence of Δt to the applied voltage.

A possible explanation for this different behavior of Δt can be seen in the photograph added in figure 4.1. The electrode gap of D2 is slightly bigger than that of D1 as one can see in the photograph, despite the effort to create an exact copy of D1, and during this part of this work it will be further shown that the electrode gap has the biggest impact on Δt.

The discharge D3 is an example of DBDI with extremely wide electrodes. Both electrodes are approximately 4.5 mm wide and are created by wrapping the copper cable several times around the capillary before it is soldered. The area of the capillary covered by the electrodes of D3 is roughly 3 times bigger than that of D1 or D2, assuming that the electrodes are cylindrical and the covered area is therefore proportional to the length of the electrode cylinders. In any case, figure 4.1 (a) reveals the total amount of charges that can be coupled into D3 is much larger than the amount of charges that can be handled by D1 and D2 which is exactly the expected

behavior. Increasing the covered surface area should increase the capacitance C of the system and in turn also increase Q.

A systematic investigation using several DBDs with different electrode widths, reveals that the charge of the DBDI does indeed increase linearly with the total electrode width or rather its capacitance as presented in figure 4.2. This further supports the fact that a DBD electrically behaves like a capacitor. The total electrode width is the sum of both the HV electrode width and the GND electrode width and figure 4.2 (a) shows the case when both electrodes are roughly the same size ($w_{HV} = w_{GND}$). Keeping the proportions of booth electrodes the same is very important as shown in figure 4.2 (b) where the results of DBDIs with either a much smaller HV or GND electrode are presented.

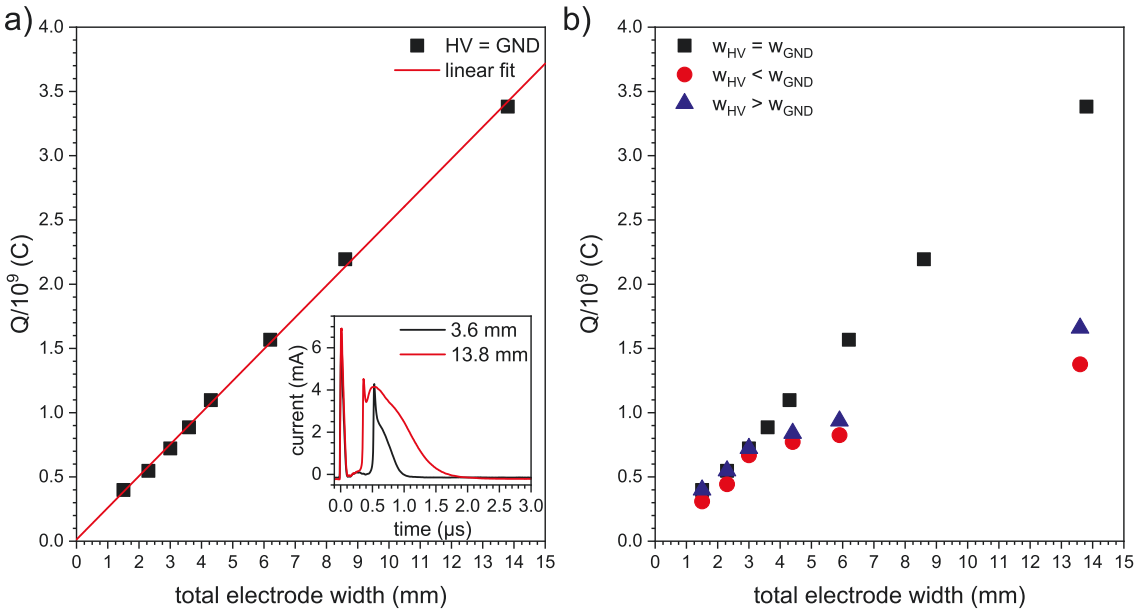

Figure 4.2: a) Charge Q in dependence of the total electrode width which is proportional to the total surface area that is covered by the electrodes. The discharge was operated with 500 ml/min He and 3.0 kV. The fit reveals that linear dependence is given and the inlet shows the representative time resolved currents for the total electrode widths of 3.6 mm and 13.8 mm. b) Effect of the ratio between HV electrode size and GND electrode size which both contribute to the total electrode width. A symmetric ratio of both electrodes, meaning HV and GND electrode are roughly the same size, leads to a linear dependence, while a strongly asymmetric ratio leads to deviation from this linearity.

The gain of total electrode width was only achieved by increasing either HV or GND electrode and keeping the respective other constant at a size of around 1.0 mm. At a total electrode width that is bigger than 4.0 mm a clear deviation from the previously linear behavior can be observed. The deviation can be explained by bottleneck effects that are caused by the extreme size difference of the two electrodes.

In the case of the large HV and small GND electrode, the HV electrode produces a large amount of charged species that cannot sufficiently discharge at the small GND electrode. This leads to the fact that the streamer that develops during the 1st plasma stage does not stop in the vicinity of the GND electrode as it usually does

but instead spreads several cm further upstream of the capillary. A much larger GND electrode compared to the HV electrode leads to effect that not enough charges are produced and the bigger GND electrode is not efficiently used.

In conclusion, increasing the total electrode width respectively the area surface is another efficient way to increase the amount of charges that are produced in a DBDI, next to the already discussed increase of the applied voltage. The benefits of such a bigger "high power" DBDI for potential optical analytical applications was published in 2016, where it was demonstrated that an increase of the overall charge Q of the plasma also leads to stronger emission signals and subsequently better limits of detection down to 0.7 ppb_V [47].

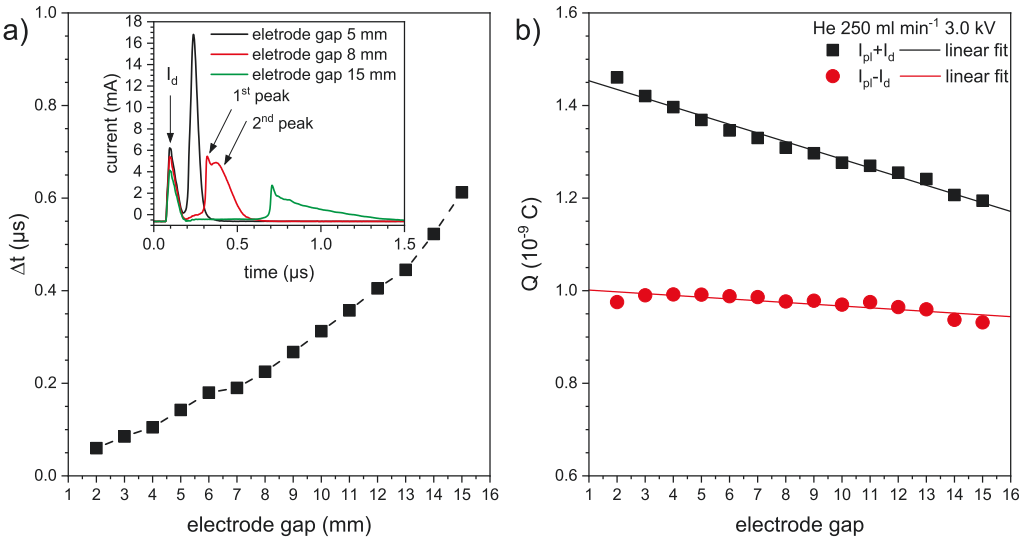

Figure 4.3: Influence of the electrode gap on the plasma transition time Δt a) and the total amount of charges b). While an increase of the electrode gap leads to a clear increase of Δt, it only changes Q on a minor scale. The increase of the electrode gap primarily decreases the displacement current I_D and only slightly decreases the plasma current I_{pl}, although it heavily impacts the shape of the plasma current peak as shown in the inset in a).

The next parameter to focus on is the gap between the electrodes, which so far was set to 10 mm. The GND electrode of the investigated DBDI was loosened from the glass capillary during the soldering to create a ring electrode that can freely move along the discharge axis. Using this method allows for a very tight contact between ring electrode and glass while still having the possibility to vary the electrode gap. The advantage of this method is, that the total surface area covered by both electrodes is always the same, therefore eliminating potential systematic errors that might be caused by using several DBDIs with different electrode gaps but also potential different overall electrodes widths.

Increase of the electrode gap leads to a steady increase of the plasma transition time Δt as presented in figure 4.3 (a) and also a strong deformation of the plasma current peak as one can see in the inset of the graph. The plasma current peak of the discharge with 8 mm electrode gap has clear defined 1st and 2nd peak features, as first described in figure 3.16. A decrease of the electrode gap leads to an overall increase of the current peak amplitude in particular of the 2nd peak contribution and

a subsequent merging of both peaks. Increasing the electrode gap leads to a decrease of the current amplitude and a strong broadening of the 2nd peak that can only be recognized as shoulder of the 1st peak for larger electrode gaps.

Despite the clear influence on Δt and the overall peak shape, the electrode gap has only a minor influence on the total amount of charges Q. Although a decrease of Q can be seen in figure 4.3 (b) it has to be noted that it only occurs in this magnitude if the charge contribution of the displacement current I_D is considered. In the measurements so far, the displacement current was usually integrated together with the plasma current I_{pl} and was seen as a linear offset of the charge value Q.

Increase of Q by either higher applied voltages or electrode width primarily increased I_{pl}, as one can see in the inset of figure 4.2 (a), but a change of the electrode gap primarily influences the charge contribution of I_D as presented in the inset of figure 4.3. This behavior is once more in good agreement with the capacitor approximation that was already used several times before. A larger electrode gap at the same time means an increase of the dielectric layer between the two electrodes which results in a smaller overall capacitance and subsequently charge of the system.

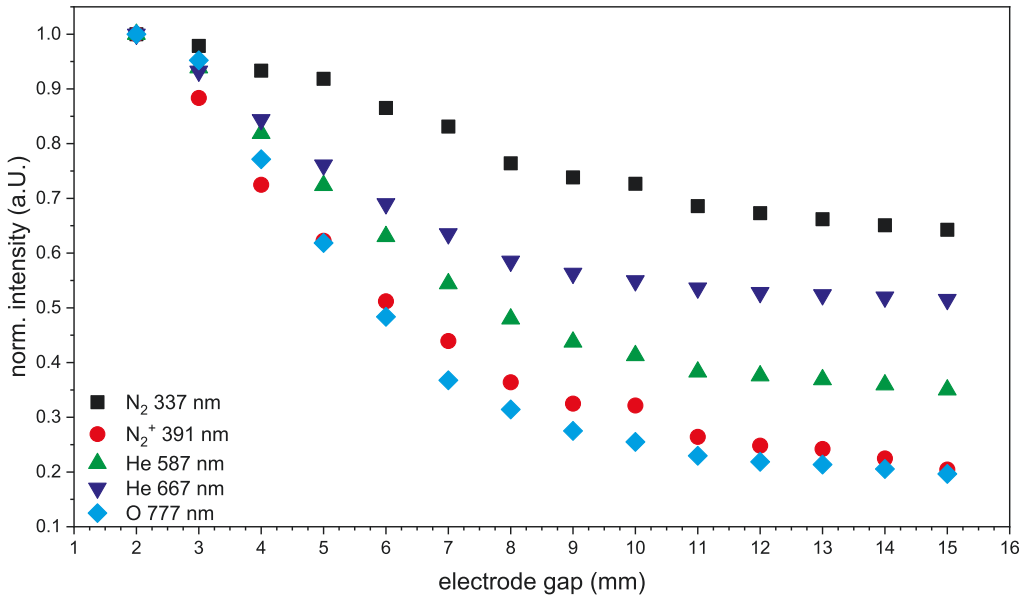

Figure 4.4: Normalized intensity of chosen emission lines for different electrode gaps.

Another parameter of the discharge not mentioned so far, but heavily influenced by the electrode gap is the volume of the plasma. The capillary structure of the DBDI leads to a very strict spatial confinement of the plasma and prohibits the plasma from freely spreading as it usually can happen in other discharge configurations. The volume that the plasma can occupy in the DBDI is given by the radius of capillary and the distance between the electrodes.

Assuming that the charges of the plasma discharge are not drastically influenced by the electrode gap, as implied by figure 4.3, would mean that a decrease of the electrode gap leads to a much shorter plasma column and therefore plasma volume, while still retaining the same amount of charge. Consequently this means that the same amount of charged and excited species are confined in much smaller volume

which efficiently increases the density of the plasma. A strong indication for a change in the effective plasma density due to the electrode gap distance can be seen in the change of the plasma emission presented in figure 4.4.

The clear decrease of emission with the increase of electrode gap indicates a reduction of excitation which can very well be caused by reduced effective plasma density and therefore less interaction and excitation between the involved species. However, these measurements require further validation due to the fact that the observed reduction of emission can also be caused by the fact that the plasma is elongated when the electrode gap is increased and the emission further upstream of the capillary is simply further away from the optical fiber.

Additional measurements are necessary but are not reasonable with the current setup. Although the movable GND electrode allows for a quick and easy change of the electrode gap, it still requires a considerable amount of mechanical force to move the electrode along the capillary. This however complicates optical measurements which require a very fine and stable alignment of the discharge. Further measurements on this matter will therefore be taken into the next part of this work, which deals with the comparison of full- and half-dielectric barrier discharge designs based on the two very popular and representative discharges in these respective fields, the dielectric barrier discharge for soft ionization DBDI and the low temperature plasma probe LTP.

4.2 Full- and half-dielectric barrier discharges: comparison of DBDI and LTP

A common plasma discharge usually consists of two electrodes and a gas in which the plasma is ignited when the voltage applied to the electrodes is high enough. A dielectric barrier discharges usually also requires two electrodes and a suited gas to ignite a plasma. The last thing necessary for a plasma to be considered a DBD is a dielectric layer that covers at least one electrode and separates the plasma from the metal surface of the electrode.

As mentioned in the theoretical part of this work, this dielectric layer leads to unique properties of the DBD but also requirements for its operation. One very important factor for the operation of a DBD that usually is neglected is the number of dielectric layers. The definition of the dielectric barrier discharge by Kogelschatz in 1997 states that at least one dielectric layer is sufficient for a plasma to be considered a DBD [57]. While this definition is certainly correct, it misses the distinction between plasmas in which only one of the electrodes is covered by a dielectric layer and plasmas in which both electrodes are fully covered. This leads to a wide variety of potential different discharges and discharge types and configurations. The resulting discharges can have very different properties and therefore can used for very different applications and approaches. Nevertheless, they are still all clustered under the term "dielectric barrier discharge" due to a lack of a more precise definition.

Two dielectric barrier discharges, that are used for very different analytic applications and also belong to either the full- or half-dielectric barrier discharge family, are the dielectric barrier discharge for soft ionization (DBDI) and the the low temperature plasma probe (LTP). The LTP is build in a glass capillary, similar to the DBDI, the only differences are the much bigger size of the LTP and the different electrode configuration. In contrast to the DBDI, the LTP only has one ring electrode that is fixed to the outside of the glass capillary and pin electrode that is inside of the capillary. The HV is applied to the outer ring electrode, as it is done for the DBDI and the inner pin electrode is pulled to ground. The inner grounded pin electrode is in direct contact with the plasma that is ignited in the LTP making the discharge a half-dielectric barrier discharge by the definition used in this part of the work.

Both discharges are used for the ionization of analytes for subsequent measurement with mass spectrometers. The main difference between the two discharges is the supply of analyte. While the DBDI in general requires a gaseous analyte that is admixed to the gas via an additional gas stream e.g. headspace, gas chromatography or laser desorption, the LTP can be used to desorp analytes directly from the surface of materials that are tested via mass spectrometry.

Using either of the two discharges for the respective other analyte supply, in other words the DBDI as a desorption source and the LTP as a direct ionization source, produces inferior mass spectra that are hardly usable. Implementation of the DBDI as a desorption source produces very low intensity spectra most likely caused by an inefficient desorption of analytes. Even if the DBDI is able to desorp the analytes from the surface of a sample, it might not be able to still ionize the desorped analyte

in this configuration due to a lack of power. Placing the LTP directly in front of the MS inlet and using it for the direct ionization on the other hand leads to strongly fragmented spectra with a low signal to noise ratio.

As already mentioned both discharges are optimized for their respective tasks and therefore quite differently-sized and also the applied voltages and gas-flows are drastically different. However, it is still questionable if the observed different performances as ionization sources can be sufficiently explained by these different sizes and different operation parameters alone. The impression remains that these differences are caused by the more fundamental difference of the DBDI being a full- and LTP being a half-dielectric barrier discharge.

A systematic study was performed that uses a special discharge, the variable dielectric barrier discharge (vDBD). This new discharge could be switched between a full- and half-dielectric operation mode with ease, which allows to completely focus on this geometric parameter. The approach and results of this study was published in 2017 and will be presented in the following section [56].

4.2.1 Experimental arrangement: The variable dielectric barrier discharge

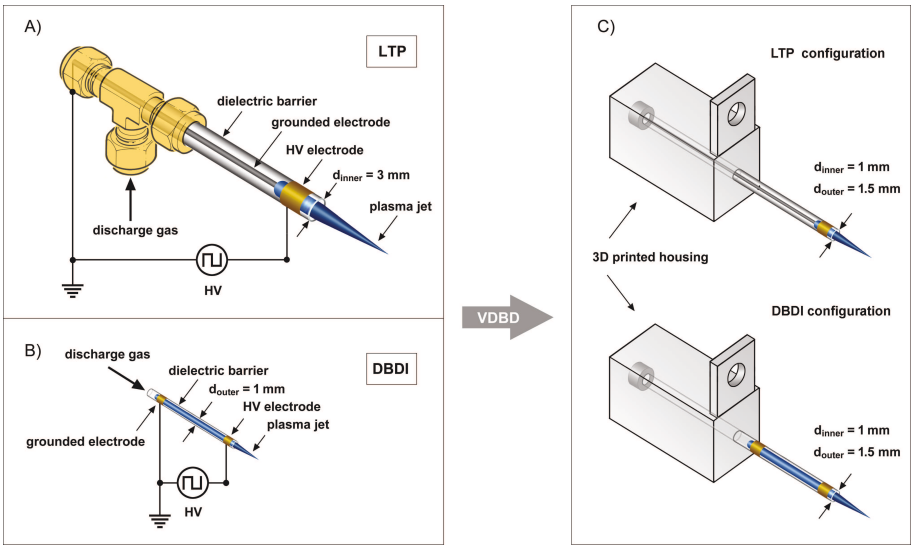

Figure 4.5: Schematics of the the LTP a), DBDI b) and vDBD c). The vDBD can be operated in two configurations, the LTP configuration (top) and the DBDI configuration (bottom) each representing the electrode configuration of the name giving discharge type [47].

The variable dielectric barrier discharge (vDBD) is a discharge platform that was developed for testing different capillary geometries and electrode configurations in a easy and reproducible way. Main part of this discharge design is the 3D printed housing, that enables a quick coupling of discharge capillary and gas supply via commercial Swagelok connectors. The diameters of the 3D housing can be easily changed and reprinted to accustom a variety of different capillary diameters.

The capillary type used throughout the systematic comparison of DBDI and LTP had an outer diameter of $d_{\text{outer}} = 1.5\,\text{mm}$ and an inner diameter of $d_{\text{inner}} = 1.0\,\text{mm}$

and therefore was right in between the standard dimensions of the DBDI and LTP. While the use of a different dielectric altogether of course changed the discharge behavior significantly, as one could guess from the detailed parameter variations of the previous parts of this work, the main focus of this comparison was to test the DBDI and LTP configuration under the same conditions. Preliminary tests revealed that the 1.5/1.0 mm capillary shows the same discharge behavior as a normal DBDI and the same three plasma stages can still be identified (see figure 4.7).

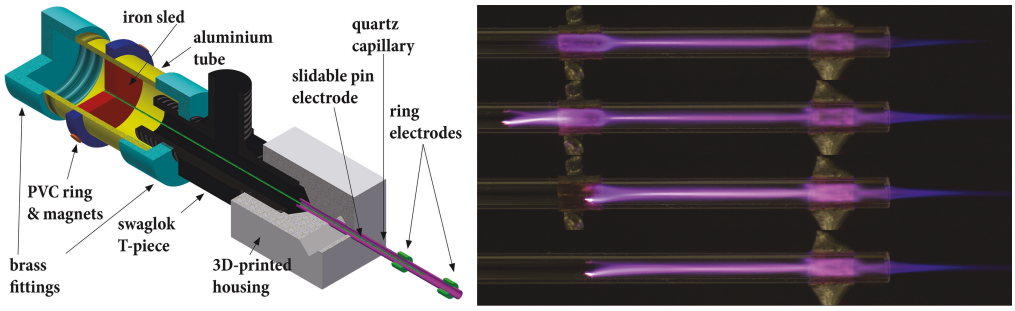

Figure 4.6: a) Custom made aluminum tube attachment for the vDBD. The attachment is used to freely move a pin electrode with the help of an iron sled and magnets under gas tight conditions. b) Several photographs of a vDBD with different electrode configurations. The vDBD is step wise changed from the DBDI like configuration (top) to the LTP like configuration (bottom). The operation of the vDBD was not interrupted in between the pictures [56, 58].

A custom-made attachment for the vDBD was developed, that helps to conveniently move the inner pin electrode in and out of the discharge while it is operated. The attachment, shown in figure 4.6, can be connected to commercial Swagelok T-fitting and mainly consists of an aluminum tube and brass fittings that form a gas tight chamber.

An iron sled is put inside the aluminum tube which can be moved with the help of strong magnets that are placed on the outside of the tube and fixed with a PVC ring. The pin electrode, usually a thin tungsten wire, is fixed to the iron sled and therefore moves when the position of the magnets is changed. Figure 4.6 (b) demonstrates the movement of the pin electrode in several pictures. The pin electrode can be freely moved to the same position that the outer ring electrode occupies and substitute it.

The ring electrode can be moved further to the back of the capillary or even completely removed to minimize interference with the LTP like configuration of the vDBD. The bigger outer diameter of the capillary that is used for the vDBD allows for an incomplete ring electrodes that only cover roughly 2/3 of the capillary circumference but still allows for a tight connection between metal and glass surface, as shown in the photographs of figure 4.6 (b). These open electrodes enable observations of the plasma below the otherwise concealed electrode region.

The vDBD is operated with the same standard square-wave HV generator as a normal DBDI, both in the DBDI configuration as well as in the LTP configuration. This is another deviation from the standard LTP that is that is also operated with a square-wave HV generator but in the range of $2.5 - 5$ kV with $2 - 5$ kHZ [12]. This difference in the HV supply might very well be a major factor for the difference in the

analytical performance of the LTP and DBDI. However, the goal of the systematic comparison is to focus on the geometric difference between full- and half-dielectric barrier discharge and if there is any, in how far it might be responsible for the different performances of the two discharges. This is why the experimental evaluation and comparison will start with the basic physical parameters such as e.g. the total amount of charges, emission and time dependent plasma development, before the actual analytical performance will be tested with a mass spectrometer.

The analytical measurements were performed with a Thermo LTQ and details regarding the exact instrument settings can be found elsewhere [56]. The analytical performance was tested with different substances such as menthone ($C_{10}H_{18}O$) and propachlor ($C_{11}H_{14}ClNO$) which is of particular interest due to fact that it is a herbicide and presents a certain relevance in an agricultural and food quality context.

The vDBD is aligned parallel and closely to the LTQ inlet and the analytes are supplied via an additional headspace capillary that is aligned perpendicular to the plasma plume that developed between discharge capillary and mass spectrometer inlet. Measurement of the protonated analyte signal intensities allows for a rather direct comparison of the analytical performance of the two discharge configurations, in particular if one considers that the vDBD can be switched rather freely between these two configurations without interrupting the operation of the plasma due to the aluminum tube attachment.

4.2.2 Measurements and results: Physical characterization

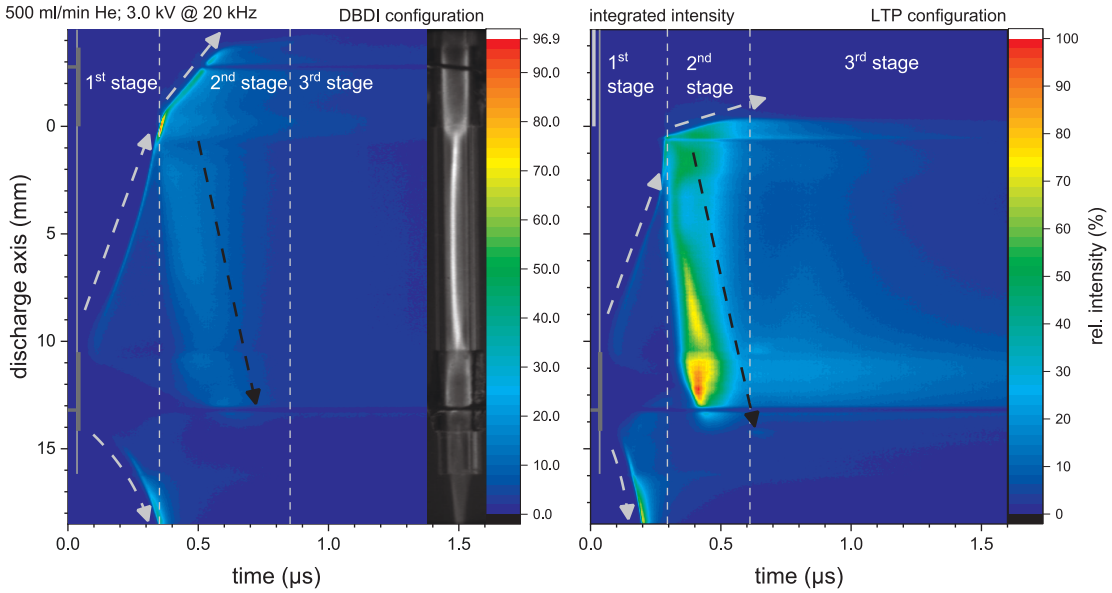

Figure 4.7: Comparison of the DBDI and LTP configurations of the vDBD. The discharge was operated with 500 ml/min He and 3.0 kV at 20 kHz. The partly open electrodes allow an insight into the usually covered region beneath the electrodes. The development of both discharge configurations can be divided into the the three stages, marked by the vertical light grey lines, that were already described during the characterization of the standard DBDI in the previous chapter.

First measurements of the vDBD in DBDI configuration, presented in figure 4.7, reveal that the plasma development is very similar to the behavior of a standard DBDI, which subsequently means that the vDBD is a suited substitute of the DBDI.

The vDBD exhibits essentially the same three plasma stages as the normal DBDI, which means that the plasma develops from an initial streamer stage that spreads from the HV electrode outwards forming the plasma jet and inwards to the grounded electrode. Using the vDBD and the partially open electrodes reveals that the streamer develops from the edges of the HV electrode where the highest electric fields can be expected.

The Streamer also forms a rather thin channel in the middle of the capillary as depicted in the photograph inset of figure 4.7 and is even more pronounced due the bigger inner diameter of the capillary that is used for the vDBD.

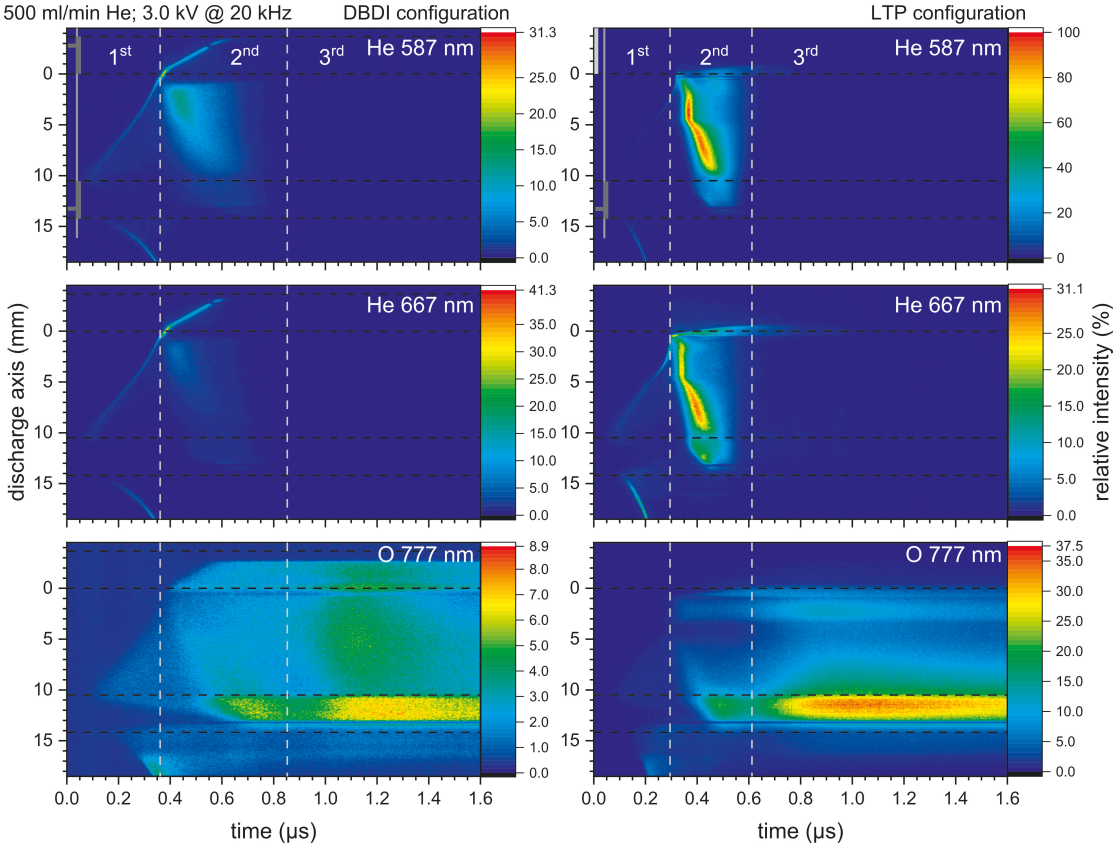

Figure 4.8: Measurements of the He 587.6 nm (top), He 667.8 nm (middle) and O 777.6 nm (bottom) lines in DBDI (left) and LTP (right) configuration. The discharges were operated with the same parameters as in 4.7. The intensity of the measurements were all normalized to the overall highest intensity measured, which was the emission of the He 587.6 nm line in LTP configuration.

The thin channel remains until the streamer reaches the vicinity GND electrode where it seemingly splits and reaches out towards the capillary walls. The streamer, now moving along the inner wall of the capillary moves further upstream, while at the same time the re-ignition of the 2nd stage plasma occurs. This reversed excitation wave moves downstream of the capillary and moves towards the former HV electrode and also splits and spreads towards the walls when it reaches the vicinity

of the electrodes. Although the open electrodes reveal some new information about the development of the plasma in a DBDI like configuration, this behavior is essentially the same as the one discussed in the previous chapter. The more interesting development is the one of the LTP like configuration that is also shown in figure 4.7. While the differences of the LTP to the DBDI configuration are quite obvious, they also share many common traits.

The development of the plasma in the LTP configuration, also starts at the edges of the HV electrode and spreads outwards, which is essentially the same as in the DBDI configuration. The streamer during this 1st plasma stage also moves towards the GND electrode and initiates the 2nd stage as soon as it reaches the electrode. However, the transition of the LTP like configuration to the 2nd stage of the plasma in particular shows some differences to the development of the DBDI configuration. Most striking is the abrupt ending of the streamer which stops directly at the tip of the wire electrode and does not propagate further upstream.

The pin electrode of the LTP configuration allows for a free flow of charges due to the absence of a dielectric layer, which means that the streamer can simply discharge at the pin electrode, in contrast to the DBDI configuration where the streamer is forced to deposit its charges on the dielectric surface.

This free access to the electrode surface and more efficient discharge of the streamer also leads to a much stronger 2nd plasma stage which is indicated by the much stronger emission of the LTP configuration during this stage. Spectrally resolved measurements further confirm the impression of a stronger 2nd plasma stage for the LTP configuration as presented in figure 4.8.

Both the He 587.6 nm emission, which is an indirect indicator of He metastables as well the O 777.6 nm emission, which is primarily caused by the collision of O_2 molecules with He metastables, suggest that the population of He metastables is more pronounced in the LTP configuration as in the comparable DBDI configuration. This overall higher emissivity and population of metastable states in the LTP configuration is most likely caused by an increase of charges that can flow through the discharge.

The pin electrode that is in direct contact with plasma allows for a free flow and electric discharge of the charged species produced during the streamer stage. The pin electrode also seems to increase the amount of charges that are present in the discharge as presented in figure 4.9 (a).

The grounded pin electrode has a major influence on the amount of charges that can flow through the discharge, especially if one considers that both discharge configurations use the same HV electrode. This stresses the importance to differentiate between full- and half-dielectric barrier discharges as the difference between these two configurations seems to be quite significant. Related to the higher amount of charges in the LTP is also the higher overall emission that can also be measured in the LTP configuration as shown in figure 4.9 (b).

Increasing the amount of charges that are available in a discharge at the same time increases the amount of excited species and as a result the overall emission due to a higher interaction of these species. The apparent stronger influence of the

decreasing applied voltage on the emission of the LTP configuration is caused by the fact that the emission of the DBDI was also normalized to the maximum value of the LTP configuration. This was done to underline the fact that the DBDI configuration has the overall weaker emission but also leads to the impression of weaker decrease of emission in the DBDI configuration.

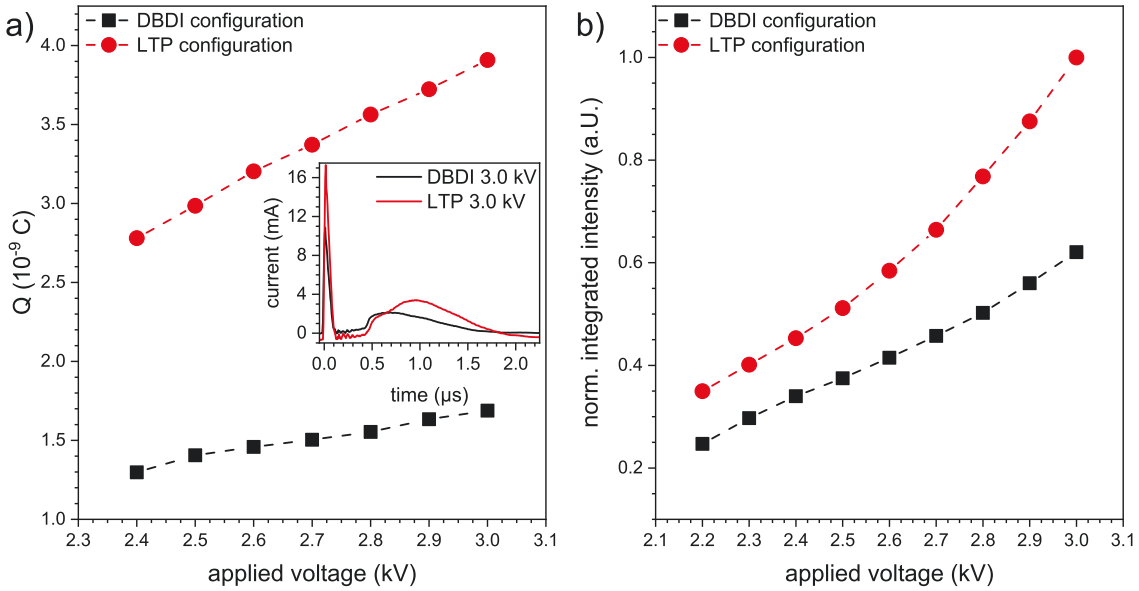

Figure 4.9: a) Total amount of charges Q generated in the DBDI and LTP configuration. The discharges were operated with 500 ml/min He each. The inset shows the time resolved currents for the DBDI and LTP configuration at 3.0 kV. Background measurements without a discharge were take to subtract the displacement current contribution before integration. b) Wavelength integrated emission of the DBDI and LTP configuration. The values were normalized to the highest measured intensity which was emitted by the LTP configuration.

The relative reduction of the DBDI emission amounts to roughly 39.8 % and therefore is only slightly less than the 34.9 % reduction reached by the LTP configuration. While the integrated reduction of emission is similar for both configurations, the wavelength resolved approach reveals high discrepancy in emission lines that can be connected to dissociative excitation processes revolving around helium metastable states.

Figure 4.10 reveals that the highest difference of emission between the two discharge configurations occurs at the He 587.6 nm and O 615.7 nm lines, the former being an indicator of the population of the He 2s $^3S_1$ metastable state and the latter being a result of collision processes of oxygen molecules with said He metastables.

The apparent rise of the O 615.7 nm emission at low voltages in the DBDI configuration is not caused by a more efficient dissociation for this configuration at lower voltages but rather by an overly steep decrease of this emission line in the LTP configuration, which drastically changes the ratio. It can be stated that the LTP configuration is an excellent source for dissociative excitation at higher voltages but quite noticeably loses this capability with falling applied voltages.

Nevertheless, the LTP configuration produces a constantly higher amount of charged species and also emission compared to a discharge operated in DBDI configuration and otherwise same conditions. While the objective observations of the LTP configuration strengthen the impression of a more powerful and efficient discharge compared to an equivalent discharge operated in DBDI configuration, these observations do not explain the reason why the LTP is the seemingly more efficient discharge yet.

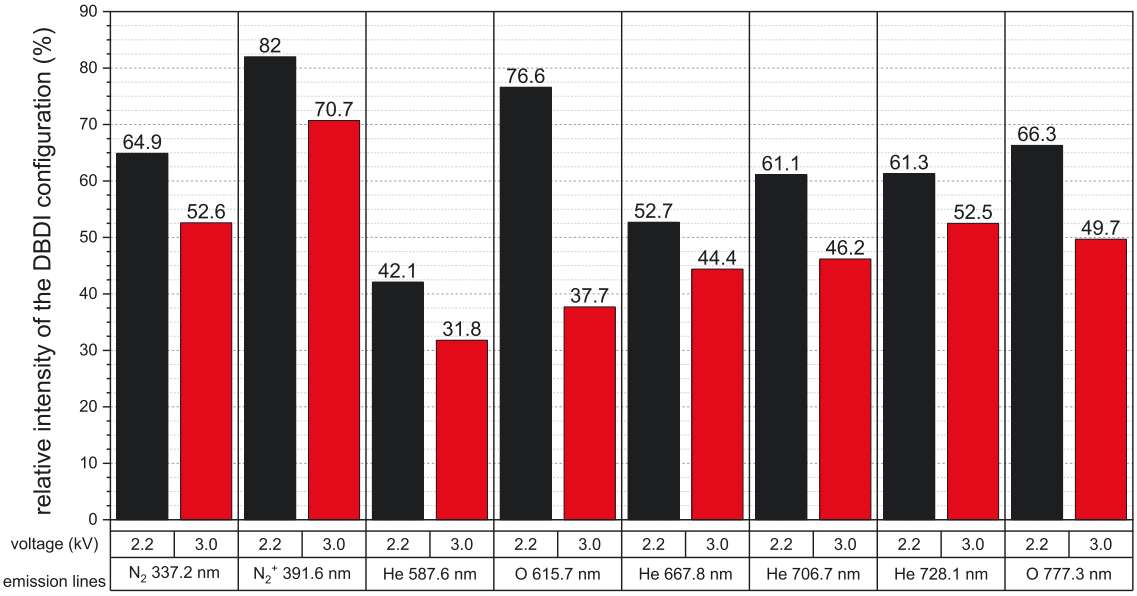

Figure 4.10: Relative intensity of several chosen emission lines in DBDI configuration. The intensities of the emission lines were normalized to the respective intensity values of the LTP configuration at the applied voltages of 2.2 kV and 3.0 kV.

The increase of charges might be connected to the direct contact of the grounded electrode with the plasma, however the simple presence of a metal surface inside the plasma cannot explain the significant amount of additional charges that are created in the LTP configuration. The streamer model used to explain the development of the plasma so far assumes that an excitation wave is created during the initial polarization caused by the change of the high electric fields.

These waves develop on the edges of the HV electrode were the electric field is the highest and begin to propagate away from the HV electrode. Considering that both discharge configurations use the same HV electrode it is not surprising that the early phases of the plasma development looks very similar for both as one can see in figures 4.7 and 4.8 but a more careful review still reveals some significant differences.

Figure 4.11 presents the development of the discharges on the basis of emission profiles that are taken out from representative points in time. This presentation of the data is more suited to highlight smaller differences between the two discharge configurations that are otherwise overlooked in the usually used 2D-contour plots of the data. It can be directly seen that both discharges do indeed start at the HV electrode shortly after the initial positive polarization happens, however the formation

of the excitation waves in the LTP configuration seems to be significantly faster and stronger than the formation that can be observed in the DBDI configuration.

This applies in particular to the formation of the outwards directed streamer which forms the plasma jet and is already strongly developed only 0.15 µs after the polarization for the LTP configuration whereas this streamer is barely noticeable for the DBDI configuration. It takes an additional 100 ns before the outward streamer of the DBDI configuration is as developed as it was for the LTP configuration, at which time the streamer of the LTP configuration has already propagated beyond the field of vision of the measurement and cannot be seen in figure 4.11 (b) anymore.

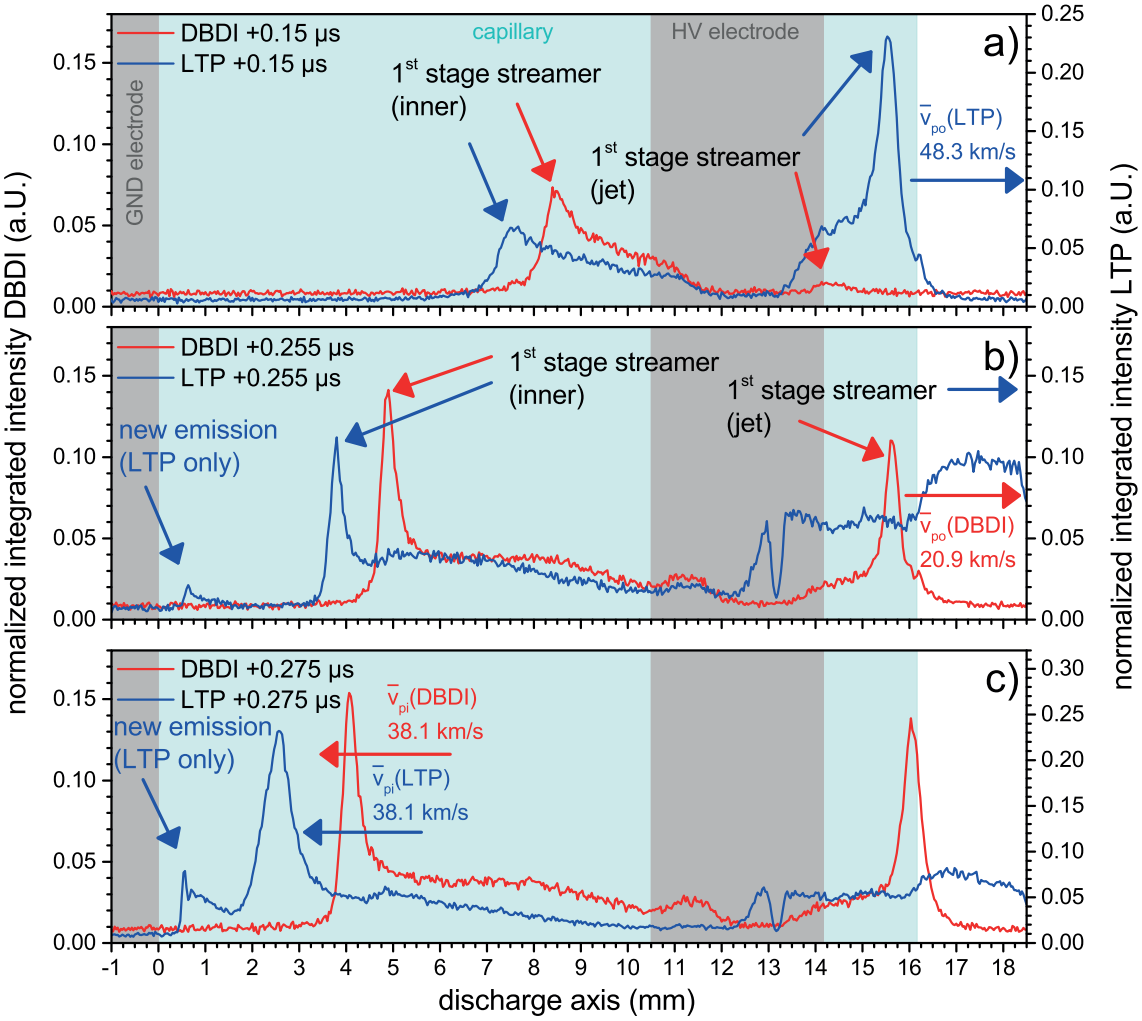

Figure 4.11: Emission profiles of discharges operated in DBDI (red) and LTP (blue) configuration. The database used is the same as in figure 4.7, the only difference is the method of presentation which is used to highlight differences between the two discharge configurations that are otherwise overlooked in the the standard 2D-contour depiction that is usually used

This behavior was already reported [56], however it still is only possible to acknowledge the fact that the outward streamer of the LTP configuration develops and also propagates much faster than the equivalent streamer of the DBDI configuration. The reported propagation speed of said streamer in LTP configuration measured dur-

ing the study in 2017 was 37.2 km/s and therefore clearly higher than the 21.4 km/s that were reached by the DBDI configuration. The mean velocities of the outward directed propagation in this quasi repetition measurements of the previous study are $\bar{v}_{po}(\mathrm{LTP}) = 48.3\,\mathrm{km/s}$ for the LTP configuration and $\bar{v}_{po}(\mathrm{DBDI}) = 20.9\,\mathrm{km/s}$ for the DBDI configuration.

This demonstrates that these results are reproducible, however a fully satisfying explanation for the faster development of the outward directed streamer propagation in the LTP configuration can still not be given at this point in time. Some of the explanation attempts in the previous study included the overall higher amount of charges that are created in the LTP configuration.

While a higher amount of charges could very well lead to a change of the discharge equilibrium over time and result in a overall stronger initial polarization during the changing high voltage, it does not satisfyingly explain why this increased polarization only influences the outwards directed streamer propagation and not the inward directed propagation.

The mean velocity of this inward directed 1$^{\mathrm{st}}$ streamer amounts to $\bar{v}_{pi}(\mathrm{LTP}) = \bar{v}_{pi}(\mathrm{DBDI}) = 38.1\,\mathrm{km/s}$ for the discharges in both configurations and is therefore exactly the same. The different positions of the two streamer peaks in 4.11 is only caused by a slightly delayed beginning of the streamer propagation for the DBDI configuration which sets in several nanoseconds later and therefore slightly lags behind the streamer that forms in the LTP configuration.

The reason for this delay could be a systematic difference between the two discharge configurations but could also be caused by a small drift of the overall discharge operation in time, which can be hardly avoided during long term measurements. The reason for this slight delay that can be observed is ultimately irrelevant, and much more interesting and important is the fact that the inward streamers have the same mean propagation velocity contrary to the outwards directed streamers where a faster development for the LTP configuration can be clearly observed.

The different propagation speeds of the outward directed streamer is unexpected considering the fact that the difference between the LTP and the DBDI configuration occurs at the grounded electrode which is positioned in the direction of the inward directed streamer and therefore would suggest a stronger dissimilarity in this part of the plasma instead of the opposite directed streamer as it can be observed.

What has to be stressed at this point is the fact that the unexpected similarities described in the previous part only refers to the inward directed 1$^{\mathrm{st}}$ stage streamers that are marked by a respective arrow in figure 4.11. The overall development of the plasma inside of the capillary still shows major differences between the two discharge configurations, as a “new emission” phenomenon appears for the LTP configuration. This phenomenon does not occur when the discharge is operated in the usual DBDI configuration and therefore will be referred to as “new” or “additional emission” in the lack of a better name.

This new emission develops during the propagation of the inward directed 1$^{\mathrm{st}}$ stage streamer and first occurs when the wave crosses roughly half the distance of the electrode gap as presented in figure 4.11 (b) and (c). The emission occurs di-

rectly at the pin electrode and retains its highest intensity at the surface of this pin electrode. At the same time however, it seems as if the emission is spreading from the pin electrode towards the streamer as if it is attracted by the excitation wave front which is closing in.

The occurrence of this new emission was already reported in the original study from 2017 but was not further elaborated on as other differences between the two discharge configurations were deemed to be more relevant at that point in time. A way of interpreting this new emission phenomenon results from a discharge configuration that can occur while using the vDBD system but was originally not intended and therefore not considered in the original study. The vDBD cannot only be operated in the LTP and DBDI configurations that were described so far, it can also be operated in a kind of "hybrid" mode.

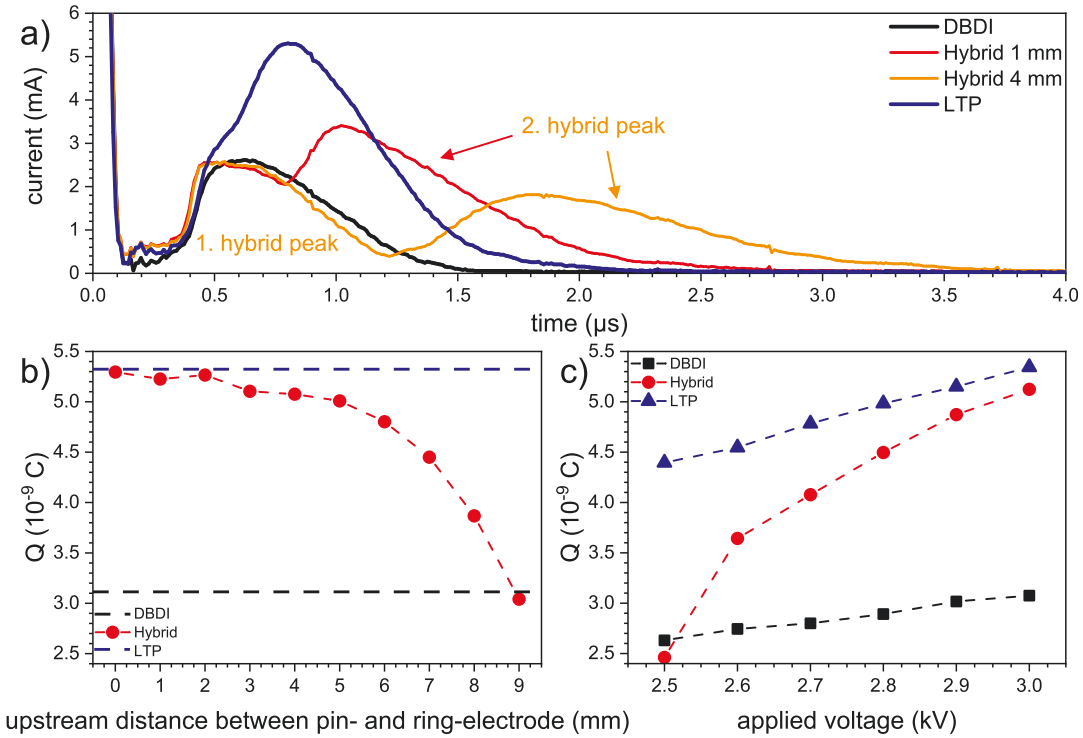

Figure 4.12: a) Time resolved currents of the vDBD in DBDI (black), Hybrid (red and orange) and LTP (blue) configuration. The hybrid discharge was measured at two distances of the inner pin and outer ring electrode: 1 and 4 mm. b) Total amount of charges Q for the hybrid discharge configuration in dependence of distance between the pin and outer ring electrode. The discharge was operated with the same amount of gas and an applied voltage of 3.0 kV. The dashed lines indicate the charge values for the LTP and DBDI configuration at the same settings. c) Total amount of charges Q in dependence of the applied voltage for the three discharge configurations. The discharge was operated with 500 ml/min of He and the distance between the pin and outer ring electrode for the hybrid discharge was approximately 4 to 5 mm.

The hybrid mode occurs when the discharge is switched from one configuration to the other while still being operated. The most common way for the hybrid discharge to occur is when the pin electrode is moved in to the plasma volume before the outer ring electrode is detached or moved further upstream. At a certain point, depending

on the remaining distance of the pin and ring electrode and the applied voltage, an additional discharge will form between the two grounded electrodes. A photo of this hybrid discharge is shown in figure 4.6 at page 64 where it was used to demonstrate that the vDBD can freely switch between the two discharge configurations. While the occurrence of such an additional discharge can be expected when a conducting surface is brought into the vicinity of a running plasma, some of the demonstrated characteristics of it were still very surprising and subsequently lead to naming this particular configuration hybrid discharge.

Figure 4.12 (a) presents the time resolved currents of all three discharge configurations. The difference between the pure LTP and DBDI configurations were already discussed in figure 4.9 (a) where the overall larger plasma peak for the LTP configuration also results in a higher amount of charges. Much more interesting is the fact that the current produced by the hybrid discharge displays two clearly separated plasma peaks, the first being mostly identical to the one created in the DBDI and the second one rising much later around 2 µs after the displacement current.

The position and shape of this second peak is highly dependent on the position of the pin electrode and the resulting distance between the pin and outer ring electrode. The bigger the distance between these two electrodes the bigger is the shift of the maximum of the second current peak in time as shown in figure 4.12 (a) and (b). Increasing the distance between the two electrodes will stretch out this additional discharge phenomenon of the hybrid configuration, continuously decreasing its contribution until it completely vanishes and the hybrid discharge switches to a pure DBDI configuration again, as presented in figure 4.12 (b).

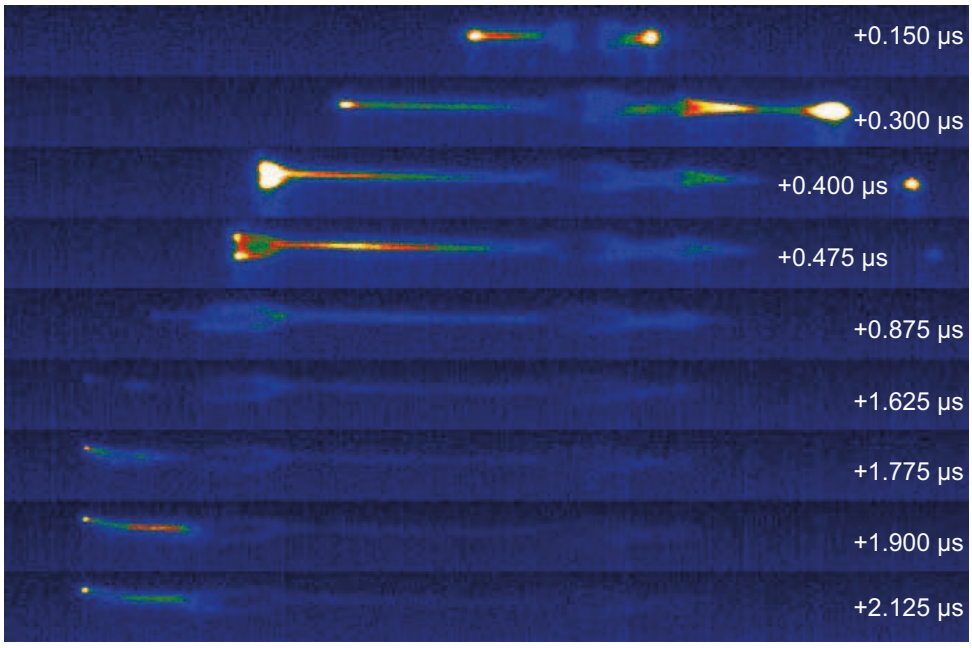

Figure 4.13: Image series of the vDBD in hybrid configuration. The discharge is shown at different points of time that are representative for the plasma development. The discharge was operated with 500 ml/min of He and an applied voltage of 3.0 kV.

This additional discharge phenomena is not a dark discharge that only produces an electrical current, the matching emission can also be measured as presented in

figure 4.13. The development of the hybrid discharge is not different from the usual DBDI during the first 1.5 µs and exhibits the usual development of the 1st stage streamers that propagate away from the HV electrode and subsequently transitions to the 2nd plasma stage. This is not surprising considering that the additional current peak of the hybrid configuration does not start to appear after 1.25 µs at an electrode distance of 4 mm.

The electrode distance in the optical measurement of the hybrid configuration is roughly the same and one can see that emission is spreading from the pin electrode toward the grounded ring electrode from 1.625 µs onward. However, it has to be noted that the initial streamer started in the 1st stage of the original plasma still seems to propagate towards the pin electrode and therefore could also play an important role in the development of the observed emission. Overall the propagation of this late emission strongly resembles the "new emission" which was discussed before regarding the LTP configuration in figure 4.11 and is most likely the same phenomenon observed under slightly different conditions.

The hybrid discharge configuration described so far can best be characterized as a phenomenon that only occurs during the transition from the DBDI to the LTP discharge configuration or vice versa. The most important factor for the hybrid discharge is the distance between the inner pin and outer ring electrode.

The hybrid configuration seamlessly switches to the LTP configuration as soon as the inner pin electrode is moved beyond the edge of the outer ring electrode. The outer ring electrode is effectively cut off at this point and does not play any role in the plasma development anymore. The switch to the LTP configuration implies that the additional plasma contribution provided in the hybrid configuration merges with the usual streamer initiated plasma created in the full-dielectric configuration. The discharge configuration referred to as half-dielectric would then be the superposition of these two discharge contributions.

While the mechanism of the full-dielectric barrier discharge was already intensively studied during the previous chapters of this work, the same cannot be said about the additional discharge contribution provided by the half-dielectric barrier configuration represented by the hybrid as well as the LTP configuration. Considering just the simple physical observables, such as the total amount of charges Q or the emission of the discharges, it clearly seems as if the half-dielectric barrier discharge is the more efficient configuration as it clearly produces the higher amount of charges and also more emission than the comparable full-dielectric barrier variant.

Closer observation reveals that this higher amount of charges as well as emission can be attributed to an additional discharge contribution that superimposes on the original discharge mechanism that is already present in the full-dielectric barrier configuration. While the operation of the hybrid discharge configuration makes a clear differentiation of the original and new discharge contributions possible it still does not reveal the exact source of the new discharge contribution and still leaves it up to speculation.

The new discharge contribution seems to originate from the pin electrode and either spreads to the grounded outer ring electrode in the hybrid configuration or

towards the HV electrode in LTP configuration where it merges with the 2nd stage coincident plasma as was shown e.g. in figure 4.11. The emission at the pin electrode starts before the 1st stage streamer either in hybrid or LTP configuration reaches the metal surface which limits the potential processes that could be responsible for its ignition.

The most likely source for the observed excitation and emission is the rapid acceleration of secondary electrons that are released from the metal surface however it is not clear by which process this electrons are emitted. Electron emission due to the bombardment of the metal surface with heavy particles such as He metastables, N_2^+ or other ions seems to be unlikely, as the emission on the surface starts clearly before the 1st stage streamer and the aforementioned species can actually reach the pin electrode. Other sources of these secondary electrons could be photons respectively the photoelectric effect.

While the streamer formation itself is heavily reliant on high energetic photons and photoionization for its propagation, it can be assumed that the actual reach of the produced VUV photons that are driving this photoionization process is very short, due to the high gas pressure and resulting density of potential absorbents. It can be assumed that the range of the photons produced in the 1st stage streamer is similar to that of the heavier particles and can also not reach the pin electrode early enough.

Another potential situation that can develop in the half-dielectric barrier configurations investigated so far is the formation of a quasi direct discharge between the grounded pin electrode and the propagating positive streamer. The positive streamer that develops during the 1st stage of the plasma is an accumulation of excited and much more importantly positive charged species that moves towards the pin electrode. This accumulation of positive charges acts in a similar way on the pin electrode as a normal positively charged electrode with a positive voltage applied to it would. This means that an electric field will develop between this virtual electrode pair, subsequently leading to the formation of plasma between them if the electric field is strong enough.

A discharge like this is of a direct nature as there is no dielectric which blocks either of the electrodes but at the time it is still not a pure direct discharge due to the fact that the supply and free flow of charges is globally seen limited by the dielectric layer that is still blocking the outer ring electrode. In this context the LTP as well as the hybrid discharge configurations cannot only be seen as half-dielectric but also half-direct discharges.

The formation of a direct discharge like plasma between the pin electrode and the virtual positive electrode formed by the 1st stage plasma streamer cannot be inarguably proven yet. No reference measurements for a direct discharge in a capillary arrangement similar to the LTP configuration exist, which means that no systematic comparison between the half-dielectric respectively half-direct and full-direct discharge is possible at this moment in time. Nevertheless, describing half-dielectric barrier discharges like the vDBD in LTP or hybrid configurations as a superposition of a regular full-dielectric barrier discharge and direct discharge contribution seems to be the most convincing explanation at the moment.

While this matter definitely deserves some further research, it can be also stated that the pure physical characterization so far was sufficient to find out that the full- and half-dielectric barrier discharge configurations exhibit some major differences in their developments. To put it simple, the half-dielectric barrier discharge seems to produce the more efficient plasma in all considered regards, simply by the fact that the plasma that is already present in the full-dielectric configuration is superimposed by an additional plasma contribution, independent of this additional plasma contribution being a direct plasma discharge or not.

The original study from 2017 aimed at finding these exact observable differences and also wanted to verify the potential impacts on the analytical performances of these two discharge types. Therefore, it was decided that a further characterization of the superposition of these two discharge mechanisms has to be left to future studies and not to neglect the comparison in front of an analytical application, which will be summarized in the following part of this work.

4.2.3 Measurements and results: Analytical performance

Both discharges the LTP and the DBDI can be used as ionization sources for analytical mass spectrometer applications. While the general purpose of the two discharges in an analytical application is essentially the production of ions, the approach of how they are implemented is clearly different. The DBDI is primarily used as an ambient ionization source similar to established other plasma based ionization sources such as e.g. corona discharges that are used for atmospheric pressure chemical ionization (CD-APCI) [9, 59]. Both these methods, the DBDI and the CD-APCI, require an additional analyte supply which vaporizes samples and transports it to the active regions of the the plasma discharge. The LTP does not necessarily require an additional analyte supply, as it can directly desorb and subsequently ionize analytes from the surface of a sample [60, 61]. This greatly simplifies the application of the LTP, due to the fact that a majority of the sample preparation is omitted.

The detailed characterization of both discharge types and the following comparative analytical tests, have been aimed at finding the reason for the different applicability of these two discharges and if the difference between a full- and a half-dielectric barrier discharge plays a fundamental role.

The variable dielectric barrier discharge (vDBD) allows for a quick change between these two discharge configurations while at the same time keeping all other external parameters constant. The vDBD is mounted in front of a Thermo LTQ mass spectrometer and essentially used in the same way as a normal DBDI. This means that the analyte is supplied externally in vaporized form by either head-space or gas chromatography (GC), which enables a direct comparison of the ionization efficiencies of both discharge configurations.

The vDBD allows for a seamless switch between both discharge configurations without stopping either the discharge or mass spectrometer operation, enabling an easy and direct comparison of the measured mass spectra. The ionization efficiency

of a discharge usually depends on many external factors which of course include the parameters of the plasma itself that can be controlled very well, but also include several factors which are more difficult to control. Some of these parameters are e.g. the position of the discharge relative to the mass spectrometer, or the composition of the atmosphere. These two factors in particular complicate an exact comparison of two discharges or discharge configurations, as an exchange of a discharge usually requires an interruption of the measurement.

Subsequent continuation of a measurement afterwards is difficult due to the fact that it usually cannot be guaranteed that the exchanged discharge is placed in the exact same position as the previous discharge. An adjustment of the discharge position depending on the signal intensity as it is usually done, defeats the purpose of a comparison measurement as it might give a completely different optimal position for the exchanged discharge.

The vDBD is therefore the best option to compare the full- and half-dielectric discharge configurations as it enables an objective comparison and guarantees that all observed changes to the measured mass spectra are only caused by the switching of the electrode configuration, which occurs "on the fly" without interruption.

Another factor that could influence the objectivity of the measurements are the parameters used to control the Thermo LTQ itself, which in contrast to the usual approach of mass spectrometer measurements where deliberately fixed. The range of the mass scan was fixed to a mass over charge ratio range of 50 m/z to 400 m/z and the automated gain control (AGC) was deactivated throughout the measurements with a maximum injection time of 100 ms[1].

Fixing the parameters of the mass spectrometer ensures that all observed changes in the measured mass spectra are only caused by a switching of the discharge mode and not by an automated correction algorithm of the mass spectrometer that usually tries to optimize the signal to noise ratio (SNR) of a measurement by minimizing the amount of background ions.

The analytes used for testing include hexane (C_6H_{14}), menthone ($C_{10}H_{18}O$) and propachlor ($C_{11}H_{14}ClNO$). While hexane and menthone represent standard chemicals which are very suited for the comparison of the two discharge modes due to their easy and well studied mass spectra, propachlor was chosen due to the fact that is a herbicide and therefore also provides an analytical relevance. Another reason for choosing these three chemicals is the fact that the ionization with the plasma is rather simple, straightforward and therefore easy to interpret.

As mentioned before, one of the biggest advantages of dielectric barrier discharges as ionization sources for analytical mass spectrometer measurements is the fact that the ionization of the molecules in question happens in a "soft" way. However this characterization only means that the analyte molecule in question is not dissociated by the plasma and remains mostly intact, but does not exactly define the ionization process the analyte was subjected to.

[1] A complete list of all MS parameters can be found of in the supporting information of the original study published in 2017 [56]

The most prominent mechanism is the protonation of an molecule which means that a proton, in other words a Hydrogen atom without its electron, attaches to a neutral molecule with the mass $[M]^0$ to form a new positively charged molecule with an increased mass of $[M+1]^+$. While the exact details of this protonation are still under investigation, it still produces easy to interpret mass spectra for hexane, menthone and also propachlor, the last one being presented in figure 4.14.

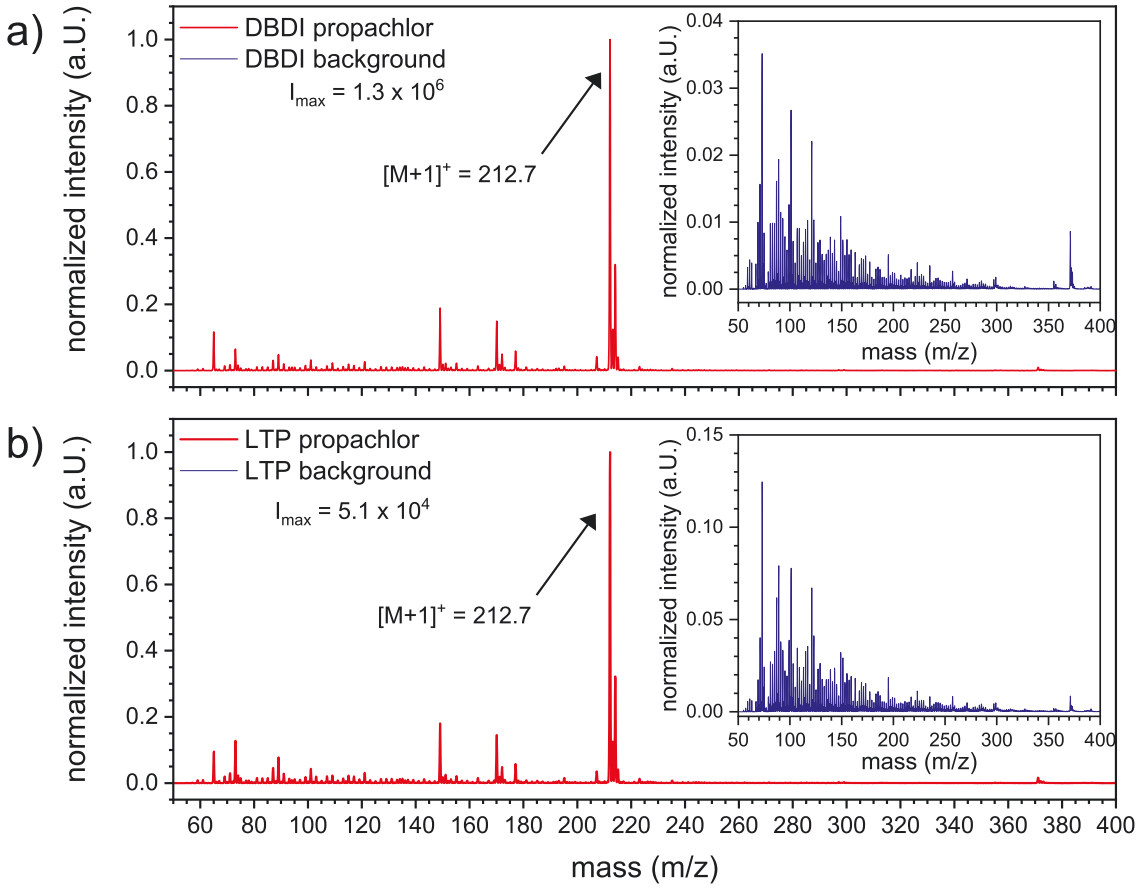

Figure 4.14: Normalized mass spectra of propachlor measured with a vDBD in DBDI (a) and LTP (b) configuration. The spectra were normalized to their respective highest intensities I_{max} and the inlets show the respective background spectra of each discharge configuration which are normalized to the same values [56].

Both discharge configurations show qualitatively very similar mass spectra, with the peak of the protonated propachlor at 212.7 m/z being the largest in the whole spectrum. Also the smaller peaks in the range of $140 - 180$ m/z and $60 - 100$ m/z have a very similar heights compared to the main ion peak. The similar mass spectra imply, that the ionization of the propachlor in both discharges follows a very similar mechanism and also yields fundamentally the same ionized species, however the ionization efficiency of both discharges seems to be different.

The ionization efficiency can simply be described as the amount of ions that are produced by a certain discharge configuration and afterwards measured by the mass spectrometer. The maximum intensity of the protonated propachlor peak in DBDI configuration is $1.30 \cdot 10^6$ counts/s which is 25 times higher than the $5.07 \cdot 10^4$

counts/s which can be measured in LTP configuration. The difference of the protonated ion signals is surprisingly high, even more so considering that the spectra look qualitatively nearly the same. This implies that the general ionization mechanism that produces the protonated ions is essentially the same in both discharge configurations and the only difference is the total yield of ions.

This is surprising due to the fact that the LTP configuration was considered to be the more efficient discharge configuration after the initial characterization. Furthermore, the observed reduction of measurable ions in the LTP configuration does not only affect the protonated ion peak but all positive species in the observed mass range and also the background species as shown in the inset of figure 4.14 (b).

While a reduction of the protonated ion peak with a simultaneous increase of ion signals at lower masses could easily be explained by an increase of fragmentation in the plasma discharge, the observed overall decrease simply implies that less positive charged ions arrive at the mass spectrometer. This is, as was mentioned before, surprising considering the LTP configuration provides the more efficient plasma but obviously is providing smaller ion current to the mass spectrometer.

The even reduction of ions throughout all mass ranges, means that the quality of the LTP as an ion source is not that much worse than that of the DBDI configuration, although the absolute signal intensity is 25 times smaller. The reason for this is the fact that the quality of a mass spectrum is not evaluated purely on the absolute intensities of the measured ion peaks but always takes the signal to noise ratio into consideration.

The ratio between the average background signals and the relevant ion peaks objectively states in how far the measured ion peak can be still differentiated from the background noise of a measurement. The SNR for the discharge configurations presented in figure 4.14 is 5931 for the LTP and 7626 for the DBDI configuration respectively which is around 1.3 times higher.

The DBDI configuration is qualitatively the better ionization source compared to an equivalent LTP configuration, but by a smaller margin than the initial lower signal intensities implied. However, the absolute reduction of positive ions in the LTP configuration by more than an order of magnitude is still a very interesting phenomenon from a mechanistic point of view, furthermore considering that a higher overall signal intensity is in general always beneficial.

A possible explanation for why the LTP configuration seemingly produces less positive ions revealed itself by chance when the vDBD was switched from one discharge configuration to the other during a mass spectrometer measurement. The pin electrode of the LTP configuration was disconnected from the electrical grounding during this switching, which means that it became a floating electrode with no direct connection to an electric circuit.

The difference between this floating state and the usual grounded state was easy to spot in the mass spectra as the amount of ions rapidly rose from a value of $5.07 \cdot 10^4$ counts/s to $1.03 \cdot 10^6$ counts/s. This signal intensity is close to what could be measured with the DBDI configuration, as shown in figure 4.15.

The floating state of the electrode also leads to an increase of SNR from 5931 to 7366 which is again close to the value that is reached in the DBDI configura-

tion. Furthermore, the floating state of the electrode also influences the vDBD when it is in DBDI configuration although the absolute signal increase is only from $1.30 \cdot 10^6$ counts/s to $1.52 \cdot 10^6$ counts/s which is only an increase by a factor 1.17 instead of the factor 20.3 reached in the LTP configuration. Also the increase of SNR with only 16.9 % for the DBDI configuration is weaker than the increase of 24.2 % in the LTP configuration but the improvement of the SNR caused by the floating electrode state is at least comparable for the two discharge configurations.

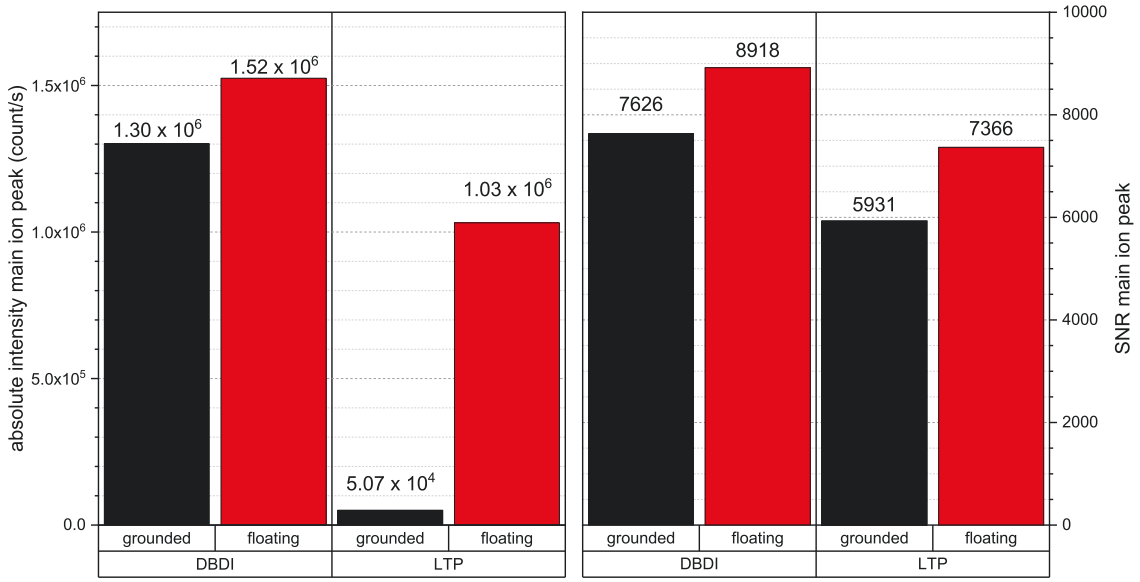

Figure 4.15: Absolute signal intensities (left) and signal to noise ratios (right) of the protonated main ion peak of propachlor. The paired bars of the DBDI and LTP configurations also show the difference between the grounded (black) and floating discharge states (red) [56].

The most notable effect of switching the electrode state from grounded to floating is the massive increase of overall positive ions that can be measured in the LTP configuration which is supposedly the less efficient ion source. One possible explanation for this strong increase could be that the floating state of the pin electrode in LTP configuration restricts the free flow of charged particles to the pin electrode.

Introduction of a metal surface to a plasma usually leads to large a amount of electrons escaping the plasma volume due to their high mobility. To counter this loss of electrons, the plasma develops an electric potential that traps electrons inside the plasma volume and accelerate positive ions out oft it to balance the initial loss of electrons and sustain the quasi neutrality of the plasma. This ambipolar diffusion due to the formation of plasma sheath potentials strongly depends on the properties of the electrodes that are introduced to the plasma.

The amount of charges that can flow through a floating pin electrode is strictly limited, as it will charge up over time until a saturation is reached. The amount of charges that can be deposited on the floating pin electrode depends on its capacitance which is usually negligibly small and leads to a seemingly instantaneous switch between grounded and floating electrode state.

Implementation of additional capacitors to enlarge the capacitance of the pin electrode leads to a larger amount of charge that can be deposited and a prolonged charging phase that can be easily observed over a long period of time as shown in figure 4.16. The system allows for a rather free flow of charges during the charging of the capacitors and therefore resembles a discharge with a still grounded pin electrode. The charging of the capacitors depend on their total capacitance and can be finished after only some minutes as for the 0.022 µF capacitor or can take up to half an hour as it is the case for the 1 µF capacitor. The quasi free flow of charges is stopped as soon as the capacitors are fully charged and the discharge converges on a state that resembles the floating discharge configuration.

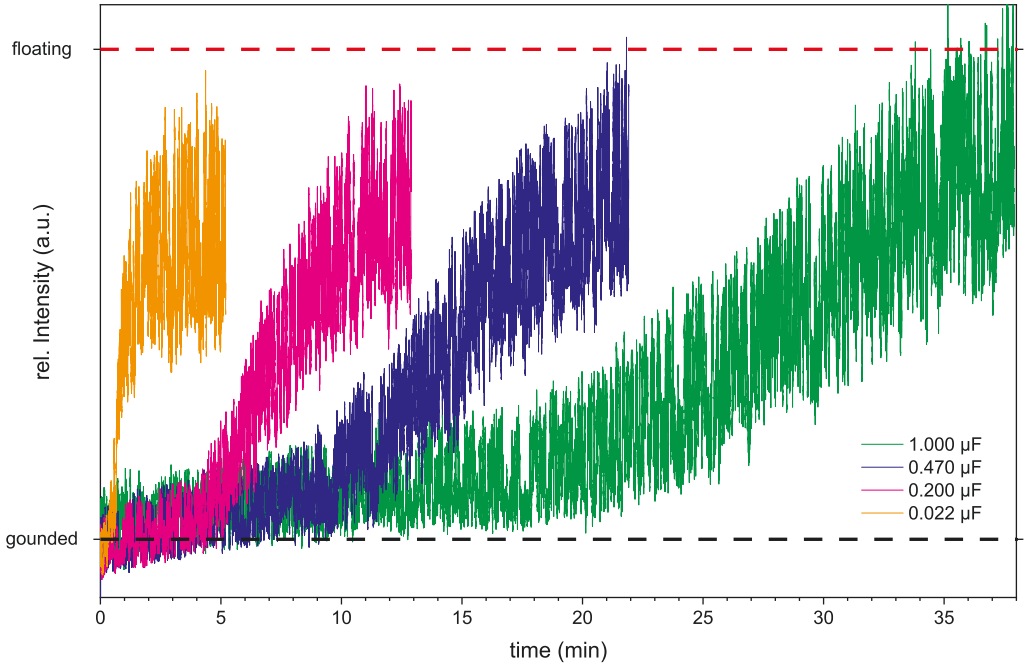

Figure 4.16: Positive ion signal of the mean ion peak of menthone measured at 155.3 m/z over time in vDBD operated in LTP configuration. The black dashed line indicates the median of the signal obtained for the grounded pin electrode state and the red dashed line the respective floating one. The colored lines show the development of the signal for different capacitors connected to the pin-electrode of the vDBD and disconnected from the ground of the electrical circuit at $t = 0$ min [56].

The increase of the positive ion signal that can be observed due to the floating electrode state is not yet fully understood and investigated but can be at least interpreted in a way that the charge transport of the LTP configuration becomes more similar to the conditions that are present in the DBDI configuration.

Charged species are able to gather and exchange in the vicinity of the electrode tip as long as the connection of the pin electrode to the external electric circuit exist. This situation is not given anymore when the pin-electrode is disconnected from the external circuit and the amount of charged particles that can flow through the pin electrode is effectively limited. The conditions ultimately become very similar to the ones given in the DBDI where the free flow and exchange of charges is always limited by the dielectric layer, which was already discussed in the physical characterization

of the two discharge configurations. In reference to these physical characterizations, the change of the discharge from a grounded to a floating state of the pin electrode also leads to a clear reduction of emitted light from plasma that is even noticeable by the naked eye.

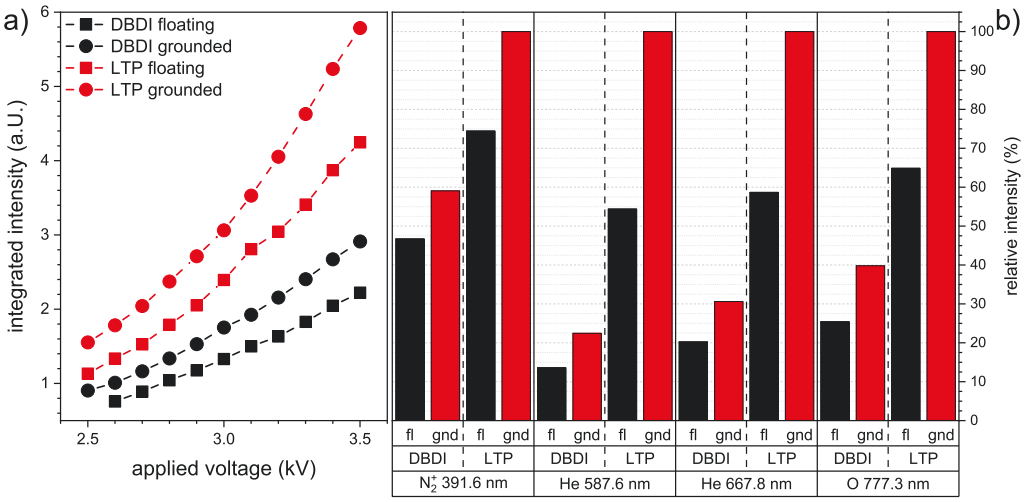

Figure 4.17: a) Integrated intensity of the vDBD in DBDI (black) and LTP (red) configuration at different operation voltages. The curves clearly show the decrease of intensity when the electrode state is switched from the grounded (dashed circle) to the floating (dashed squares) state. b) Relative intensity of the N_2^+ 391.6 nm, He 587.6 nm and 667.8 nm and O 777.3 nm emission lines at an applied voltage of 3.5 kV. The bars are additionally sorted for the different discharge configurations and electrode states. The intensities of the emission lines are all normalized to the highest intensity measured for each line, which was in all cases the grounded LTP configuration.

The LTP configuration is clearly the brighter discharge configuration even for the floating electrode state, as figure 4.17 shows. However the relative reduction of emission due to the floating electrode state is stronger for the LTP configuration as for the DBDI configuration. This result very well complements the measurement of the menthone signal presented in figure 4.15 where the floating electrode state also improves the intensity and quality of both discharge configurations signal leading to overall better mass spectrometer signals. Nevertheless, the relative improvement of the intensity and quality was much larger for LTP configuration than for the DBDI configuration, which means that the floating electrode state clearly impacts the LTP configuration in a more noticeable way.

In contrast to the physical characterization it is not possible to definitely state in how far the floating electrode state leads to a reduction of charged species by the further restriction of the flow and exchange of charged species as it was done in e.g. figure 4.9 (a). The floating electrode state leads to a disconnection of the whole discharge from the grounded part of the electric circuit and therefore prevents the measurement of the discharge current. Careful evaluation of optical measurements presented in figure 4.17 reveals that the reduction of emission that can be observed in the LTP and DBDI configuration due to the floating electrode state, correlates fairly well with the increase of the ion signal.

Switching the electrode state clearly decreases the overall emission from the plasma in both configurations. The decrease seems to be more pronounced in the LTP configuration, however this has to be accounted to the overall higher emissivity of the LTP configuration that is already known from figure 4.9 (b). This simply leads to a stronger decrease in absolute numbers for the LTP configuration, but the relative decrease of emission for both discharge configurations accounts to approximately 20-25 % which is a very close range to each other.

The same conclusion arises at a closer examination of certain emission lines that are presented in 4.17 (b) where a quick glance at the strong decrease of the line emission for the LTP configuration leads to the impression that the decrease for the DBDI configuration is much weaker. However, the relative decrease of emission for each emission line caused by the floating electrode state is comparably strong for both discharge configurations.

More important than the difference in absolute intensity between the emission lines of the two discharge configurations, already mentioned in figure 4.10, is the varying impact of the floating electrode state on the different emission lines. The relatively weak decrease of the N_2^+ 391.6 nm line by 25.5 % for the LTP and 20.9 % for the DBDI configuration and the much stronger decrease of the He 587.6 nm line by 45.6 % and 39.4 % respectively, implies a shift to the whole discharge mechanism.

While figure 4.17 (a) shows that restraining the flow of charges does most likely reduce the overall excitation in the discharge, figure 4.17 (b) reveals that in particular the population of the high energetic He and He metastables states is affected more by the floating electrode states than the positive ion species of the plasma. The reduction of these He metastable states could lead to a "weaker" discharge and subsequently less dissociation which correlates very well with the relative reduction of the O 777.3 nm emission which also decreases by 35.1 % in the floating LTP configuration and 36.0 % in the DBDI configuration respectively.

Summarizing the results from above: The floating electrode state seems to lead to a shift in the discharge mechanism that influences both discharge configurations in a similar way. The floating electrode seems to lead to an overall reduction of excitation in the plasma which seems to affect the population of highly excited He metastable atoms stronger than the population of positive ion species such as N_2^+.

This shift of the discharge mechanism could very well lead to a better signal to noise ratio, as it can be observed in figure 4.15 (b), due to the fact that reduced dissociation of the plasma would most likely lead to the detection of less background ions. However, the over proportionate strong increase of the menthone ion signal by more than an order of magnitude in the LTP configuration presented in figure 4.15 (a), cannot be sufficiently explained by the already discussed factors alone.

The grounded LTP configuration of the vDBD is a significantly worse ion source for the Thermo LTQ MS compared to an equivalent DBDI configuration in regards of absolute ion yield, as the amount of protonated ions that reach the detection device is 25 times smaller. This is a remarkable reduction, considering that the same amount of analyte is supplied for both discharge configurations of the vDBD.

One explanation for the smaller ion signal could be an increased dissociation of the analyte and therefore decrease of protonated signal, however the comparable signal to noise ratios of both discharge configurations and no noticeable increase of fragmented ions in the presented mass spectra of figure 4.14 do not indicate a loss of analyte ions through an increase of dissociation and fragmentation. Switching the electrode state from grounded to floating simply leads to a higher amount of positive ions that can be detected with the Thermo LTQ mass spectrometer when the vDBD is operated in LTP configuration. It seems as if the overall ion current from the discharge to the MS instrument is strongly influenced by the electrode state and simply increases when the wire electrode of the LTQ configuration is set to floating.

These results show that the focus of the ongoing investigations should not only lie on understanding the mechanism of the soft ionization that occurs but also on the transport of the generated reactive species and subsequently charged analyte species. Current studies show that the process called "soft ionization" cannot be defined by a single mechanism so far and the formation of positively and also negatively charged analyte ions are very complex chemical reactions often involving substitution reactions with radical oxygen or similar chemically active species [33, 34]. Therefore, it is even more important in this context to carefully consider how the ionized molecules are transported and moving towards the detecting instrument.

The regular distance between a DBD based plasma ion source and the inlet of the mass spectrometer is at least 10 mm to avoid arcing between the plasma and mass spectrometer. Assuming the standard DBDI with an inner diameter of 466 µm is operated with a usual flow of $100 - 200$ ml/min of He this means that the mean linear velocity of the gas stream inside of the discharge capillary is in the range of $9.8 - 19.5$ m/s for a non turbulent flow. These velocities are certainly quite high and produce quite strong and easily noticeable gas streams, however the movement of single particles and atoms becomes negligible on the timescales of the plasma excitation.

Previous parts of this work have shown that excitation mechanisms in the plasma discharge usually only occur in the first few microseconds after the initial polarization. The distance that could be covered by a single particle in these few microseconds by gas flow alone is at most in the range of $0.02 - 0.08$ mm. The potential distance a particle could cover in a half period is roughly 0.5 mm which means that a particle that is produced in the plasma would need approximately ten full discharge periods to cover the aforementioned 10 mm between plasma source and mass spectrometer inlet, purely driven by the gas-flow alone.

These approximations assume that the linear velocity of the gas leaving the capillary remains constant which it most likely will not due to turbulence created between the high velocity gas flow and the ambient atmosphere outside of the capillary and also the difficult to estimate pumping flow of the mass spectrometer. Nevertheless gas flow alone appears to be a too slow to explain a sufficient amount of charged species to eventually reach the mass spectrometer before they decay and recombine under atmospheric conditions.

A reasonable assumption is that the charges species created by the plasma are not only transported by the gas flow, but are additionally accelerated by relatively constant potentials that might develop between plasma and mass spectrometer inlet. The existence of such plasma potentials and their development is relatively well studied and also used in several technical applications and they could very well be responsible for the formation of a strong ion current between plasma source and mass spectrometer [18, 62, 63].

Plasma potentials are heavily influenced by the external electrical circuit and can therefore be manipulated to a certain degree. Such a manipulation, although somewhat unintentional, seems to have occurred by the introduction of the floating electrode state which might have lead to the formation of floating plasma potential that created a more favorable ion current for the soft ionization process.

This means that the effects caused by the difference between floating and grounded electrode state observed from figure 4.15 onward might not indicate a drastic change in the the generation of reactive species and subsequently more ionized analyte but a change of the transport of these generated ions to the mass spectrometer. First tests with electrical circuits allowing for additional and deliberate offsets of the plasmas potential in relation to the grounded mass spectrometer show clear changes in the ion yield that can be measured with the mass spectrometer. However these are just preliminary tests and need further careful consideration and planning before the role of ion transport for the soft ionization mechanism can be properly investigated.

Further investigations in these direction would have exceeded the scope of the work already published in 2017 [56] and also the scope of the this overarching dissertation. The initial intention of the comparison between the full-dielectric barrier discharge represented by the DBDI like configuration and the half-dielectric barrier discharge represented by the LTP, was to find and characterize fundamental differences in the discharge development and combine those findings with potential discrepancies that might occur in further applications.

Detailed measurements confirm that there is a fundamental difference between the full- and half-dielectric barrier discharges that is independent of other external parameters of the discharge and only depends on the grounded electrode being in direct contact with the plasma or not. While further measurements revealed interesting effects like e.g. the floating state of the grounded electrode, the initial objective of the comparison can be regarded as fulfilled and further investigations should be discussed in separate studies.

However, a final topic regarding half dielectric barrier discharges and their special characteristics still remains and will be discussed in the next and final chapter of this dissertation.

5 POLARITY OF HALF DBDS: THE INVERSE LTP CONFIGURATION

The polarity of the applied voltage is a factor that only played a minor role in the characterization of the DBDI so far. The two ring electrodes of the standard DBDI are fixed to the outside of the glass electrode and are therefore in a broader sense equivalent in their positions. This means that it does not matter which of the two electrodes is connected to the HV and which to the ground output of the HV generator for the general development of the plasma itself. The excitation of the plasma is mainly independent of the much slower gas flow and other external factors and only depends on the direction of the electric field.

Switching of the two electrodes would, as demonstrated in figure 5.1 on page 88, only lead to a plasma igniting and extending from the upstream electrode. The phenomenon referred to as "plasma jet" would extend further upstream and the inner 1^{st} stage streamer would propagate downstream in the direction of the capillary orifice until it reaches the grounded electrode and transition to the 2^{nd} plasma stage that would be directed upstream again. The general process can therefore be seen as a simple inversion of the usual development of the plasma in the DBDI.

Switching the polarity of the electrodes becomes a more interesting factor in the case of a half-dielectric barrier discharge such as the LTP like configurations of the vDBD, as one of the electrodes in this configuration is in direct contact with the plasma that forms inside of the capillary. The previous chapter already revealed some significant differences between the development of the plasma in the DBDI and LTP configurations that are only caused by the grounded wire electrode of the LTP which is in direct contact with the plasma.

This chapter of this work will deal with the effect of the electrode polarity and its impact on the development of the plasma and changes to the overall discharge parameters. The majority of the investigations will focus on the LTP and inverse LTP (iLTP) like configurations, due to the fact that the electrode polarity does not play a major role for full-dielectric barrier discharges such as the DBDI.

The conclusion of this last chapter will be the presentation of a new type of discharge, the flexible micro tube plasma (FμTP), that was developed from the findings of the iLTP configuration and represents a new, robust and easy to handle plasma source for the soft ionization of analytes for mass spectrometer applications.

5.1 Influence of the polarity on the DBDI and LTP configurations

The characterization of the electrode polarity is in general a continuation of the characterization of the vDBD from the previous chapter 4.2 onward. Switching the polarity of the electrodes in full dielectric barrier configuration like the DBDI mainly influences the propagation direction of the excitation waves inside of the capillary but does not change anything major to the general mechanism, as can be seen on the left side of figure 5.1.

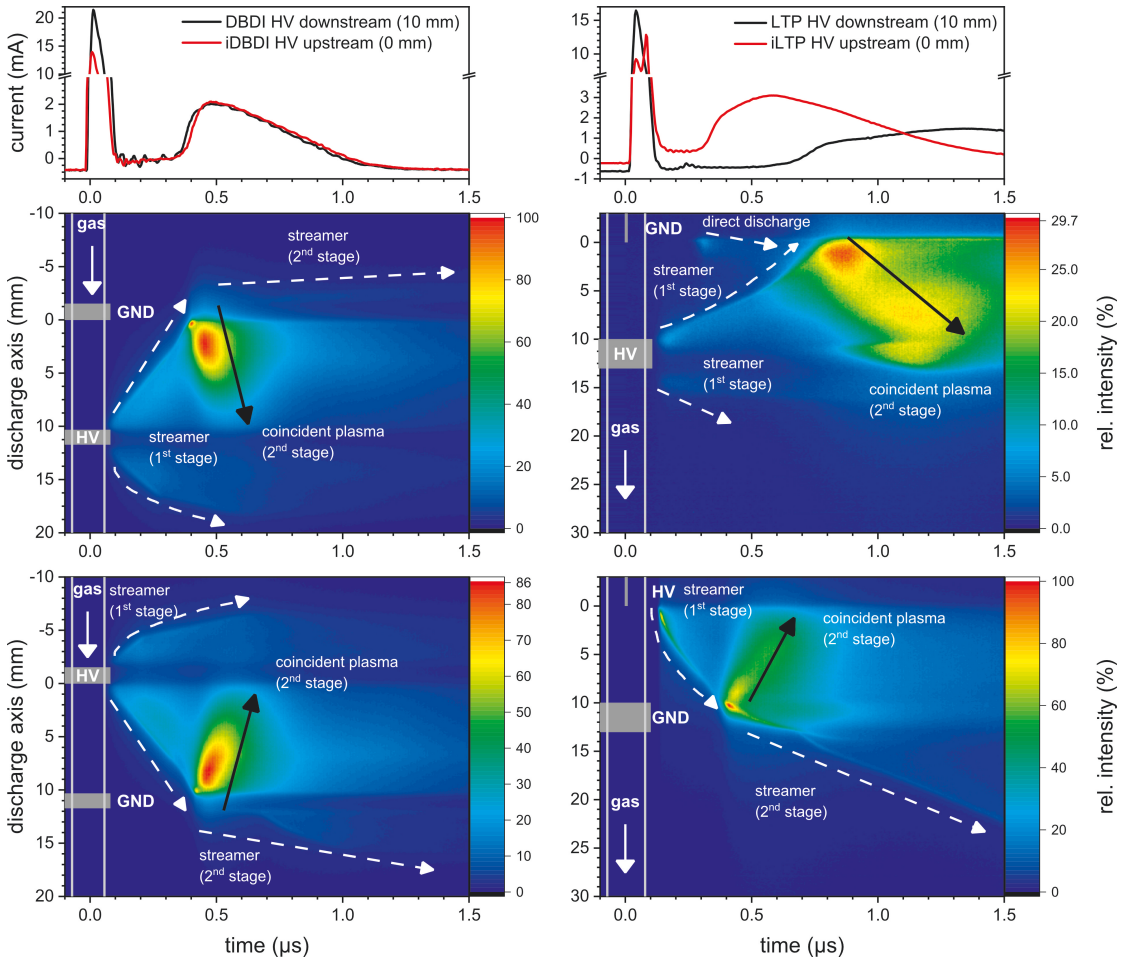

Figure 5.1: Emission measurements of the full-dielectric DBDI (left) and half-dielectric LTP (right) configurations. The top row of measurements shows the usual polarity of the electrodes with the HV electrode downstream of the gas flow and the GND upstream. The reverse polarity is shown in the bottom row of measurements.

The electrodes are essentially symmetric and equivalent to one another and the only break of the systems symmetry is the flow of the applied gas. However the propagation of the gas particles due to the flow is at maximum in the range of only some 10 m/s assuming an inner diameter of the capillary of 0.5 mm, a gas flow of 500 ml/min and a completely laminar and undisturbed gas flow through the capillary. Even assuming these ideal conditions, a gas velocity of 10 m/s is orders of magnitudes

slower than the propagation velocity of the streamer which typically reaches several 10 km/s depending on the discharge type and the applied voltage. The movement of gas particles in an otherwise symmetrical system should therefore not influence the development of the plasma in a major way and can indeed be mostly neglected as will be shown by the further discussion of the results shown in figure 5.1.

The left column of this figure shows the typical configuration of the DBDI with the HV electrode downstream of the gas in the middle of the figure and the inverted iDBDI version with the HV electrode upstream above the grounded electrode at the bottom of the figure. The only major difference between these TSSR-OES measurements from the ones already explained in previous chapters such as e.g. figure 4.7 on page 65, is the fact the capillary is exceptionally long to place the electrodes as far away from the capillary orifice as possible. This further increases the symmetry of the whole system and decreases the influence of disturbing effects such as gas diffusion and mixing that usually occur at the capillary orifice. The symmetry of the system ultimately leads to very similar plasma discharges developing for the normal DBDI and its inverted polarity case the iDBDI, which will be described in detail in the following.

Both discharges start with excitation waves spreading from the respective HV electrode and towards the grounded electrode. In addition a second wave forms at the opposite electrode edge and extends further down- or upstream the capillary. This additional excitation wave would normally form the plasma jet that extends outward of the capillary, but due to the extra long capillary it can not reach the orifice and extinguishes after it reaches its maximum length. The propagation speed and relative intensities of the excitation waves in both polarity cases is nearly the same and clearly shows that the movement of the gas particles due to the superimposing gas flow plays only a minor role in the propagation of the excitation waves.

The reversal of the electrode polarity in a symmetric full dielectric barrier discharge such as this special setup DBDI, only leads to a simple reversal of the excitation direction. Other differences in the left column of 5.1, such as the slightly lower emission intensity that is measured in the upstream HV electrode case, can be explained by the fact that the two ring electrodes are not completely identical. It can be concluded that the polarity respectively the position of the electrodes might only be considered due to technical reasons of a given analytical application, as it only plays a minor role in the excitation mechanisms of a full-dielectric barrier discharge configuration such as the DBDI.

The excitation waves also originate from the respective HV electrode of the LTP and iLTP configurations, as was the case for the DBDI and iDBDI configurations. However, in the case of the iLTP the excitation wave only develops in the direction of the grounded electrode and does not split off in the opposite direction as it can be observed for the HV ring electrodes of the DBDI, iDBDI and normal LTP configurations. The reason for the absence of this split off streamer lies in the asymmetry of the pin electrode which suppresses the development in the opposite direction.

This asymmetry leads to a focused formation of the excitation wave of the 1st stage streamer into one single direction, which is more pronounced as in the case of

the normal LTP and its outer ring electrode. The focusing of the 1st stage streamer leads to a higher propagation velocity of the excitation wave which can be seen in the much smaller dependence of Δt on the applied voltage for the iLTP version presented in figure 5.2 (a). The earlier occurrence of the coincidence plasma for the iLTP configurations can in addition easily be made out in the emission of the plasma presented in figure 5.1. The transition to the 2nd plasma stage already occurs at 0.43 µs for the iLTP configuration which is clearly faster than the transition at 0.85 µs for the normal LTP configuration.

Another difference between the two discharge configurations is the amount of emission they both produce. The maximum emission both for LTP and iLTP configuration occurs at the transition of the plasma to the 2nd stage. However, the intensity of the peak emission of the normal LTP configuration only reaches roughly 30 % of the intensity that is reached in the iLTP configuration. Integration of the emission also shows that the overall emission of the normal LTP configuration is much lower compared to the iLTP configuration although the emission seems to spread over a much longer time frame.

Figure 5.2 (b) shows that LTP and iLTP configuration produce nearly the same amount of charged species, which is not such a surprise due to the fact that the electrical capacitance and with it the charge of the system should not change by the simple switch of electrode polarity. This however means that the correlation between the amount of charges of a plasma and the emission it produces is not valid for all cases anymore.

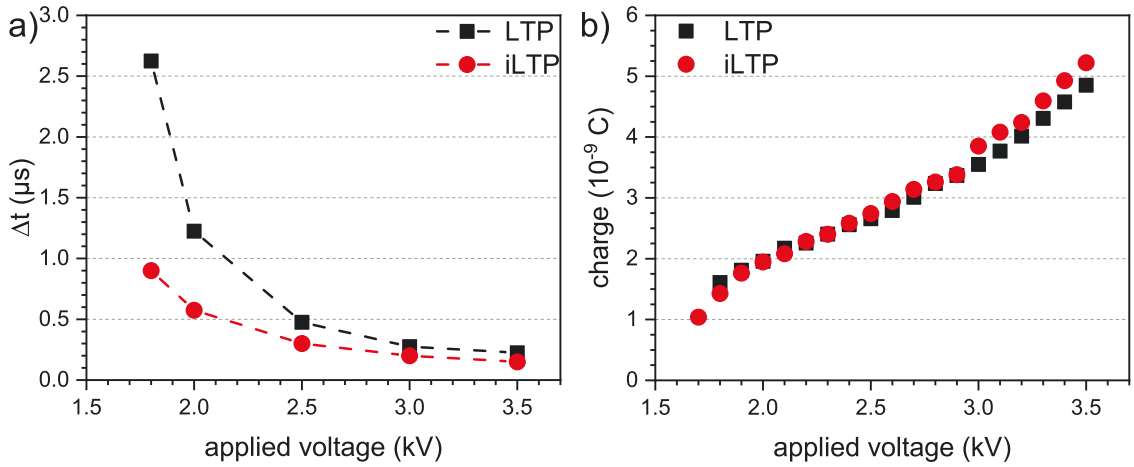

Figure 5.2: a) Time delay Δt in dependence of the applied voltage for the LTP (black) and iLTP (red) configurations. The weaker dependence for the iLTP configuration indicates a faster transition from the 1st to the 2nd plasma stage compared to the LTP configuration. b) Amount of charges Q for the LTP (black) and iLTP (red) configurations in dependence of the applied voltage. The amount of charges is nearly identical for both configurations.

The comparison of full- and half-dielectric barrier discharge in chapter 4.2 showed that this correlation between charges and emission was a good approximation in most of the cases. Increasing the total amount of charges Q by e.g. increasing the applied voltage, switching from a full- to half-dielectric barrier configuration or change of the electrode width also increased the emission as e.g. described in figure 4.9 on page

68. However, the influence of the gap between the electrodes already indicated that this correlation is not necessarily always true.

Similar to the present observations, figure 4.3 (b) on page 59 showed that the gap between the electrodes influences the charges only in a minor way, while figure 4.4 showed a strong impact of the gap on the emission of the plasma. First explanations of this behavior revolved around the density of the plasma and in how far a change to the gap between the electrodes could influence it. Increase of the gap would effectively stretch out the plasma and increase the volume in which the charged species could interact, while not changing their amount. This could very well decrease the chance of interaction between the charged species and decrease the overall excitation in the plasma.

The change of the electrode polarity in the iLTP configuration could lead to a contrary behavior, where a more focused development of the 1st stage streamer in only one single direction could increase the chances of charged particles to interact and subsequently increase the excitation of the developing plasma. Verification of both these assumptions requires a better knowledge about the densities of relevant species inside the plasma discharges or a better definition and understanding of the effective volume that a plasma in a dielectric environment occupies.

Further investigations in this direction are not practical at this point in time. A reasonable measurement of particle densities in these kind of atmospheric plasmas would require too much effort and would subsequently distract from the most important difference between the LTP and iLTP discharge configurations that still needs to be discussed. This difference occurs after the 1st stage streamer reaches the grounded electrode and ignites the coincident plasma at the transition to the 2nd plasma stage.

As was already explained in the previous chapter 4.2, the streamer of the normal LTP configuration stops at the pin electrode and is completely discharged, due to the fact that electrode is in direct contact with the plasma volume and not covered by any dielectric layer. In the case of the iLTP however, the streamer is only partly discharged at the grounded ring electrode, which is outside of the capillary and therefore not in direct contact with the plasma. This subsequently leads to a continuation of the initial streamer during the 2nd stage of the plasma.

This behavior can also be observed in the DBDI and iDBDI configuration, in particular if the applied voltage is very high or the grounded electrode is very small. This will lead to a bottleneck effect as discussed in the context of figure 4.2 on page 58. The continuation of the streamer during the 2nd plasma stage is therefore not really surprising in itself. Due to the fact that the streamer of the iLTP configuration is much more focused from the start this subsequently also leads to a strongly pronounced and long streamer during the 2nd plasma stage as presented in figure 5.3.

The scale of the continuing streamer in the iLTP configuration is much more impressive than the ones known from the DBDI configurations and can easily reach several centimeters. The length of the streamer is very depended on the applied voltage, as one can see from figure 5.3, were the length of the iLTP streamer measured from the edge of the grounded ring electrode can linearly be increased by 7.2 cm/kV.

Using the maximum voltage of the generator allows the streamer to reach a final length of approximately 15 cm which is 15 times longer than the plasma between the electrodes. This length is most likely caused by a dielectric guiding effect as reported by other studies [64].

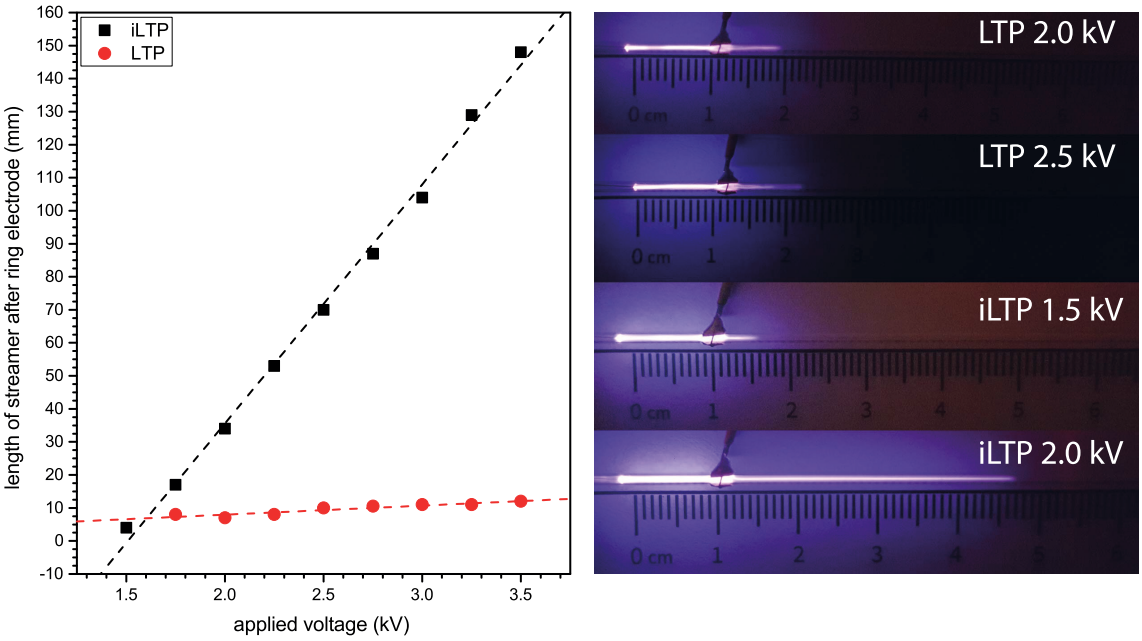

Figure 5.3: Streamer length in dependence of the applied voltage for the LTP (red) and iLTP discharge. The discharges where operated in a 20 cm long quartz capillary with an inner diameter of 1.0 mm and outer diameter of 1.5 mm that was flushed with 500 ml/min of He 5.0. The streamer length depicted on the left side of this figure was measured from the outer edge of the see through ring electrode at approximately 1.2 cm on the scale

The dielectric guiding is caused by the polarization and further charging of the capillary which prevents charges from the streamer to settle and discharge on the surface of the capillary. The streamer is therefore guided further through the center of the capillary and travels until all the initial excitation is completely used up. It has to be stated that the described behavior is only valid for this special case and discharge configuration used for these measurements.

The maximum length of the streamer and its dependence on the applied voltage are determined most likely by several geometric parameters such as e.g. the ratio of inner and outer diameter, the material composition of the glass itself and the width of the grounded electrode which discharges the streamer that passes under it. These parameters all influence the capacitance of the system and therefore also the dielectric guiding effect and have to be better understood before any predictions regarding the general behavior of these elongated streamers can be done.

Extensive parameter studies would exceed the scope of this work and are also not necessary at this point of time. The most important parameter which can influence the propagation of the streamer during the 1st and 2nd plasma stage that is not connected to the geometry of the discharge itself, is the applied voltage as one can see in figure 5.2 (a) and 5.3. Figure 5.2 (a) clearly shows that an increase of the applied

voltage leads to smaller Δt values leading to a faster transition to the 2nd plasma stage and effectively accelerating the propagation of the streamer. At the same time the increase of voltage also leads to drastic increase of the maximum length of the streamer as illustrated in figure 5.3.

Other parameters that can be changed during the operation of the plasma such as e.g. the gas flow or its composition on a minor scale do not influence the streamer in a meaningful way. This means that the length of the streamer is only dependent on a single major parameter which is the applied voltage. This small amount of relevant parameters and the simple fact that the iLTP configuration produces these very long 2nd stage plasmas open up new approaches to analytical applications that subsequently lead to the creation of a new discharge type, the flexible micro tube plasma (FμTP).

This miniaturized plasma based ionization source is based on the findings of the iLTP configuration and was specifically developed for mass spectrometer and ion mobility spectrometer applications. The next part of this work will briefly describe the steps that lead from the characterization of the iLTP configuration and the subsequent development of the FμTP which can be seen as a culmination of all the characterization effort of dielectric barrier discharges in this whole work.

5.2 The flexible micro tube plasma: a new design for plasma based soft-ionization

The flexible micro tube plasma (FμTP) is an advancement from the old DBDI design and tackles many of the problems that deal with coupling of ionization source and mass spectrometer, robustness and overall user-friendliness by implementing the findings of the previous characterization chapters. The most important finding for the development of the FμTP was the discovery of the pronounced streamer propagation in the iLTP configuration.

As mentioned before, the development of the streamer seems to depend on the dielectric guiding effect that develops in the dielectric capillary during the operation of the plasma. The operation of a plasma charges the surface of the capillary over time and without sufficient means to discharge it again, it forces the excitation wave to further propagate along the charged capillary surface.

This behavior can also be observed in DBDI configurations were either the ratio between HV- and grounded-electrode width or very high voltages lead to insufficient discharging of the propagating streamers. This insufficient discharging will lead to a bottleneck effect that was already described in figure 4.1 on page 56 and can lead to a very pronounced overshoot of the streamer discharge beyond the grounded electrode. However, this overshoot is only in the range of some 1 mm to 10 mm for a typical DBDI.

The most obvious advantages of the new discharge design is the fact the HV electrode is inside of the insulating dielectric, making a direct contact and short circuits nearly impossible. This danger is further minimized by the very long streamers of the iLTP configuration, which can be guided over several centimeters and therefore

potentially further increasing the distance between the HV wire and orifice of the dielectric.

Another advantage of the streamer covering these large distances is the fact that the active HV electrode can be placed far away from applications that are easily disturbed by fluctuating high electric fields usually created by the operation of plasma. One of these applications that is normally disturbed by the operation of plasma in its vicinity is the electrospray ionization source (ESI), which is one of the most common mass spectrometer ionization source. Placing a DBDI next to a ESI can suppress the development of an electrospray due to the interference between the electric fields of both sources.

Combination of a plasma based ionization source with an electrospray based source might increase the performance of a given analytical application, due to the fact that the plasma source might ionize analytes that were not yet ionized in the electrospray process. The synchronization of these two very different ion-source types so far failed due to the fact that the generation of the plasma always suppressed the development of a sufficiently strong electrospray [65, 66].

First test of the FµTP showed that it might be a suitable workaround for this problem as its HV electrode can be placed far enough away from the ESI to the electrospray process but still provide enough reactive species to noticeably enhance the ionization process [58].

The FµTP used in this study is in principle a miniaturized version of the iLTP configuration, which uses commercially available high performance liquid chromatography (HPLC) equipment to allow for very tight connections with minimal gas leakage. The polyimide coated capillaries perfectly fit in the HPLC connections and their flexible nature greatly reduces the risk of accidentally breaking the discharge apart. The biggest difference between the FµTP and the bigger iLTP, other than the obvious size and material, is the fact that the FµTP does not use a grounded electrode.

Further tests with the iLTP configuration revealed that the development of the 1^{st} stage streamer will also occur in the absence of a grounded electrode as one can see from figure 5.4. The removal of the grounded electrode leads to a complete suppression of the coincident plasma and no apparent transition to a 2^{nd} plasma stage can be identified.

Although it seems as if the emission of the groundless iLTP version is less intense than the emission of its grounded counterpart, this impression is only partly correct. The emission at the tip of the wire amounts to approximately 80 % of the maximum measured intensity in both cases meaning that both streamers start out similarly bright.

However, the highest intensity can only be measured in the case of the standard iLTP configuration at the moment of the 2^{nd} stage transition. The standard version of the iLTP is overall brighter compared to the not grounded version, but only due to the fact that the part of the discharge that is responsible for the majority of the emission does simply not occur in the un-grounded case.

Both discharge configurations produce very similar streamers and the un-grounded iLTP configuration is the second possibility to create a “streamer only discharge” where the transition of the discharge to a 2^{nd} stage is suppressed. This new method

seems to be much more reliable compared to the plasma tuning method that was briefly presented in previous parts of this work (see chapter 3.4.1) and also already published by Schütz et al. in 2016 [52]. The removal of the grounded electrode completely and securely prevents accidental re-ignition of a coincident plasma, that occasionally can occur when the plasma tuning method is used.

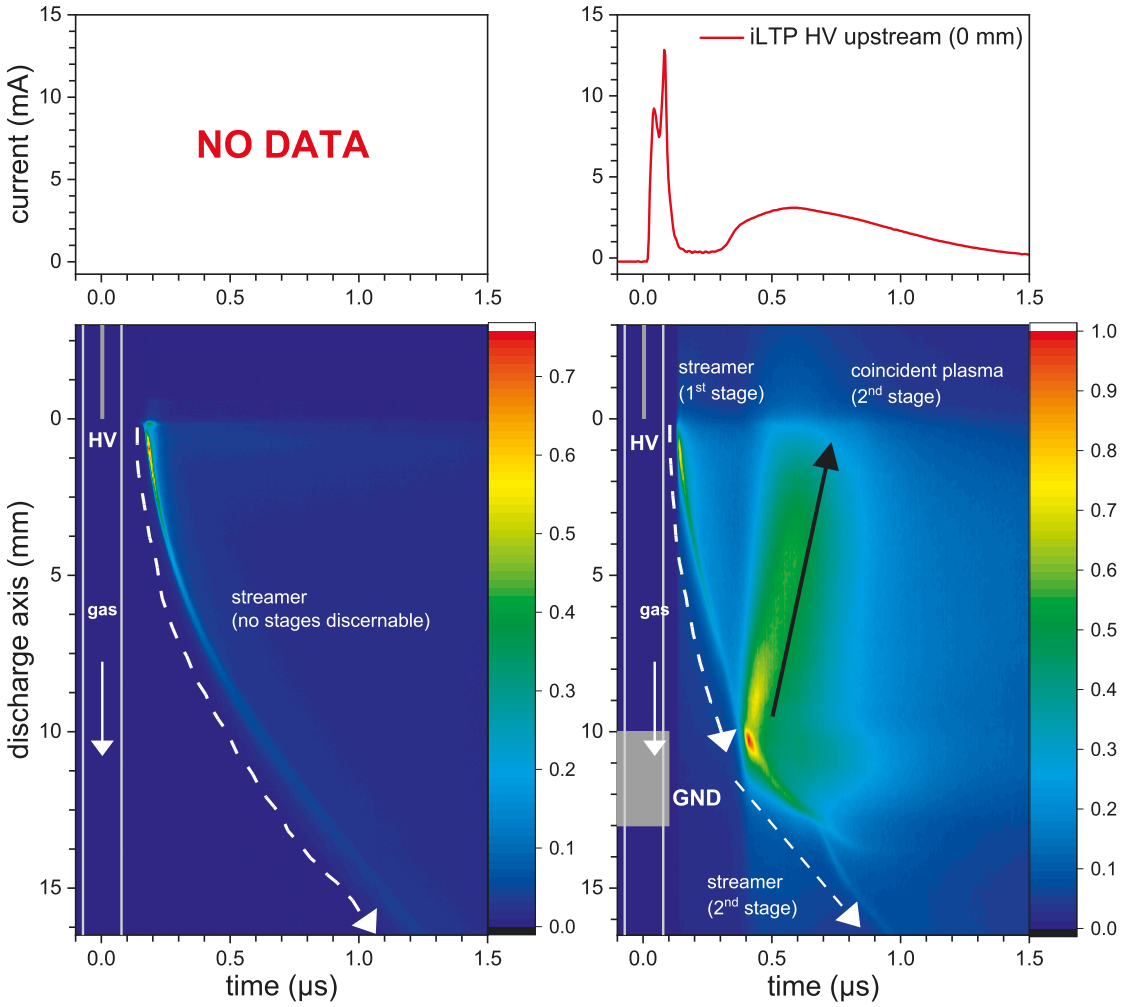

Figure 5.4: Emission measurements of the iLTP configuration with (right) and without (left) a grounded electrode. Removal of the grounded electrode leads to a complete suppression of the 2nd stage transition and directly related to this the creation of an inner coincident plasma. Both discharges were operated with an applied voltage of 3.0 kV and a gas flow of 500 ml/min He 5.0.

The special geometry that allows for a reliable operation mode where only a streamer discharge can be ignited and the possibility to use commercial, miniaturized equipment for the construction of the discharge, subsequently lead to the decision to define a new discharge design, the flexible micro tube plasma (FµTP) to differentiate it from the other DBD designs used so far.

At this point it should be mentioned that both the groundless iLTP configuration as well as FµTP should still be referred to as half dielectric barrier discharges although the dielectric barrier is not shielding the plasma actively from a grounded electrode anymore. The guiding effect of the dielectric capillary plays a major role in the

development and mechanisms of these plasmas and make the long distance streamers possible in the first place.

The exact impact of the dielectric on the discharge is still not fully understood and in particular the influence of physical properties connected to the geometry of the dielectric such as e.g. the capacitance are not yet investigated. A systematic investigation of these properties should be considered as the next logical step in the characterization and investigation of plasma based ionization sources for analytical applications.

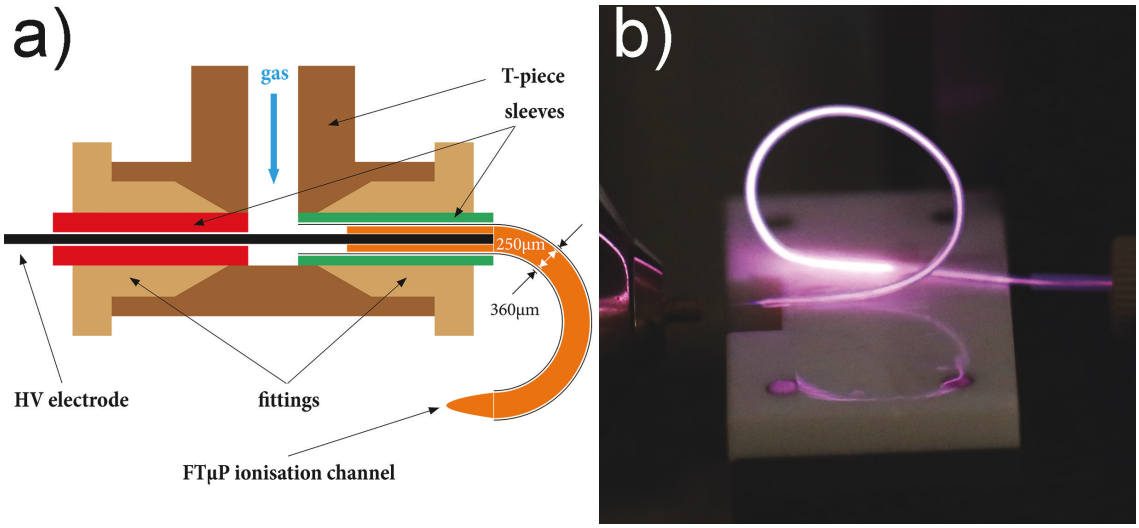

Figure 5.5: a) Schematic of the flexible micro tube plasma (FµTP). The FµTP is built in commercially available HPLC equipment which allows for a very robust and gas tight construction. b) Photograph of the FµTP in a representative MS setup. The flexible nature of the coated capillaries allow for curves and bends in the plasma discharge itself and simplify the implementation to a given mass spectrometer setup [58].

The development of the FµTP can be seen as an appropriate example on how diligent investigation and characterization of basic discharge parameters can lead to more effective plasma designs that further improve the overall efficiency of analytic applications. This small outlook on the newest development regarding miniaturized dielectric barrier discharges is thus a fitting conclusion of the experimental section of this work.

6 SUMMARY AND OUTLOOK

This work focused on the systematic characterization of capillary dielectric barrier discharges with the aim to identify fundamental discharge mechanisms that can be used for the improvement of these discharges for analytic applications.

It was found that the plasma in a capillary DBD arrangement develops in a streamer like fashion on a nanosecond time scale. While doing so, the plasma initially starts in the direct vicinity of the powered HV electrode right after the application of a positive high voltage which leads to the polarization of the dielectric material.

The plasma then extends from this HV electrode towards the grounded electrode and if the HV electrode is a symmetric ring also in the opposite direction of the grounded electrode to form the outwards directed plasma jet. The plasma transitions into a second spark like stage as soon as the initial plasma streamer reaches the grounded electrode and closes the quasi neutral conducting plasma channel between the electrodes. The plasma then fades out and slowly diminishes during this 3rd plasma stage which is dominated by metastable collisions that lead to an increased degree of dissociation of molecular components of the gas mixture.

After the positive half cycle finishes, the plasma ignites once more when the polarity of the applied voltage switches and a negative polarization occurs. Surprisingly the development of the plasma during the negative half-cycle is very similar to that of the positive half-cycle, due to the fact that the plasma propagates in the same direction. A closer examination reveals that the propagation of the excitation front is blurred out over a longer period of time than during the positive HV half-cycle which indicates that the negative plasma development is not initiated by the formation of focused steamer event.

Instead it seems as if the sudden switch of the HV polarity leads to a very fast ejection of residual electrons that remain in the vicinity of the HV electrode after the plasma diminished during the 3rd stage positive voltage half-cycle. This fast ejection of electrons will also lead to to the formation of an excitation wave front that is dominated by unfocused electron collisions and is therefore distinguishable from a classical streamer development during the positive HV half-cycle.

Further investigation in this matter are necessary to verify that the observed behavior during the negative voltage half-cycle can be explained by the suggested mechanism or if other factors play a significant role.

A systematic comparison of half- and full-dielectric barrier discharges, represented by the LTP and DBDI like discharge configurations, revealed that both discharge types are very similar to each other regarding the development and formation of the plasma. Both discharges start with an initial streamer in the vicinity of a powered

HV electrode that extend towards the grounded electrode and also both discharge types exhibit a spark like discharge behavior as soon as the initial streamer reaches the grounded electrode and closes the plasma channel.

However, the half-dielectric LTP configuration showed an additional emission forming in the vicinity of the grounded electrode wire, which is inserted into the dielectric capillary to create the half-dielectric configuration. The most notable part about this new emission is the fact that it emerges before the propagation of the streamer is fully finished. The reason for this early emission at the grounded wire tip is not yet fully understood.

One hypothesis is that a similar situation to direct discharge develops between the wire electrode and the approaching positively charged streamer head that acts as virtual electrode and generates a direct discharge plasma between this virtual electrode pair. This means that a half-dielectric discharge might also behave like a half-direct discharge but this investigation is still not fully concluded.

The overall conclusion to the comparison of LTP and DBDI like discharge configurations is that the LTP configuration seems to create the more efficient plasma from a purely physical point of view. The LTP configuration generates more charges and emission compared to an equivalent DBDI configuration that is operated with the otherwise same parameters. This higher physical efficiency suggests that also the generation of reactive species by the LTP configuration could be higher which in turn might increase its ionization efficiency.

While the generation of reactive species might indeed be higher, mass spectrometer measurements comparing the two configurations actually showed that the ionization efficiency of the DBDI is higher by up to an order of magnitude compared to the LTP configuration. As this result was unexpected at first it became even more unexpected as soon as it was found out that the ionization efficiency of the discharge configurations was highly dependent on the "status" of the grounded electrode. The "grounding status" describes whether the grounded electrode is connected to an actual mass (grounded) or not (floating) and was previously assumed to be an unimportant factor as the grounded state seemed to be the most logical default state for the grounded electrode.

The ionization efficiency of a discharge in LTP configuration can be greatly influenced by a floating grounded electrode. One reason for this could be an artificial restriction of the electric flow as the floating wire electrode cannot drain an infinite amount of charges from the discharge anymore. This suggestion is supported by preliminary measurements that used different capacitors to allow for different amounts of charges to drain through the wire electrode before it reaches its floating potential.

Another reason for the increase in ionization efficiency could be a change in the electric potential that develops between discharge and mass spectrometer. While it is hard to quantify and measure it can be assumed that a certain electric field will develop between a plasma discharge and a mass spectrometer. A good indication for this is the actual ion current that is produced with the help of the plasma and transported into the mass spectrometer and subsequently creates the desired mass spectrum. Changes to the grounding status of the grounded electrode could fairly

easy alter these fields between the discharge and mass spectrometer and therefore influence the overall transport of ionic species to the instrument.

The last subject of this work was the polarity of dielectric barrier discharges and the development of the flexible micro tube plasma (FμTP). Continuing from the systematic comparison of the LTP and DBDI configurations a previously unimportant parameter similar to the grounding status showed up which was the polarity of the electrodes.

The polarity of the electrodes defines which of the electrode is connected to the powered HV output and which is connected to the ground of the HV generator. It is a parameter that usually does not play a major role for full-dielectric configurations such as the DBDI, as their electrodes are both on the outside of the capillary.

The polarity suddenly becomes a much more important parameter for half-dielectric configurations such as the LTP, due to the fact that they have an inner and outer electrode. Applying the HV to the inner wire electrode creates the so called inverse LTP configuration which has an even higher yield of emission compared to the normal LTP configuration and most strikingly creates very long plasma channels in the range of several 1 cm to 10 cm.

The length of these plasma channels mainly results from a very pronounced streamer propagation and most strikingly even occurs in the absence of an outer grounded electrode. This mean the streamer develops and starts propagating but can never form a closed plasma channel. The iLTP configuration is an option to create a "jet only" plasma that fully suppresses the formation of a spark like coincident plasma similar to the plasma tuning method presented by Schütz at al. in 2016 [52].

The FμTP is a miniaturized discharge that uses the iLTP configuration to its advantage to create a very efficient plasma for soft ionization. The development of this very small, robust and also simplified discharge can be seen as the pinnacle and culmination of the characterization effort that was done in this work.

Development of the FμTP represents a satisfactory conclusion to the experimental part of this work, however several open questions still remain. These questions mainly revolve around the ionization efficiency of the plasmas generated by dielectric barrier discharges. Initial consideration on this topic mainly revolved around the identification of reactive species and potentially influencing these by manipulation of the discharge gas composition.

The studies conducted with argon and argon-propane mixtures showed that manipulation of gas mixture can definitely impact the operation of a DBD and open up new approaches for applications. However, further investigations with the new FμTP in pure argon show that the addition of propane is not prerequisite for soft ionization of molecules. Propane is a useful addition to ignite argon in a standard DBDI at a reasonable voltage regime necessary for the soft ionization.

The FμTP or more precisely the iLTP electrode configuration also enables the ignition of an argon plasma in this reasonalbe voltage range without the addition of propane. This contradicts the assumption that propane takes up the role as a proton donor in argon discharge as a replacement for nitrogen that supposedly takes this

role in helium discharge. This contradiction at the same time calls into question in how far nitrogen plays an important role for the soft ionization in helium discharge.

The studies on influence of trace impurities in the noble gas discharge undoubtedly shows the importance of nitrogen and propane on a helium respectively argon discharge [54]. These additional gas components clearly impact the photoionization processes in the noble gas discharges, however this does not necessarily mean that they also influence the formation of soft ionized analytes or reactive species.

These new insights emphasize the need to further investigate the soft ionization mechanism. It is still necessary to better understand the formation of reactive species in the plasma and how these species form charged molecules complexes with analytes. However, the systematic comparison of the DBDI and LTP configurations shows that it is not enough to try and only comprehend the formation of the soft ionized molecules but it is at least as important to understand the transport of the charged molecule complexes.

The distance between plasma source and mass spectrometer inlet is relatively large and charges molecules created in the vicinity of the plasma source have to travel this distance in one way or another. Better understanding of these transport processes, that are potentially dominated by electric potentials that develop between plasma source and mass spectrometer, might lead to further improvements of DBD based ionization sources for analytical applications.

BIBLIOGRAPHY

[1] A. J. Dempster: "A new Method of Positive Ray Analysis". *Physical Review* 11 (4 1918), pp. 316–325.
DOI: 10.1103/PhysRev.11.316.

[2] D. L. Albritton, T. M. Miller, D. W. Martin, and E. W. McDaniel: "Mobilities of Mass-Identified H_3^+ and H^+ Ions in Hydrogen". *Physical Review* 171 (1 1968), pp. 94–102.
DOI: 10.1103/PhysRev.171.94.

[3] Q. Hu, R. J. Noll, H. Li, A. Makarov, M. Hardman, and R. Graham Cooks: "The Orbitrap: a new mass spectrometer". *Journal of Mass Spectrometry* 40.4 (2005), pp. 430–443.
DOI: 10.1002/jms.856.

[4] A. B. Kanu, P. Dwivedi, M. Tam, L. Matz, and H. H. Hill Jr.: "Ion mobility–mass spectrometry". *Journal of Mass Spectrometry* 43.1 (2008), pp. 1–22.
DOI: 10.1002/jms.1383.

[5] D. T. Snyder, C. J. Pulliam, Z. Ouyang, and R. G. Cooks: "Miniature and Fieldable Mass Spectrometers: Recent Advances". *Analytical Chemistry* 88.1 (2016). PMID: 26422665, pp. 2–29.
DOI: 10.1021/acs.analchem.5b03070.

[6] M. Dole, L. L. Mack, R. L. Hines, R. C. Mobley, L. D. Ferguson, and M. B. Alice: "Molecular beams of macroions". *The Journal of Chemical Physics* 49.5 (1968), pp. 2240–2249.
DOI: 10.1063/1.1670391.

[7] J. B. Fenn, M. Mann, C. K. Meng, S. F. Wong, and C. M. Whitehouse: "Electrospray ionization for mass spectrometry of large biomolecules". *Science* 246.4926 (1989), pp. 64–71.
DOI: 10.1126/science.2675315.

[8] E. C. Horning, M. G. Horning, D. I. Carroll, I. Dzidic, and R. N. Stillwell: "New picogram detection system based on a mass spectrometer with an external ionization source at atmospheric pressure". *Analytical Chemistry* 45.6 (1973), pp. 936–943.
DOI: 10.1021/ac60328a035.

[9] D. I. Carroll, I. Dzidic, R. N. Stillwell, K. D. Haegele, and E. C. Horning: "Atmospheric pressure ionization mass spectrometry. Corona discharge ion source for use in a liquid chromatograph-mass spectrometer-computer analytical system". *Analytical Chemistry* 47.14 (1975), pp. 2369–2373.
DOI: 10.1021/ac60364a031.

[10] R. G. Cooks, Z. Ouyang, Z. Takats, and J. M. Wiseman: "Ambient mass spectrometry". *Science* 311.5767 (2006), pp. 1566–1570.
DOI: 10.1126/science.1119426.

[11] N. Na, M. Zhao, S. Zhang, C. Yang, and X. Zhang: "Development of a dielectric barrier discharge ion source for ambient mass spectrometry". *Journal of the American Society for Mass Spectrometry* 18.10 (2007), pp. 1859–1862.
DOI: 10.1016/j.jasms.2007.07.027.

[12] J. D. Harper, N. A. Charipar, C. C. Mulligan, X. Zhang, R. G. Cooks, and Z. Ouyang: "Low-temperature plasma probe for ambient desorption ionization". *Analytical chemistry* 80.23 (2008), pp. 9097–9104.
DOI: 10.1021/ac801641a.

[13] C. Meyer, S. Müller, E. L. Gurevich, and J. Franzke: "Dielectric barrier discharges in analytical chemistry". *Analyst* 136 (12 2011), pp. 2427–2440.
DOI: 10.1039/C0AN00994F.

[14] M. M. Nudnova, L. Zhu, and R. Zenobi: "Active capillary plasma source for ambient mass spectrometry". *Rapid Communications in Mass Spectrometry* 26.12 (2012), pp. 1447–1452.
DOI: 10.1002/rcm.6242.

[15] B. Gilbert-López, H. Geltenpoth, C. Meyer, A. Michels, H. Hayen, A. Molina-Díaz, J. F. García-Reyes, and J. Franzke: "Performance of dielectric barrier discharge ionization mass spectrometry for pesticide testing: a comparison with atmospheric pressure chemical ionization and electrospray ionization". *Rapid Communications in Mass Spectrometry* 27.3 (2013), pp. 419–429.
DOI: 10.1002/rcm.6469.

[16] S. Brandt, A. Schütz, F. D. Klute, J. Kratzer, and J. Franzke: "Dielectric barrier discharges applied for optical spectrometry". *Spectrochimica Acta Part B: Atomic Spectroscopy* 123 (2016), pp. 6–32.
DOI: 10.1016/j.sab.2016.07.001.

[17] S. Brandt, F. D. Klute, A. Schütz, and J. Franzke: "Review: Dielectric barrier discharges applied for soft ionization and their mechanism". *Analytica Chimica Acta* 951 (2016).
DOI: 10.1016/j.aca.2016.10.037.

[18] H. M. Mott-Smith and I. Langmuir: "The Theory of Collectors in Gaseous Discharges". *Phys. Rev.* 28 (1926), p. 727.
DOI: 10.1103/PhysRev.28.727.

[19] J. W. Coburn and H. F. Winters: "Plasma etching-A discussion of mechanisms". *Journal of vacuum Science and Technology* 16.2 (1979), pp. 391–403. DOI: 10.1116/1.569958.

[20] H. Abe, M. Yoneda, and N. Fujiwara: "Developments of Plasma Etching Technology for Fabricating Semiconductor Devices". *Japanese Journal of Applied Physics* 47.3R (2008), p. 1435. DOI: 10.1143/JJAP.47.1435.

[21] C. S. Wu, L. Wang, W. J. Ren, and X. Y. Zhang: "Plasma arc welding: Process, sensing, control and modeling". *Journal of Manufacturing Processes* 16.1 (2014). Recent Developments in Welding Processes, pp. 74–85. DOI: 10.1016/j.jmapro.2013.06.004.

[22] K. Salonitis and S. Vatousianos: "Experimental Investigation of the Plasma Arc Cutting Process". *Procedia CIRP* 3 (2012). 45th CIRP Conference on Manufacturing Systems 2012, pp. 287–292. DOI: 10.1016/j.procir.2012.07.050.

[23] H. Höcker: "Plasma treatment of textile fibers". *Pure and Applied Chemistry* 74.3 (2002), pp. 423–427. DOI: 10.1351/pac200274030423.

[24] G. G. Lister, J. E. Lawler, W. P. Lapatovich, and V. A. Godyak: "The physics of discharge lamps". *Reviews of modern physics* 76.2 (2004), p. 541. DOI: 10.1103/RevModPhys.76.541.

[25] J. A. C. Broekaert: "State of the art of glow discharge lamp spectrometry. Plenary lecture". *Journal of Analytical Atomic Spectrometry* 2.6 (1987), pp. 537–542. DOI: 10.1039/JA9870200537.

[26] M. Tendler, P. Rutberg, and G. van Oost: "Plasma based waste treatment and energy production". *Plasma Physics and Controlled Fusion* 47.5A (2005), A219. DOI: 10.1088/0741-3335/47/5A/016.

[27] K. Moustakas, D. Fatta, S. Malamis, K. Haralambous, and M. Loizidou: "Demonstration plasma gasification/vitrification system for effective hazardous waste treatment". *Journal of Hazardous Materials* 123.1 (2005), pp. 120–126. DOI: 10.1016/j.jhazmat.2005.03.038.

[28] M. Vleugels, G. Shama, X. T. Deng, E. Greenacre, T. Brocklehurst, and M. G. Kong: "Atmospheric plasma inactivation of biofilm-forming bacteria for food safety control". *IEEE Transactions on Plasma Science* 33.2 (2005), pp. 824–828. DOI: 10.1109/TPS.2005.844524.

[29] N. N. Misra, B. K. Tiwari, K. S. M. S. Raghavarao, and P. J. Cullen: "Nonthermal Plasma Inactivation of Food-Borne Pathogens". *Food Engineering Reviews* 3.3 (2011), pp. 159–170.
DOI: 10.1007/s12393-011-9041-9.

[30] N. Na, C. Zhang, M. Zhao, S. Zhang, C. Yang, X. Fang, and X. Zhang: "Direct detection of explosives on solid surfaces by mass spectrometry with an ambient ion source based on dielectric barrier discharge". *Journal of mass spectrometry* 42.8 (2007), pp. 1079–1085.
DOI: 10.1002/jms.1243.

[31] W. Vautz, A. Michels, and J. Franzke: "Micro-plasma: a novel ionisation source for ion mobility spectrometry". *Analytical and bioanalytical chemistry* 391.7 (2008), pp. 2609–2615.
DOI: 10.1007/s00216-008-2181-y.

[32] H. Hayen, A. Michels, and J. Franzke: "Dielectric barrier discharge ionization for liquid chromatography/mass spectrometry". *Analytical chemistry* 81.24 (2009), pp. 10239–10245.
DOI: 10.1021/ac902176k.

[33] L. Gyr, F. D. Klute, J. Franzke, and R. Zenobi: "Characterization of a Nitrogen-Based Dielectric Barrier Discharge Ionization Source for Mass Spectrometry Reveals Factors Important for Soft Ionization". *Analytical Chemistry* 91.10 (2019). PMID: 31035763, pp. 6865–6871.
DOI: 10.1021/acs.analchem.9b01132.

[34] S. Hagenhoff, A. Korf, U. Markgraf, S. Brandt, A. Schütz, J. Franzke, and H. Hayen: "Screening of semifluorinated n-alkanes by gas chromatography coupled to dielectric barrier discharge ionization mass spectrometry". *Rapid Communications in Mass Spectrometry* 32.13 (2018), pp. 1092–1098.
DOI: 10.1002/rcm.8139.

[35] F. Paschen: "Ueber die zum Funkenübergang in Luft, Wasserstoff und Kohlensäure bei verschiedenen Drucken erforderliche Potentialdifferenz". *Annalen der Physik* 273.5 (1889), pp. 69–96.
DOI: 10.1002/andp.18892730505.

[36] V. Horvatic, A. Michels, N. Ahlmann, G. Jestel, D. Veza, C. Vadla, and J. Franzke: "Time-resolved spectroscopy of a homogeneous dielectric barrier discharge for soft ionization driven by square wave high voltage". *Analytical and bioanalytical chemistry* 407.26 (2015), pp. 7973–7981.
DOI: 10.1007/s00216-015-8969-7.

[37] M. Teschke, J. Kedzierski, E. G. Finantu-Dinu, D. Korzec, and J. Engemann: "High-speed photographs of a dielectric barrier atmospheric pressure plasma jet". *IEEE Transactions on Plasma Science* 33.2 (2005), pp. 310–311.
DOI: 10.1109/TPS.2005.845377.

[38] X. Lu, M. Laroussi, and V. Puech: "On atmospheric pressure non equilibrium plasma jets and plasma bullets". *Plasma Sources Science and Technology* 21.3 (2012), p. 034005.
DOI: 10.1088/0963-0252/21/3/034005.

[39] A. Fridman: "Plasma Chemistry". (2008).
DOI: 10.1017/CBO9780511546075.

[40] S. Wu, X. Lu, D. Liu, Y. Yang, Y. Pan, and K. Ostrikov: "Photo-ionization and residual electron effects in guided streamers". *Physics of Plasmas* 21.10 (2014), p. 103508.
DOI: 10.1063/1.4897393.

[41] S. Nijdam: "Attraction of positive streamers to surfaces and free electrons". English. In: Invited paper; 69th Annual Gaseous Electronics Conference (GEC 2016), October 10-14, 2016, Bochum, Germany, GEC 2016 ; Conference date: 10-10-2016 Through 14-10-2016. 2016, JW3.00001.
DOI: 10.1103/BAPS.2016.GEC.JW3.1.

[42] V. Horvatic, S. Müller, D. Veza, C. Vadla, and J. Franzke: "Atmospheric Helium Capillary Dielectric Barrier Discharge for Soft Ionization: Determination of Atom Number Densities in the Lowest Excited and Metastable States". *Analytical Chemistry* 86.1 (2014). PMID: 24320177, pp. 857–864.
DOI: 10.1021/ac403518s.

[43] R. C. G. Sterling H. F. and. Swann: "Chemical vapour deposition promoted by r.f. discharge". *Solid-State Electronics* 8.8 (1965), pp. 653–654.
DOI: 10.1016/0038-1101(65)90033-X.

[44] V. Horvatic, A. Michels, N. Ahlmann, G. Jestel, D. Veza, C. Vadla, and J. Franzke: "Time- and spatially resolved emission spectroscopy of the dielectric barrier discharge for soft ionization sustained by a quasi-sinusoidal high voltage". *Analytical and Bioanalytical Chemistry* 407.22 (2015), pp. 6689–6696.
DOI: 10.1007/s00216-015-8827-7.

[45] V. Horvatic, A. Michels, N. Ahlmann, G. Jestel, C. Vadla, and J. Franzke: "Time-resolved line emission spectroscopy and the electrical currents in the plasma jet generated by dielectric barrier discharge for soft ionization". *Spectrochimica Acta Part B: Atomic Spectroscopy* 113 (2015), pp. 152–157.
DOI: 10.1016/j.sab.2015.09.017.

[46] S. Müller, T. Krähling, D. Veza, V. Horvatic, C. Vadla, and J. Franzke: "Operation modes of the helium dielectric barrier discharge for soft ionization". *Spectrochimica Acta Part B: Atomic Spectroscopy* 85 (2013), pp. 104–111.
DOI: 10.1016/j.sab.2013.04.005.

[47] F. D. Klute, A. Michels, A. Schütz, C. Vadla, V. Horvatic, and J. Franzke: "Capillary Dielectric Barrier Discharge: Transition from Soft Ionization to Dissociative Plasma". *Analytical Chemistry* 88.9 (2016), pp. 4701–4705.
DOI: 10.1021/acs.analchem.5b04605.

[48] A. L. Schmeltekopf and H. P. Broida: "Short-Duration Visible Afterglow in Helium". *The Journal of Chemical Physics* 39.5 (1963), pp. 1261–1268. DOI: 10.1063/1.1734425.

[49] E. E. Ferguson, F. C. Fehsenfeld, and A. L. Schmeltekopf: "Ion-Molecule Reaction Rates Measured in a Discharge Afterglow". In: *Chemical Reactions in Electrical Discharges*. 1969. Chap. 6, pp. 83–91. DOI: 10.1021/ba-1969-0080.ch006.

[50] F. D. Klute, A. Schütz, S. Brandt, S. Burhenn, P. Vogel, and J. Franzke: "Characterization of dielectric barrier discharges for analytical chemistry". *Journal of Physics D: Applied Physics* 51.31 (2018), p. 314003. DOI: 10.1088/1361-6463/aace24.

[51] S. S. Ivković, G. B. Sretenović, B. M. Obradović, N. Cvetanović, and M. M. Kuraica: "On the use of the intensity ratio of He lines for electric field measurements in atmospheric pressure dielectric barrier discharge". *Journal of Physics D: Applied Physics* 47.5 (2014), p. 055204. DOI: 10.1088/0022-3727/47/5/055204.

[52] A. Schütz, F. D. Klute, S. Brandt, S. Liedtke, G. Jestel, and J. Franzke: "Tuning Soft Ionization Strength for Organic Mass Spectrometry". *Analytical Chemistry* 88.10 (2016). PMID: 27121975, pp. 5538–5541. DOI: 10.1021/acs.analchem.6b01131.

[53] C. Meyer, S. Müller, B. Gilbert-Lopez, and J. Franzke: "Impact of homogeneous and filamentary discharge modes on the efficiency of dielectric barrier discharge ionization mass spectrometry". *Analytical and Bioanalytical Chemistry* 405.14 (2013), pp. 4729–4735. DOI: 10.1007/s00216-013-6902-5.

[54] F. D. Klute, A. Schütz, A. Michels, C. Vadla, D. Veza, V. Horvatic, and J. Franzke: "An experimental study on the influence of trace impurities on ionization of atmospheric noble gas dielectric barrier discharges". *Analyst - The Royal Society of Chemistry* 141.20 (2016), pp. 5842–5848. DOI: 10.1039/C6AN01352J.

[55] A. Schütz, F. J. Lara-Ortega, F. D. Klute, S. Brandt, M. Schilling, A. Michels, D. Veza, V. Horvatic, J. F. García-Reyes, and J. Franzke: "Soft Argon–Propane Dielectric Barrier Discharge Ionization". *Analytical Chemistry* 90.5 (2018). PMID: 29461807, pp. 3537–3542. DOI: 10.1021/acs.analchem.7b05390.

[56] F. D. Klute, S. Brandt, P. Vogel, B. Biskup, C. Reininger, V. Horvatic, C. Vadla, P. B. Farnsworth, and J. Franzke: "Systematic Comparison between Half and Full Dielectric Barrier Discharges Based on the Low Temperature Plasma Probe (LTP) and Dielectric Barrier Discharge for Soft Ionization (DBDI) Configurations". *Analytical Chemistry* 89.17 (2017). PMID: 28727447, pp. 9368–9374. DOI: 10.1021/acs.analchem.7b02174.

[57] U. Kogelschatz, B. Eliasson, and W. Egli: "Dielectric-barrier discharges. Principle and applications". *Le Journal de Physique IV* 7.C4 (1997), pp. C4–47. DOI: 10.1051/jp4:1997405.

[58] S. Brandt, F. D. Klute, A. Schütz, U. Marggraf, C. Drees, P. Vogel, W. Vautz, and J. Franzke: "Flexible Microtube Plasma (FμTP) as an Embedded Ionization Source for a Microchip Mass Spectrometer Interface". *Analytical Chemistry* (2018). PMID: 30063325.
DOI: 10.1021/acs.analchem.8b01493.

[59] A. Habib, D. Usmanov, S. Ninomiya, L. C. Chen, and K. Hiraoka: "Alternating current corona discharge/atmospheric pressure chemical ionization for mass spectrometry". *Rapid Communications in Mass Spectrometry* 27.24 (2013), pp. 2760–2766.
DOI: 10.1002/rcm.6744.

[60] Y. Zhang, X. Ma, S. Zhang, C. Yang, Z. Ouyang, and X. Zhang: "Direct detection of explosives on solid surfaces by low temperature plasma desorption mass spectrometry". *Analyst* 134.1 (2009), pp. 176–181.
DOI: 10.1039/B816230A.

[61] J. F. García-Reyes, F. Mazzoti, J. D. Harper, N. A. Charipar, S. Oradu, Z. Ouyang, G. Sindona, and R. G. Cooks: "Direct olive oil analysis by low-temperature plasma (LTP) ambient ionization mass spectrometry". *Rapid Communications in Mass Spectrometry* 23.19 (2009), pp. 3057–3062.
DOI: 10.1002/rcm.4220.

[62] E. V. Shun'ko: "V-A characteristic of a cylindrical probe in a plasma with electron flow". *Physics Letters A* 147.1 (1990), pp. 37–42.
DOI: 10.1016/0375-9601(90)90010-L.

[63] J. Schulze, E. Schüngel, and U. Czarnetzki: "The electrical asymmetry effect in capacitively coupled radio frequency discharges – measurements of dc self bias, ion energy and ion flux". *Journal of Physics D: Applied Physics* 42.9 (2009), p. 092005.
DOI: 10.1088/0022-3727/42/9/092005.

[64] E. Robert, E. Barbosa, S. Dozias, M. Vandamme, C. Cachoncinlle, R. Viladrosa, and J. M. Pouvesle: "Experimental Study of a Compact Nanosecond Plasma Gun". *Plasma Processes and Polymers* 6.12 (2009), pp. 795–802.
DOI: 10.1002/ppap.200900078.

[65] S. Brandt: "Synchronisierung zweier dielektrisch behinderten Ionisierungstechniken". Masterarbeit. 2014.

[66] I. Reginskaya, M. Schilling, G. Adali, G. Jestel, D. Janasek, and J. Franzke: "Emitter-assigned multi-dielectric barrier-nano-electrospray ionization mass spectrometry". *Analytical and bioanalytical chemistry* 407 (2015).
DOI: 10.1007/s00216-015-8821-0.

PUBLICATIONS

F. D. Klute, A. Michels, A. Schütz, C. Vadla, V. Horvatic, and J. Franzke: "Capillary Dielectric Barrier Discharge: Transition from Soft Ionization to Dissociative Plasma". *Analytical Chemistry* 88.9 (2016). PMID: 27032869, pp. 4701–4705.
DOI: 10.1021/acs.analchem.5b04605.

F. D. Klute, A. Schütz, A. Michels, C. Vadla, D. Veza, V. Horvatic, and J. Franzke: "An experimental study on the influence of trace impurities on ionization of atmospheric noble gas dielectric barrier discharges". *Analyst - The Royal Society of Chemistry* 141.20 (2016), pp. 5842–5848.
DOI: 10.1039/C6AN01352J.

F. D. Klute, S. Brandt, P. Vogel, B. Biskup, C. Reininger, V. Horvatic, C. Vadla, P. B. Farnsworth, and J. Franzke: "Systematic Comparison between Half and Full Dielectric Barrier Discharges Based on the Low Temperature Plasma Probe (LTP) and Dielectric Barrier Discharge for Soft Ionization (DBDI) Configurations". *Analytical Chemistry* 89.17 (2017). PMID: 28727447, pp. 9368–9374.
DOI: 10.1021/acs.analchem.7b02174.

F. D. Klute, A. Schütz, S. Brandt, S. Burhenn, P. Vogel, and J. Franzke: "Characterization of dielectric barrier discharges for analytical chemistry". *Journal of Physics D: Applied Physics* 51.31 (2018), p. 314003.
DOI: 10.1088/1361-6463/aace24.

COOPERATIVE PUBLICATIONS:

S. Brandt, F. D. Klute, A. Schütz, and J. Franzke: "Review: Dielectric barrier discharges applied for soft ionization and their mechanism". *Analytica Chimica Acta* 951 (2016).
DOI: 10.1016/j.aca.2016.10.037.

S. Brandt, A. Schütz, F. D. Klute, J. Kratzer, and J. Franzke: "Dielectric barrier discharges applied for optical spectrometry". *Spectrochimica Acta Part B: Atomic Spectroscopy* 123 (2016), pp. 6–32.
DOI: https://doi.org/10.1016/j.sab.2016.07.001.

A. Schütz, F. D. Klute, S. Brandt, S. Liedtke, G. Jestel, and J. Franzke: "Tuning Soft Ionization Strength for Organic Mass Spectrometry". *Analytical Chemistry* 88.10 (2016). PMID: 27121975, pp. 5538–5541.
DOI: 10.1021/acs.analchem.6b01131.

S. Brandt, F. D. Klute, A. Schütz, U. Marggraf, C. Drees, P. Vogel, W. Vautz, and J. Franzke: "Flexible Microtube Plasma (FμTP) as an Embedded Ionization Source for a Microchip Mass Spectrometer Interface". *Analytical Chemistry* (2018). PMID: 30063325.
DOI: 10.1021/acs.analchem.8b01493.

S. Burhenn, J. Kratzer, M. Svoboda, F. D. Klute, A. Michels, D. Veža, and J. Franzke: "Spatially and Temporally Resolved Detection of Arsenic in a Capillary Dielectric Barrier Discharge by Hydride Generation High-Resolved Optical Emission Spectrometry". *Analytical Chemistry* 90.5 (2018). PMID: 29457722, pp. 3424–3429.
DOI: 10.1021/acs.analchem.7b05072.

A. Schütz, F. J. Lara-Ortega, F. D. Klute, S. Brandt, M. Schilling, A. Michels, D. Veza, V. Horvatic, J. F. García-Reyes, and J. Franzke: "Soft Argon–Propane Dielectric Barrier Discharge Ionization". *Analytical Chemistry* 90.5 (2018). PMID: 29461807, pp. 3537–3542.
DOI: 10.1021/acs.analchem.7b05390.

S. Burhenn, J. Kratzer, F. D. Klute, J. Dědina, and J. Franzke: "Atomization of arsenic hydride in a planar dielectric barrier discharge: Behavior of As atoms studied by temporally and spatially resolved optical emission spectrometry". *Spectrochimica Acta Part B: Atomic Spectroscopy* 152 (2019), pp. 68–73.
DOI: https://doi.org/10.1016/j.sab.2018.12.006.

L. Gyr, F. D. Klute, J. Franzke, and R. Zenobi: "Characterization of a Nitrogen-Based Dielectric Barrier Discharge Ionization Source for Mass Spectrometry Reveals Factors Important for Soft Ionization". *Analytical Chemistry* 91.10 (2019). PMID: 31035763, pp. 6865–6871.
DOI: 10.1021/acs.analchem.9b01132.

CONFERENCE CONTRIBUTIONS:

F. D. Klute, A. Michels, S. Brandt, A. Schütz, and J. Franzke: "Optimization of a Dielectric Barrier Discharge for soft Ionization or Excitation of Dissociated Molecules". *SciX 2016 (FACSS 43)* (2016).
.

F. D. Klute et al.: "Influence of metastables, quasi metastables and gas impurities on the positive ion formation of a noble gas atmospheric DBD". *CESPC-7* (2017).
.

F. D. Klute, S. Burhenn, P. Vogel, A. Michels, C. Lewis, D. Thurston, B. Biskup, P. B. Farnsworth, and J. Franzke: "On the roles of metastable and quasi-metastable species in atmospheric noble gas dielectric barrier discharges". *SciX 2017 (FACSS 44)* (2017).
.

LIST OF FIGURES

DANKSAGUNGEN

Ich möchte diese Gelegenheit nutzen und mich bei allen Personen bedanken die mich die letzten Jahre unterstützt haben und ohne die ich diese Arbeit nicht hätte fertig stellen können.

Zuallererst bedanke ich mich bei PD. Dr. Joachim Franzke für die Bereitstellung dieser Arbeit und die geduldige und kompetente Betreuung. Vielen Dank für die interessanten und angeregten Diskussionen die es geschafft haben meinen Ehrgeiz und eigenen Anspruch jederzeit aufrecht zu erhalten. Ohne diese Motivation hätte ich dieses zum Teil recht komplexe Thema niemals zufriedenstellend bearbeiten können.

Gleichzeitig danke ich der DFG für die Förderung dieses Themas unter der Projektnummer 262732688 wodurch diese Arbeit überhaupt erst ermöglicht wurde.

Des weiteren möchte ich mich bei Professor Manfred Bayer bedanken der sich dazu bereit erklärt hat ein Zweitgutachten für diese Arbeit zu erstellen.

Als nächstes danke ich meinen Kolleginnen und Kollegen des Leibniz-Institut für analytische Wissenschaften ISAS - e.V., insbesondere denen der Arbeitsgruppe Miniaturisierung. Die Arbeit der letzten Jahre war eine anspruchsvolle aber trotz allem erfreuliche Erfahrung, die nur durch die gute und enge Zusammenarbeit zustande kommen konnte. Diese Arbeit wäre ohne die umfangreichen Kooperationen mit vor allem Alexander Schütz und Sebastian Brandt in dieser Form nicht möglich gewesen, weshalb ich euch im speziellen an dieser Stelle danken möchte.

Außerdem möchte ich meinen Kooperationspartnern Damir Veža, Cedomil Vadla und Vlasta Horvatic danken, für die wunderbare Vorarbeit zur Charakterisierung dielelektrisch behinderter Plasmen. Ohne die Unterstützung und den regen Austausch hätte ich es niemals geschafft so schnell in dieses Komplexe Thema einzusteigen und relevante Erkenntnisse zu gewinnen. Gleiches gilt für Professor Paul B. Farnsworth von der Brigham Young University in Provo Utah und seiner Arbeitsgruppe. Dank des kurzen aber sehr erfolgreichen Forschungsaufenthalts konnte ich nicht nur einen Einblick in das amerikanische Universitätsleben werfen, sondern auch Absorptionsmessungen durchführen die in unseren eigenen Laboren in der Form nicht möglich gewesen wären.

Abschließend bedanke ich mich bei meinen Freunden und meiner Familie. Die Arbeit an diesem Thema hat viel Zeit und Aufmerksamkeit in Anspruch genommen. Erschwerend kommt hinzu, dass man diese Art der Arbeit nur schwer im Büro lassen kann, egal was man sich vorab vorgenommen hat. Deswegen vielen

Dank für das Verständnis der letzten Jahre an alle!

Insbesondere danke ich meiner Lebenspartnerin Beatrix Biskup. Du hast nun den größten Teil meines Studiums zu mir gehalten und dass du im Gegensatz zu den Meisten meiner Bekannten, Freunden und Familie genau verstehst worin meine Arbeit besteht macht die Sache vermutlich eher schwerer als leichter. Danke dass du diese Zeit mit mir gemeistert hast.